REPORT NO.
UCB/SESM 85/07

S. E. S. M.
DEPARTMENT OF CIVIL ENGINEERING

FRACTIONAL DERIVATIVE REPRESENTATION OF SEISMIC RESPONSE OF BASE-ISOLATED MODELS : THEORY AND EXPERIMENTS

by

CHAN GHEE KOH
and
JAMES M. KELLY

NOVEMBER 1985

COLLEGE OF ENGINEERING
UNIVERSITY OF CALIFORNIA
BERKELEY, CALIFORNIA

FRACTIONAL DERIVATIVE REPRESENTATION OF SEISMIC RESPONSE OF BASE-ISOLATED MODELS : THEORY AND EXPERIMENTS

by

Chan Ghee Koh

Graduate Student in Civil Engineering

University of California, Berkeley

James M. Kelly

Professor of Civil Engineering

University of California, Berkeley

Division of Structural Engineering and Structural Mechanics
Department of Civil Engineering
College of Engineering
University of California, Berkeley

November 1985

Abstract

The concept of fractional derivatives is used in the mathematical formulation of stress-strain relationship for viscoelastic materials. Several simple fractional derivative models are introduced. In particular, the fractional oscillator which consists of a mass and a fractional Kelvin element is suggested as a more accurate model for the elastomeric bearings used in base isolation systems. Solution procedures for obtaining the dynamic response of base-isolated structure idealized as a single-degree-of-freedom system are presented. Numerical step-by-step algorithms are developed to the analysis of linear systems in time domain, and can be extended to treat the nonlinear systems as well. Alternative approaches, namely the Laplace transformation and Fourier transformation methods, are also employed in the analysis of linear systems for comparison purposes. Numerical examples show that the solutions obtained by the step-by-step scheme are in good agreement with the Laplace and Fourier solutions.

The fractional derivative model is used to fit the results of an experimental test program in which a base-isolated bridge was subjected to simulated earthquake loading on a large shaking table. In fitting the amplification factor curve obtained from the tests of the bridge deck when subjected to harmonic excitations, the linear fractional derivative model is found to be better than the conventional models. A nonlinear fractional derivative model is proposed to account for the strain effect of rubber in correlation with the earthquake simulated tests. This model is found to give good agreement with the experimental results. The solution procedure is then extended to the dynamic analysis of a base-isolated multi-degree-of-freedom system.

Acknowledgments

The research reported here was sponsored in part by the National Science Foundation under grant no. CEE-8213604.

Table of Contents

List of Figures

List of Tables

CHAPTER 1
INTRODUCTION

1.1 Brief Historical Review of Fractional Calculus

The generalization of derivatives and integrals to arbitrary order, now contained in the theory of Fractional Calculus, is not a new concept. Its existence was first questioned as early as in 1695 by Leibniz. Some analytical works on this subject were carried out by Abel, Liouville and Riemann in the first half of the nineteenth century.[1] The first significant application of fractional calculus was due to Heaviside who introduced fractional differentiation in his investigation of the transmission line theory.[2] This concept was then extended by Gemant who observed that the stiffness and damping properties of viscoelastic materials appeared to be related to fractional powers of frequency,[3] and thus suggested the use of fractional time derivatives in the stress-strain relation for certain types of materials.[4] Other applications outside pure mathematics now include those to rheology, potential theory, electrochemistry, diffusion and general transport theory.[5] It appears that many problems in physical science can be expressed and solved succinctly by recourse to fractional calculus. However, its applications are still considerably few, mainly because of its unfamiliarity and the lack of recent development in the theory.

1.2 Applications of Fractional Calculus to Viscoelasticity

As mentioned earlier, Gemant first suggested the use of fractional derivatives in the viscoelastic model. Later, Scott-Blair used this approach to model the observations made by Nutting that the stress relaxation phenomenon could be described by fractional powers of time.[6] In late 60's and 70's, Caputo and Minardi found good agreements with the experimental results in frequency domain, when applying this concept to model the viscoelastic properties of geological strata, some metals and glasses.[7,8,9] In about the same period, other related works include those contributed by Slonimsky,[10] Smit and de Vries.[11] Besides presenting the fractional calculus formulation of viscoelastic stress-strain law, both of these papers give some

physical insight into the fractional derivative models.

More recently, Bagley and Torvik have shown that the generalized (fractional) derivative constitutive equations are effective in modeling several viscoelastic materials having distinctly different mechanical properties.[12,13,14] This is attained with fewer parameters than the conventional viscoelastic models which contain time derivatives of integral orders only. Stiassnie also obtains a similar conclusion by considering a two-stage standard test to a polymeric material.[15] Rogers shows that the use of polynomial operator of fractional degree describes the complex shear modulus accurately and efficiently.[16] In particular, he develops a generalized fractional Maxwell model that always produces causal response and also offers a feasible explanation between fractional calculus and molecular dynamics. The model parameters are determined by means of Bode diagrams. Very recently, Koeller[17] has shown that Rabotnov's theory of hereditary solid mechanics[18] is equivalent to requiring that the stress in the dashpot is proportional to the fractional derivative of the corresponding strain. He then generalizes this theory and obtains creep and relaxation functions for various fractional calculus models.

1.3 Physical Justification of Fractional Derivative Models (FDM)

So far most of the applications of fractional calculus in science and engineering are in solving diffusion problems, including heat in solids, vorticity in fluids, chemical species in homogeneous media, and electricity in resistive- capacitative lines.[5] In these somewhat idealized problems, the fractional order of derivative is usually 1/2 and, in some cases, 1/4 . In the theory of viscoelasticity, the fractional calculus approach has originally evolved as an empirical method of describing the mechanical properties of viscoelastic materials. Such approach is justified by the fact that it is effective in fitting the storage modulus and the loss factor curves by one equation with only a few parameters. Otherwise, these two curves are normally fitted by two independent empirical equations. Conceptually, the fraction calculus approach is a more reasonable one since the storage and loss moduli are actually interrelated.[19]

Among other researhers[10,11] in the attempts to trace the physical origin of the fractional derivative models, Bagley and Torvik show that the fractional derivative does arise naturally in at least the following cases:

(i) In a half-space of Newtonian viscous fluid undergoing the motion induced by the sinusoidal motion of a plate on the surface, the shear stress at any point is proportional to the time semi-derivative, i.e. derivative of order 1/2, of the fluid velocity.[20]

(ii) For polymer solutions and polymer solids with no crosslinking and under certain restrictions, the shear stress can be expressed in terms of the time semi-derivative of the shear strain.[21]

In the second case, the semi-derivative arises as a result of the retardation spectrum being proportional to the half-power of retardation time. Similarly, a related molecular theory taking into account the intermolecular hydrodynamic forces is developed by Zimm[22] and, if put in the fractional derivative form, the fractional order is found to be 2/3 . Certainly for real materials with crosslinking and more complicated microscopic structure, one would not expect the fractional order to be exactly 1/2 or 2/3 . Nevertheless, these observations provide a link between microscopic theories of ideal viscoelastic media and macroscopic behaviors of real materials. More importantly, the fractional derivative model in viscoelasticity theory is not totally empirical.

1.4 Characteristics of Rubber and its Engineering Applications

A rubber (or elastomer) is a polymeric material (natural of synthetic), with long flexible molecular chains having the ability to deform elastically when vulcanized. Vulcanization is a process by which the rubber molecules are linked with adjacent molecules at intervals along their lengths, usually by sulphur, to form a stable crosslinked elastic material.[23] Rubber is a very versatile and adaptable material and has been used in engineering for over 100 years. Its physical properties such as strength, modulus, fatigue resistance and heat resistance can be varied at will over a wide range by adding different types and levels of vulcanizing agents,

fillers and protective agents.[24] Rubber has the following advantages over many other engineering materials: (i) High compressive strength; (ii) Good energy absorption; (iii) Ability to undergo large deformations and recover (160,000 times more elastic than steel in shear); (iv) Good electrical insulation properties; (v) Resistance to fatigue, abrasion and corrosion; and (vi) Can be moulded.[25] As an engineering material, rubber has a wide range of applications, for examples, to bridge bearings, dockside fenders, suspension systems, acoustic insulation, vibration isolation and flexible couplings. Particularly because of its first three characteristics, rubber in the form of multilayer elastomeric bearings has made the century-old concept of base isolation a reality.

1.5 Base Isolation Systems

The conventional earthquake resistant designs rely on strength and ductility of the structural components to resist the earthquake induced forces and to dissipate the seismic energy, thereby preventing the collapse of structures in case of earthquake. In contrast, base isolation approach aims to reduce the damaging horizontal seismic force transmitted to the structures. In principle, this is achieved by building the structure on a system of foundation bearings that serves to decouple the structure from the horizontal ground motion. During earthquakes, the superstructure virtually floats as a rigid body and is thus isolated from the horizontal ground motion to some extent. As such, not only is the primary structure protected from earthquake destruction, damages to its contents and occupants are greatly reduced as well.

Base isolation concept has long been discussed, but the main problem has always been that of controlling the very large relative displacement that can occur. With the advance in rubber technology, special multilayer elastomeric bearings can be designed to sustain these amplitude substantially. These bearings have been developed following the extensive and confident use of rubbers in bridge bearings[26] and acoustic isolation bearings for buildings.[27] Many years of experience with bridge bearings show that rubber, with the appropriate protective agents, is reliable and resistant to environmental damage, including oil and fire.[28] Recognition of the superior engineering properties of rubber has led to the use of elastomeric

bearings in several base-isolated buildings that have been built or are still under construction. A good review of the development of base isolation, experimentation on this concept and the implementation to actual structures is presented by Kelly.[29]

1.6 Motivation for Use of FDM in Base Isolation Systems

With a suitably designed base isolation system, the superstructure of the building moves almost as a rigid body during an earthquake. Large relative movement and large energy dissipation take place only across rubber bearings. It is therefore essential to construct a good constitutive model for rubber bearing in order to predict the seismic response accurately. In most of the dynamic analyses for rubber base isolation systems, linear viscous damping is assumed. This means that the loss factor is linearly proportional to the frequency, which is not true for rubber and many other engineering materials. Typical storage modulus and loss factor curves for vulcanized and unvulcanized natural rubbers[30] are shown in Figs. 1.1 and 1.2. It is clear that linear viscous model (i.e. a mass connected to a Kelvin model) is not a good idealization of the actual behavior of rubbers. It tends to overdamp the high-frequency response. To this end, one might proceed to use generalized Kelvin (or Maxwell) model as in the standard viscoelasticity approach, involving derivatives of integral orders only in the constitutive equation. However, as seen in many previously mentioned papers, more terms are usually required than it would be in the fractional calculus approach. As a result, one obtains a high order constitutive equation which is not convenient for computation, especially in dynamic problems.

Another commonly used model is the hysteretic damping model (or sometimes known as the rate-independent damping model), in which the stiffness and loss factor are assumed to be frequency independent. This is certainly not true for a wide range of frequency. A drawback is that this model is physically unrealizable because it implies non-causal response, i.e. response exists prior to the application of the excitation.[31] This may vitiate the usefulness of this model in transient problems. Another disadvantage is that this model is convenient only in Fourier (frequency) approach. In real time analysis, one might define the damping force in

phase with the velocity but proportional in magnitude to the displacement.[32] However, it is rather cumbersome to use this model as a jump in damping force arises whenever there is a change in the direction of motion. The alternative ad-hoc representation of damping force in time domain is a stiffness term divided by excitation frequency. This approach is clearly not appropriate for transient problems. The fractional derivative model, if properly constructed, has no such problems.

The above advantages of the fractional derivative model over conventional approaches motivate the study of its possible application to construct a more realistic constitutive model for rubber bearings so that the seismic response of base-isolated structures can be more accurately predicted .

CHAPTER 2

LINEAR FRACTIONAL DERIVATIVE MODEL

2.1 Definitions and Properties of Fractional Derivatives

Derivatives and integrals are sometimes called *differintegrals* in one word for brevity in fractional calculus. Fractional differintegration is an operator that generalizes the differentiation or integration to non-integral order. There are several definitions which are equivalent to one another. One commonly used definition due to Riemann and Liouville is the following:

$$
\begin{aligned}
{}_aD_t^q\,[f(t)] &\equiv \frac{d^q\, f(t)}{[d(t-a)]^q} \\
&\equiv \begin{cases}
\dfrac{1}{\Gamma(n-q)}\,\dfrac{d^n}{dt^n}\left[\displaystyle\int_a^t \frac{f(\tau)}{(t-\tau)^{q-n+1}}\,d\tau\right], & n>q\geq 0\,,\ n \text{ integer} \qquad (2.1a) \\
\dfrac{1}{\Gamma(-q)}\displaystyle\int_a^t \frac{f(\tau)}{(t-\tau)^{q+1}}\,d\tau, & q<0 \qquad (2.1b)
\end{cases}
\end{aligned}
$$

In the theory of viscoelasticity , we are concerned with the influence of the entire response history on the current response. The lower limit (a) should thus be $-\infty$. However, if we assume $f(t) = 0$, $t < 0$, then ${}_{-\infty}D_t^q$ is identical to ${}_0D_t^q$. Hence a is usually taken as 0 and the short hand notation for such derivative is written as $D^q[f(t)]$, or sometimes simply $D^q f$ if the independent variable is understood. Furthermore q is taken to be non-negative from here onwards, as is normally done in the applications to viscoelasticity.

An algebraic definition for fractional derivatives as a limit of a (backward) difference quotient is[33]

$$D^q[f(t)] = \lim_{h\to 0^+} \frac{\Delta_h^q f(t)}{h^q} \qquad (2.2)$$

where

$$\Delta_h^q\, f(t) = \sum_{j=0}^{\infty} (-1)^j \begin{bmatrix} q \\ j \end{bmatrix} f(t-jh) \qquad (2.3)$$

$$\begin{bmatrix} q \\ j \end{bmatrix} = \frac{\Gamma(q+1)}{\Gamma(q-j+1)\,j!} \qquad (2.4)$$

Some important properties :

In the following , we assume that the differintegral of the functions can be determined (i.e. the functions are 'differintegrable') , and n is an integer.

(i) Linearity :

$$D^q[c_1 f_1(t) + c_2 f_2(t)] = c_1 D^q[f_1(t)] + c_2 D^q[f_2(t)] , \tag{2.5}$$

where c_1 , c_2 are constants .

(ii) Laplace transformation[5] :

$$L\{D^q[f(t)]\} = s^q L\{f(t)\} - \sum_{k=0}^{n-1} s^k \; D^{q-1-k}[f(0)] , \qquad n-1<q\leq n \tag{2.6}$$

where

$$L\{f(t)\} \equiv \int_0^\infty exp(-st)\, f(t)\, dt \tag{2.7}$$

For $0<q<1$, Eq. (2.7) reduces to

$$L\{D^q[f(t)]\} = s^q L\{f(t)\} \tag{2.8}$$

Because of this relatively simple form , the range $0<q<1$ is preferred.

(iii) Fourier transformation :

Under the usual condition that the Fourier transform of $f(t)$ defined as below exists

$$F\{f(t)\} = \int_{-\infty}^{\infty} f(t)\, exp(-i\omega t)\, dt \tag{2.9}$$

and the additional condition that $f(t)=0$, $t<0$, we have

$$F\{D^q[f(t)]\} = (i\omega)^q \; F\{f(t)\} , \quad q>0 \tag{2.10}$$

in which

$$i^q = \cos\frac{\pi q}{2} + i \sin\frac{\pi q}{2} \tag{2.11}$$

For proof of Eq. (2.10) , see Appendix A .

(iv) Composition rule[5] :

In general ,

$$D^q D^Q f = D^{q+Q} f - D^{q+Q}[f - D^{-Q} D^Q f] \tag{2.12}$$

Certainly , it would be nice to have

$$D^q D^Q f = D^{q+Q} f \tag{2.13}$$

This is in fact true for the following cases:

(a) q is a positive integer .

(b) Q is a positive integer , n , and $f(0)=f'(0)=\cdots=f^{n-1}(0)=0$.

(c) f can be expressed as follows :

$$f(t) = t^p \sum_{j=0}^{\infty} a_j \, t^j \quad , p>-1 \quad , a_0 \neq 0 \quad , D^Q f \neq 0 \tag{2.14}$$

A particular case of (c) is when $p=0, Q<1$,

$$f(t) = \sum_{j=0}^{\infty} a_j \, t^j \tag{2.15}$$

This says that Eq. (2.13) holds as long as $f(t)$ can be expressed as a polynomial in t and $Q<1$.

2.2 General Fractional Derivative Model

The conventional viscoelastic models, such as generalized Maxwell or Kelvin models, can be represented in general by the following stress-strain ($\tau-\gamma$) relationship[34] :

$$\sum_{k=0}^{K} b_k D^k \, \tau(t) = \sum_{j=0}^{J} a_j D^j \, \gamma(t) \tag{2.16}$$

The general fractional derivative model is an extension of the above model, having the following constitutive equation:

$$\sum_{k=0}^{K} b_k D^{r_k} \, \tau(t) = \sum_{j=0}^{J} a_j D^{q_j} \, \gamma(t) \tag{2.17}$$

where q_j and r_k are the fractional orders of time derivatives, usually in the range between 0

and 1 for reasons that would be clear later.

In the frequency domain, Eq. (2.17) yields

$$[\sum_{k=0}^{K} b_k (i\omega)^{r_k}]\ \bar{\tau}(\omega) = [\sum_{j=0}^{J} a_j (i\omega)^{q_j}]\ \bar{\gamma}(\omega) \tag{2.18}$$

where $\bar{\tau}(\omega)$ and $\bar{\gamma}(\omega)$ are the Fourier transforms of $\tau(t)$ and $\gamma(t)$, respectively .

The complex shear modulus is then given by

$$G(\omega) = \frac{\sum_{j=0}^{J} a_j (i\omega)^{q_j}}{\sum_{k=0}^{K} b_k (i\omega)^{r_k}} \tag{2.19}$$

This can be decomposed into the real and imaginary parts, i.e.

$$G(\omega) = G_1(\omega) + i\ G_2(\omega) \tag{2.20}$$

where $G_1(\omega)$ and $G_2(\omega)$ are known as the storage (elastic) modulus and the loss modulus, respectively, and their ratio

$$\tan\delta = \frac{G_2(\omega)}{G_1(\omega)} \tag{2.21}$$

is called the loss factor (or loss tangent).

Note that $G_2(\omega)$ must not be negative. Otherwise, physically it means that the energy is created instead of dissipated during the loading and unloading process.

2.3 Spring-pot Element

The simplest form of Eq. (2.17) is

$$\tau(t) = G_0 \eta^q\ D^q[\gamma(t)] \quad , \quad 0 \le q \le 1 \tag{2.22}$$

where G_0 and η have the dimensions of shear modulus and time, respectively.

For $q=0$ and $q=1$, this equation becomes the respective stress-strain equation for a purely elastic material obeying Hooke's law of elasticity and a purely viscous material obeying Newton's law of viscosity. Thus, it is reasonable and natural to propose this constitutive relation for viscoelastic material which is known to behave in between. Koeller shows that

this model does allow a continuous transition of mechanical properties from the solid state to the fluid state when q is varied from zero to one.[17] Smit and de Vries,[11] as a matter of fact, make a remark that q indicates the state of material on a scale ranging from 0 for the purely elastic case to 1 for the purely viscous case. They refer this element as the 'intermediate model' while Koeller calls it the 'spring-pot' because the element is intermediate between a spring and a dash-pot. Figuratively, it is represented by a diamond as shown in Fig. 2.1 .

The storage modulus and the loss factor are, respectively,

$$G_1(\omega) = G_0 (\eta\omega)^q \cos\frac{\pi q}{2} \tag{2.23}$$

$$\tan\delta = \tan\frac{\pi q}{2} \tag{2.24}$$

Note that $\eta\omega$ is dimensionless and thus called the normalized frequency. This simple model is attractive for some applications where the loss factor is frequency independent. Caputo[35] incorporates this concept in the wave equation for a dissipative medium . Stiassnie[15] indeed uses just the spring-pot element to obtain reasonably good agreement with the experimental results for a polymeric compound subjected to a standard creep-relaxation test. This element, however, gives $G_1(\omega) = 0$ and it therefore cannot characterize materials which do not relax to zero stress. This problem can be resolved by adding a spring in the model, as illustrated in the following section.

2.4 Fractional Kelvin (FKV) Model

If the dashpot in the conventional Kelvin model is replaced by a spring-pot element, one obtains the so called 'fractional Kelvin model'. For this model, the stress-strain relation is

$$\tau(t) = G_0 (1 + a\eta^q D^q) \gamma(t) \quad , \; a > 0 \tag{2.25}$$

from which

$$G_1(\omega) = G_0 [1 + a(\eta\omega)^q \cos\frac{\pi q}{2}] \tag{2.26}$$

$$\tan\delta = \frac{a(\eta\omega)^q \sin\frac{\pi q}{2}}{1 + a(\eta\omega)^q \cos\frac{\pi q}{2}} \tag{2.27}$$

Note that, for $a > 0$, the range $0 \leq q \leq 1$ should be imposed in order to avoid negative storage and loss moduli over the entire (positive) frequency range. When $q = 1$, this model recovers to the Kelvin model for which $G_1(\omega)$ is constant and $\tan\delta$ is linearly proportional to ω .

Figures 2.2 and 2.3 present the curves of storage modulus and loss factor for different values of q over four decades of normalized frequency. When these figures are compared with Figs. 1.1 and 1.2 , this model seems promising for describing the properties of natural rubber in the rubbery region, i.e. in the frequency range before the storage modulus and the loss factor increase sharply.

2.5 Numerical Example

To compare the effectiveness of the fractional derivative models and the conventional viscoelastic models, a numerical example of fitting the storage modulus and loss factor curves is presented here. The experimental data for a lightly vulcanized Hevea (natural) rubber are taken from p.458 of Reference 19. The frequency range considered here is 10^{-2} – 10^{2} rad/s , which covers the dominant frequency range for most seismic problems. The following models are used to fit these data by the least square method:

Conventional : (a) Hysteretic damping model

(b) Kelvin model

(c) Standard linear solid

Fractional : (d) Spring-pot element

(e) Fractional Kelvin model

The loss factor curve (Fig. 2.4) is first used to determine all the model parameters except the stiffness constant (G_0) , which is then found by fitting the storage modulus curve (Fig. 2.5). It can be seen clearly that the fractional derivative models fit the experimental data much better than the conventional models do. Among all these models, FKV model is the best for describing the viscoelastic properties in the rubbery range that is the usual operating region

for base isolation problems.

2.6 Fractional Standard Linear Solid (FSLS) Model

The conventional standard linear solid has the the following constitutive relationship:

$$\tau(t) + b\dot{\tau}(t) = G_0 [\gamma(t) + \dot{\gamma}(t)] \tag{2.28}$$

Its counterpart in the fractional derivative theory is given by

$$(1 + bD^q)\, \tau(t) = G_0 (1 + aD^q)\, \gamma(t) \tag{2.29}$$

In the frequency domain , the complex shear modulus is

$$G(\omega) = G_0 \frac{1+a(i\omega)^q}{1+b(i\omega)^q} \tag{2.30}$$

It can be shown easily that the storage and loss moduli are non-negative if $0 \le q \le 1$, $a > b$. With just an additional parameter over the FKV model, this model can fit the experimental data fairly well over an enormous range of frequency , as shown in Figs. 2.6 and 2.7. However, in the frequency range of interest in seismic problems, FKV model is preferred.

CHAPTER 3

RESPONSE OF SDOF FRACTIONAL OSCILLATOR

3.1 Single-degree-of-freedom 'Fractional Oscillator'

Consider a base deck mounted on an elastomeric base isolation system with no super-structure. The elastomeric base isolation system is usually idealized as a single-degree-of-freedom (SDOF) oscillator, i.e. a lumped mass connected to a Kelvin model. The latter is here replaced by a fractional Kelvin model, as shown in Fig. 3.1, and the system might be called a SDOF 'fractional oscillator'. The system is linear if the parameters (m,k,c,q) are constants.

The equation of motion of the base deck due to ground motion is

$$m\ddot{v}(t) + cD^q v(t) + kv(t) = f(t) \tag{3.1}$$

where

m = mass of the deck,

c = damping constant of rubber bearings,

k = static stiffness of rubber bearings in horizontal shear direction,

v(t) = relative displacement of the deck with respect to the ground,

f(t) = forcing function $= -m\ddot{u}_g(t)$; $\ddot{u}_g(t)$ is the ground acceleration.

The fact that D^q ($\equiv {}_0D_t^q$) is used in Eq. (3.1) requires the following assumption:

$$v(t) = 0 \ , \ t < 0 \tag{3.2}$$

Otherwise, ${}_{-\infty}D_t^q$ should be used instead. Equation (3.1) can be solved by the following methods:

(1) Laplace transformation method.

(2) Fourier transformation method.

(3) Step-by-step integration scheme in time domain.

The first two methods are applicable only for linear systems.

3.2 Laplace Transformation Method

Let $\bar{f}(s)$ and $\bar{v}(s)$ denote the Laplace transforms of $f(t)$ and $v(t)$, respectively. Taking the Laplace transform of Eq. (3.1) and using Eq. (2.6), we obtain

$$\bar{v}(s) = \frac{\bar{f}(s)}{m\,s^2 + c\,s^q + k} \tag{3.3}$$

The response is evaluated by the following complex inversion integral (numerically in general):

$$v(t) = \frac{1}{2\pi i}\int_{a-i\infty}^{a+i\infty} \bar{v}(s)\,exp(st)\,ds \quad \text{for some } a \tag{3.4}$$

3.3 Fourier Transformation Method

Let $F(\omega)$ and $V(\omega)$ denote the Fourier transforms of $f(t)$ and $v(t)$, respectively. Taking the Fourier transform of Eq. (3.1) and using Eq. (2.10), we obtain

$$V(\omega) = \frac{F(\omega)}{-m\,\omega^2 + c\,(i\omega)^q + k} \tag{3.5}$$

In this approach, assumption (3.2) is not necessary so long as ${}_0D_t^q$ is replaced by ${}_{-\infty}D_t^q$ in Eq. (3.1). The response is evaluated by the inverse Fourier transformation as follows:

$$v(t) = \frac{1}{2\pi}\int_{-\infty}^{\infty} V(\omega)\,exp(i\omega t)\,d\omega \tag{3.6}$$

For numerical computation, the discrete Fourier transform would be used instead of the continuous Fourier transform. An efficient numerical algorithm known as the Fast Fourier Transform (FFT) algorithm can be used for this purpose.

3.4 Numerical Scheme in Time Domain

To facilitate the incorporation of nonlinearity, such as reduced stiffness due to the

amplitude effect, in later works, Eq. (3.1) is preferably solved in time domain, rather than Fourier or Laplace domains. A numerical step-by-step solution technique has to be developed to compute the response of the base isolated structure subjected to an arbitrary ground motion.

The acceleration can be approximated by a central difference as follows:

$$\ddot{v}(t) = \frac{1}{h^2} [\, v(t+h) - 2v(t) + v(t-h) \,] + O(h^2) \tag{3.7}$$

where h is the time step size used in the numerical scheme. Only the truncation error is considered in the error analysis. Let v_n be the numerical solution of $v(t=nh)$ at the n^{th} step. Then the numerical representation of Eq. (3.7) is

$$\ddot{v}_n = \frac{1}{h^2} [\, v_{n+1} - 2v_n + v_{n-1} \,] \tag{3.8}$$

As for $D^q v(t)$, $0 \le q < 1$, we obtain from Eq. (2.1a)

$$D^q v(t) = \frac{1}{\Gamma(1-q)} \frac{d}{dt} \int_0^t \frac{v(\tau)}{(t-\tau)^q} \, d\tau \tag{3.9}$$

An equivalent form of Eq. (3.9) is[5]

$$D^q v(t) = \frac{1}{\Gamma(1-q)} [\, \frac{v(0)}{t^q} + \int_0^t \frac{\dot{v}(\tau)}{(t-\tau)^q} \, d\tau] \tag{3.10}$$

Change of variables in the above integral gives

$$D^q v(t) = \frac{1}{\Gamma(1-q)} [\, \frac{v(0)}{t^q} + \int_0^t \frac{\dot{v}(t-\tau)}{\tau^q} \, d\tau \,] \tag{3.11}$$

Note that the first term and thus the singularity in either Eq. (3.10) or Eq. (3.11) disappear if the system is initially at rest, i.e. $v(0) = 0$. Moreover, the singularity would never occur in the numerical step-by-step scheme since $t=0$ is used as the initial time to determine the responses that follow, rather than a time at which the solution is to be determined. Thus, it is fine to include this term in the numerical scheme.

3.4.1 Linear L1-Algorithm

The integral in Eq. (3.11) at $t = nh$ can be written as

$$I(t=nh) = \int_0^t \frac{\dot{v}(t-\tau)}{\tau^q}\, d\tau = \sum_{j=0}^{n-1} \int_{jh}^{(j+1)h} \frac{\dot{v}(t-\tau)}{\tau^q}\, d\tau \tag{3.12}$$

If $v(t)$ is assumed to be piecewise linear in each subinterval $[jh,(j+1)h]$, we obtain the L1-algorithm.[5] It would be called the linear L1-algorithm here to be distinguished from the quadratic L1-algorithm proposed later. In this algorithm, the velocity term in the subinterval is approximated by

$$\dot{v}(t-\tau) \approx \frac{v_{n-j} - v_{n-j-1}}{h}, \quad jh \le \tau \le (j+1)h \tag{3.13}$$

which is independent of τ in the subinterval.

Integration of Eq. (3.12) in each subinterval leads to

$$I(t=nh) = \frac{1}{(1-q)\,h^q} \sum_{j=0}^{n-1} (v_{n-j} - v_{n-j-1})\,[(j+1)^{1-q} - j^{1-q}] \tag{3.14}$$

Hence the linear L1-algorithm for Eq. (3.11) is

$$D^q v_n = \frac{1}{\Gamma(1-q)} \left\{ \frac{v_0}{t^q} + \frac{1}{(1-q)\,h^q} \sum_{j=0}^{n-1} (v_{n-j} - v_{n-j-1})\,[(j+1)^{1-q} - j^{1-q}] \right\} \tag{3.15}$$

or

$$D^q v_n = \frac{1}{h^q\,\Gamma(2-q)} \left\{ \frac{(1-q)v_0}{n^q} + \sum_{j=0}^{n-1} (v_{n-j} - v_{n-j-1})\,[(j+1)^{1-q} - j^{1-q}] \right\} \tag{3.16}$$

Equation (3.16) can be written in the quadrature form as follows:

$$D^q v_n = \frac{1}{h^q} \sum_{j=0}^{n} w_j v_j, \quad 0 \le q < 1 \tag{3.17}$$

where

$$w_0 = \frac{1}{\Gamma(2-q)} \left[(n-1)^{1-q} - n^{1-q} + (1-q)n^{-q} \right]$$

$$w_n = \frac{1}{\Gamma(2-q)}$$

$$w_{n-j} = \frac{1}{\Gamma(2-q)} \left[(j+1)^{1-q} - 2j^{1-q} + (j-1)^{1-q} \right], \quad 1 \le j \le n-1$$

It is shown in Appendix B that the truncation error introduced in the approximation of $D^q v(t)$ by Eq. (3.17) is *at most* of order h^{1-q} , i.e.

$$D^q v(t) = \frac{1}{h^q} \sum_{j=0}^{n} w_j v_j + O(h^{1-q}) \tag{3.18}$$

Substitution of Eqs. (3.7) and (3.18) into Eq. (3.1) leads to

$$\frac{m}{h^2} (v_{n+1} - 2v_n + v_{n-1}) + \frac{c}{h^q} \sum_{j=0}^{n} w_j v_j + k v_n = f(nh) + O(h^2) + O(h^{1-q}) \tag{3.19}$$

This suggests the following multi-step numerical scheme:

$$\bar{w}_{n+1} \, v_{n+1} = f(nh) - \sum_{j=0}^{n} \bar{w}_j v_j \tag{3.20}$$

where

$$\bar{w}_j = \frac{c}{h^q} w_j \,, \quad 0 \le j \le n-2$$

$$\bar{w}_{n-1} = \frac{m}{h^2} + \frac{c}{h^q} w_{n-1}$$

$$\bar{w}_n = -\frac{2m}{h^2} + \frac{c}{h^q} w_n + k$$

$$\bar{w}_{n+1} = \frac{m}{h^2}$$

The global truncation error can easily be shown as $O(h^{2-q})$. The error becomes close to first order when q is close to one. For this reason, a quadratic L1-algorithm that has accuracy of an order higher than the linear L1-algorithm is proposed in the following section. Furthermore, the assumption of piecewise linearity is, in a strict sense, inconsistent with Eq. (3.7) that requires $v(t=nh)$ be at least twice differentiable.

3.4.2 Quadratic L1-Algorithm

The quadratic L1-algorithm is a refinement of the linear counterpart by assuming that v(t) is piecewise parabolic in two consecutive subintervals, $(j-1)h \le t \le (j+1)h$, for evaluation of the integral in the first subinterval. The ultimate form is the same as Eq. (3.20) except for the different quadrature weights, which are derived in Appendix C. The order of the quadratic L1-algorithm is $3-q$. The question that remains is the stability of these two numerical

algorithms. This will be discussed later .

3.4.3 Shifted L1-Algorithms

The implementation of either linear or quadratic L1-algorithm in the form of Eq. (3.20) is not convenient since $n = t/h$ grows and becomes very large as t increases. To reduce the number of terms required in the quadrature formula, we approximate ${}_0D_t^q v(t)$ by ${}_sD_t^q v(t)$, where s is the shifted lower limit of the fractional derivative. Let $s = t - t_w$; t_w is a fixed 'time window' , only inside which the influence of the response history on the current response is to be included. See Fig. 3.2 .

If $t = nh$, $t_w = Nh$, Eq. (3.17) is approximated by

$$ {}_sD_t^q v_n = \frac{1}{h^q} \sum_{j=0}^{N} w_j \, v_{n-N+j} , \qquad 0 \le q < 1 \tag{3.21} $$

in which the quadrature weights still remain unchanged. The modified L1-algorithm with shifted derivative could be called the 'shifted' L1-algorithm.

For $s \le 0$, Eqs. (3.17) and (3.21) are equivalent since $v(t) = 0$, $t<0$. For $s>0$, the difference is

$$ \begin{aligned} \Delta &\equiv {}_0D_t^q v(t) - {}_sD_t^q v(t) \\ &= \frac{1}{\Gamma(1-q)} \left[\frac{v(0)}{t^q} - \frac{v(s)}{(t-s)^q} + \int_0^s \frac{\dot{v}(t-\tau)}{\tau^q} \, d\tau \right] \end{aligned} \tag{3.22} $$

Integration of Eq. (3.22) by part gives

$$ \Delta = -\frac{q}{\Gamma(1-q)} \int_0^s \frac{v(\tau)}{(t-\tau)^{1+q}} \, d\tau \tag{3.23} $$

or

$$ \Delta = -\frac{q}{\Gamma(1-q)} \int_{t_w}^{t} \frac{v(t-\tau)}{\tau^{1+q}} \, d\tau \tag{3.24} $$

Hence, a bound for the difference can be obtained as follows:

$$ |\Delta| \le \frac{q}{\Gamma(1-q)} \max_{0 \le t \le s} |v(t)| \; \left| \int_{t_w}^{t} \frac{1}{\tau^{1+q}} \, d\tau \right| $$

$$= \frac{1}{\Gamma(1-q)} \max_{0 \le t \le s} | v(t) | \left[\frac{1}{t_w^q} - \frac{1}{t^q} \right] \tag{3.25}$$

For $q=0$ and $q=1$, inequality (3.19) gives a zero bound, which is consistent with the fact that the zeroth and first derivatives are invariant with the time shift.

A larger bound is given by

$$| \Delta | \le \frac{1}{\Gamma(1-q)} \max_{0 \le t \le s} | v(t) | \frac{1}{t_w^q} \tag{3.26}$$

Note that $1/\Gamma(1-q)$ is between 0 and 1 for $0 \le q < 1$. We should then try to make $t_w \ge 1$ to keep this bound as small as possible. This gives us a crude guide line that $N \ge 1/h$. The last inequality is a rather pessimistic bound. The integrand in Eq. (3.23) tends to cancel out since the seismic response $v(t)$ is usually oscillatory with almost zero-mean. As such, we would expect the actual difference be much smaller than this bound. Both linear and quadratic versions of shifted L1-algorithm will be checked by considering some forcing functions for which the alternative solutions can be obtained by Laplace or Fourier transformation methods.

3.4.4 Stability of L1-Algorithms

If the damping term is neglected, the numerical scheme is essentially a central difference method. Equation (3.22) can be alternatively put in the following form:

$$\begin{Bmatrix} v_{n+1} \\ v_n \end{Bmatrix} = \mathbf{A} \begin{Bmatrix} v_n \\ v_{n-1} \end{Bmatrix} + \begin{Bmatrix} 1 \\ 0 \end{Bmatrix} f(nh) h^2/m \tag{3.27}$$

where

$$\mathbf{A} = \begin{bmatrix} 2-\omega^2 h^2 & -1 \\ 1 & 0 \end{bmatrix} \quad ; \quad \omega^2 = k/m$$

For stability, the absolute value of the eigenvalues of **A** must be smaller or equal to one. Thus,

$$h \le T/\pi \tag{3.28}$$

This would be an approximate stability criterion if we include the damping term, which is

usually small. Nevertheless, the time step should be considerably smaller than T/π so as to discretize the vibration response with reasonable accuracy. In general, $h \leq T/10$ is a good rule of thumb, and thus the stability is not a problem in practice.

3.5 Numerical Examples

The response of a SDOF fractional oscillator due to the following excitations are studied by implementing the shifted L1-algorithms:

(1) Unit impulse function, $\delta(t)$.

(2) Unit step function, $h(t)$.

(3) Sinusoidal function, $\sin \bar{\omega} t$ where $\bar{\omega}$ is the forcing frequency.

(4) El Centro Earthquake ground motion, May 18, 1940 (NS component).

For comparison, Laplace and Fourier methods are used to obtain the transient and the steady-state solutions, respectively, whereas the Fast Fourier Transform technique is employed in the case of earthquake excitation. The following two systems are considered:

(a) $m = 1 , k = 1 , c = 0.1 , q = 0.5$

(b) $m = 1 , k = 10 , c = 3 , q = 0.13$

System (a) has q=0.5 that permits us to obtain analytical solutions for excitations (1)-(3) by the Laplace transformation method (Appendix D). System (b) has dynamic properties similar to those of the lightly vulcanized natural rubber discussed in Sect. 2.5 . The static stiffness k=10 gives a natural period of about 2 seconds, a typical characteristic period of rubber bearings used in base isolation .

3.5.1 Impulsive Excitation

The equation of motion is

$$(mD^2 + cD^q + k) v(t) = \delta(t) \tag{3.29}$$

Integrating from $t = 0^-$ to $t = 0^+$, we have

$$m\,(\dot{v}(0^+) - \dot{v}(0^-)) + c\int_{0^-}^{0^+} D^q v(t)\,dt + k\int_{0^-}^{0^+} v(t)\,dt = 1 \tag{3.30}$$

Assuming the system is at rest before the excitation, we have $\dot{v}(0^-) = 0$. The second integral is zero too since the displacement $v(t)$ should be a continuous function. This further implies that $\dot{v}(t)$ cannot be an impulse-like function; neither can $D^q v(t)$ be one by Eq. (3.10) . Thus $\int_{0^-}^{0^+} D^q v(t)\,dt = 0$. Equation (3.30) becomes

$$\dot{v}(0^+) = \frac{1}{m} \tag{3.31}$$

The initial velocity is used to determine v_1 in the numerical scheme, simply by

$$v_1 = h\,\dot{v}(0^+) \tag{3.32}$$

We consider system (a) here for the reason mentioned earlier. Based on the static stiffness, the natural period (T) is 2π seconds. The common rule of thumb for the step size in numerical time domain solutions is $h \le 0.1T$ which is about 0.6 second here. For the first trial, we take $h = 0.5\ s$ and $N = 4$, thus $t_w = 2\ s$. Figures 3.3 and 3.4 show the numerical solutions obtained by the linear and quadratic L1-algorithms, respectively. Both solutions are fairly good as compared to the 'exact' solution obtained by the Laplace method, the quadratic solution being slightly better than the linear solution. If N is changed to 50 so that the time window is greatly increased to $t_w = 25\ s.$, the solutions are not improved though (Fig. 3.5) . This implies that the main error source is the coarseness of time step, rather than the width of time window. With a smaller time step, $h = 0.4\ s.$ and $N = 5$, we get somewhat improved results (Figs. 3.6 and 3.7) . The quadratic solution is again slightly better than the linear solution. Finally, using a smaller time step, $h = 0.2\ s.$, we obtain very good solutions by both algorithms (Fig. 3.8) .

3.5.2 Step Excitation

The essential difference between the responses in this case and in the previous case is that, the system now oscillates about a non-zero mean position. The numerical shifted

solutions are not as good as in the previous case, as expected from the discussion in Sect. 3.4.3 . Otherwise, the observations made from the numerical results are similar to those in the previous section. The same parameters are considered and the results are presented in Figs. 3.9-3.13 for different values of h and N .

3.5.3 Sinusoidal Excitation

The forcing function is $\sin\bar{\omega}t$, $t>0$. The transient solution as well as the steady-state solution are studied here, by comparing the results with the Laplace and Fourier solutions. We take $h = 0.5\ s.$, $N = 4$ as before for the first trial, and $\bar{\omega} = 1$ for resonance. The transient solutions are good, as shown in Fig. 3.14 , whereas the steady-state solutions in Fig. 3.15 show some discrepancy in the amplitude of vibration. Once again, the quadratic solution is slightly better than the linear solution. With $h = 0.4\ s.$, $N = 5$, the solutions are improved significantly (Figs. 3.16 and 3.17) . In particular, the quadratic solution is almost exact in this case. No instability is observed at all as time marches on to even $t = 100$.

3.5.4 Earthquake Excitation

The first 20-second ground acceleration of El Centro 1940 Earthquake (NS component) is taken as the ground excitation to system (b) that simulates a base isolation system of $T \approx 2\ s.$ First, the FFT technique is employed to obtain a solution for comparison. The input signal is sampled at every 0.04 s. ; this means that the frequency content is captured up to about 12.5 Hz. Then, the linear L1-algorithm with the same time step, i.e. $h = 0.04\ s.$, is used. With such a small time step, the linear algorithm is little different from the quadratic algorithm. We take $N = 25$ to make $t_w = 1\ s.$ As shown in Fig. 3.18 , the multi-step solution is found to be in good agreement with the FFT solution. With $N = 40$ so that t_w is increased to 1.6 s., we obtain almost perfect agreement (Fig. 3.19) .

The number of floating point operations (flop) in these two approaches are comparable. (An addition and a multiplication is counted as one flop.) The effort in computing the FFT of a function discretized at 2^p points is $2^{p+1}p$ flop. When using the FFT algorithm for a non-

periodic function, a trailing zero-excitation with a duration equal or longer than the duration of the input time history is usually added to its tail. This is to ensure that the initial response is not affected by the response near the end of actual excitation. In the example, the 'period' of total excitation is taken to be 40.96 s. With $h = 0.04\ s.$, p is 10 . Thus the computation of the response by inverse FFT alone requires 20,480 flop. In the shifted L1-algorithm with $t_w = Nh$, we need N flop to compute the response at each time. The total number of flop is thus Nt/h . For $t = 20\ s.$ and $h = 0.04\ s.$, the computation takes 12,500 flop if $N = 25$, and 20,000 flop if $N = 40$. Therefore, the seemingly tedious multi-step L1-algorithm is actually at least as efficient as the FFT approach.

3.6 Response of System with Non-zero Initial Displacement

The solution procedures discussed so far are applicable to systems that are assumed to be at rest before $t=0$. Now suppose a system has a non-zero displacement $v(t) = v_0$ for $t \le 0$. In this case, we use ${}_{-\infty}D_t^q$ in place of D^q $(\equiv {}_0D_t^q)$. Let $v^*(t) = v(t) - v_0$ .The equation of motion becomes

$$m\,\ddot{v}^*(t) + c\,{}_{-\infty}D_t^q v^*(t) + c\,{}_{-\infty}D_t^q v_0 + k\,v^*(t) + k\,v_0 = f(t) \tag{3.33}$$

The general form of Eq. (3.10) for arbitrary a is

$${}_aD_t^q v(t) = \frac{1}{\Gamma(1-q)}\left[\frac{v(a)}{(t-a)^q} + \int_a^t \frac{\dot{v}(\tau)}{(t-\tau)^q}\,d\tau\right] \tag{3.34}$$

which, for $a = -\infty$ and $v(t) = v_0$, leads to ${}_{-\infty}D_t^q v_0 = 0$. Also, note that ${}_{-\infty}D_t^q v^*(t) = {}_0D_t^q v^*(t)$ since $v^*(t) = 0$ for $t \le 0$. The equation to be solved thus reduces to one with zero response history prior to $t=0$:

$$m\ddot{v}^*(t) + cD^q v^*(t) + kv^*(t) = f(t) - kv_0 \tag{3.35}$$

This equation can then be dealt with by the solution procedures developed before.

CHAPTER 4
CORRELATION OF FRACTIONAL DERIVATIVE MODELING WITH SHAKING TABLE TEST RESULTS

4.1 Experimental Program

An extensive series of shaking table tests of base-isolated bridge deck superstructures has recently been carried out at the Earthquake Simulator Laboratory of the Earthquake Engineering Research Center of UCB. In the tests a one-half scale model of a bridge deck was mounted on multilayer natural rubber bearings. The bridge deck model was loaded by additional lead weights to increase the inertia to achieve dynamic similitude such that the stress and acceleration are the same in the model and the prototype. The total weight of the model was about 100 kips (45 tonnes). The input earthquake signal is subjected to a time compression by a factor equal to the square root of the scale factor. A cross-section of the bridge deck model on bearings is shown in Fig. 4.1. The bearings are mounted on load cells to allow continuous monitoring of shear forces. A side elevation of the model is shown in Fig. 4.2.

Rubber Bearings

The rubber bearings used in the test are shown in plan and cross-section in Fig. 4.3. They have fourteen layers of 3/8 in. (9.5 mm) -thick rubber and thirteen 1/8 in. (3.2 mm) steel reinforcing plates. At each end there is a 1/2 in. (12.7 mm) -thick steel plate with holes for dowels which key the bearings to the load cells below and the bridge deck above. The formulation from which the bearings were made was developed by the Malaysian Rubber Producers' Research Association (MRPRA). To develop the frequency characteristics for the bridge deck, it was necessary to select a fairly soft rubber and that chosen was MRPRA EDS 39^{36} with a nominal shear modulus at 50% strain of 100 psi (0.70 Mpa) and an IRHD of 55. The rubber as compounded by the manufacturer had a hardness of 50 and a 50% shear modulus of 105 psi (0.73 Mpa), and a minimum elongation at break of 550%.

Shaking Table

The shaking table is a 20ft x 20ft x 1ft (6.1m x 6.1m x 0.3m) prestressed concrete slab, driven independently in the vertical direction by servo-controlled actuators. The 100 kip (45 tonnes) dead weight of the table, plus the weight of the model, is supported by differential air pressure during operation, thus relieving the vertical actuators of any static load-carrying function. The table is displacement controlled. A digitized record of a particular earthquake history is converted to analogue form, using a digital to analogue converter, and integrated twice, using an analogue integrator. The amplitude scaling of the displacement record during a test is controlled by a span setting. A horizontal span of 1000 will generate a displacement time history with the maximum displacement of 5 in. (12.7 cm), while lower span numbers reduce the maximum table displacement in proportion.

Data Acquisition

The data acquisition system, centered around a NOVA 1200 minicomputer equipped with a Daiblo 31 magnetic disc unit, is capable of discretely sampling up to 128 channels at rates of up to 100 samples/sec./channel. Transducer signals, in analog form, pass through a NEFF system 620 analog-digital processor. The digitized data are them temporarily stored on a magnetic disc before being transferred to a magnetic tape for permanent storage.

4.2 Harmonic Tests

Among a large number of different types of dynamic test, one test series involved steady state harmonic tests at fixed shaking table displacement over a range of frequency from 0.2 Hz to 2.8 Hz. The bridge deck at these frequencies acts as a rigid mass and the total system can be idealized as a single-degree-of-freedom system if the torsional and lateral vibrations are not significantly excited.

In these steady state harmonic tests, the table displacement was set at 0.35 inch. and the table frequency varied in steps from 0.2 Hz to 2.8 Hz. The relative displacement of the model with respect to table was measured after a steady state had been achieved. The

amplification factor defined as peak relative displacement of model divided by peak displacement of table is the quantity of most interest and the results are shown in Table 4.1.

4.2.1 Amplification Factor for Various Mathematical Models (Linear)

It can be derived from Eq. (3.1) that the amplification factor (A) for a fractional oscillator system (or fractional derivative model) is given by

$$A = \frac{\beta^2}{[(1-\beta^2+2\xi\beta^q\cos\frac{\pi q}{2})^2+(2\xi\beta^q\sin\frac{\pi q}{2})^2]^{1/2}} \tag{4.1}$$

where

$\beta = \frac{\bar{\omega}}{\omega_0}$ is the frequency ratio ;

$\xi = \frac{c}{2m\,\omega_0^{2-q}}$ is the damping ratio

in which

$\bar{\omega}$ is the forcing frequency of input motion (rad./s) and

$\omega_0 = \sqrt{k/m}$ is the undamped natural frequency of the system.

When $q = 1$, Eq. (4.1) reduces to

$$A = \frac{\beta^2}{[(1-\beta^2)^2+(2\xi\beta)^2]^{1/2}} \tag{4.2}$$

for a conventional SDOF oscillator.

If we use hysteretic damping in place of viscous damping by substituting $(k+ic)$ for $(k+ic\omega)$ in frequency domain representation of the model, the amplification factor for the hysteretic model is then given by

$$A = \frac{\beta^2}{[(1-\beta^2)^2+(2\xi)^2]^{1/2}} \tag{4.3}$$

where $\xi = \frac{c}{2m}$.

4.2.2 Correlation of Experimental Results with Mathematical Models

To fit the experimental data for amplification factor shown in Table 4.1, the abovementioned three models, namely, the fractional derivative model, the linear viscous model and

the hysteretic model are considered here. Since the damping of the rubber bearing (lightly filled only) for the test is small, the peak of the amplification factor curve would occur approximately at the undamped natural frequency. Hence ω_0 is chosen to be 1.4π rad./s (0.7 Hz), thereby reducing the number of parameters to be determined in each of the models by one. The parameters obtained for the best fit in least-square sense are as follows:

(1) ξ = 5.78% , q = 0.7 for fractional derivative model;

(2) ξ = 5.84% for linear viscous model;

(3) ξ = 5.85% for hysteretic model.

The least-square curves in these three cases are compared with the experimental data in Figs. 4.4 , 4.5 and 4.6, respectively. It is clear by comparing these figures that the FDM gives a much better fit than the other two models, which give least-square curves very similar to each other. It should be noted that though the rubber used is lightly filled, it still has some significant nonlinearity; in particular, the stiffness is strain-dependent. Thus, while the FDM can accommodate the peculiar frequency sensitivity of rubber, it cannot, being linear in the context, account for nonlinearity in the shear modulus of rubber and therefore the stiffness of the system.

4.3 Earthquake Simulator Tests

Another shaking table test series involved the study of seismic response of the base-isolated bridge deck. The following six earthquake records with indicated span setting (H) were used as the input signals to shaking table:

(1) El Centro 1940 S00E component (H = 100* , 200* , 400* , 750) ;

(2) Taft 1952 S69E component (H = 750) ;

(3) Parkfield 1966 N65E component (H = 150* , 750) ;

(4) Pacoima Dam 1971 S14W component (H = 750) ;

(5) Cal Tech A artificial record (H = 750) ;

(6) Caltrans artificial record (H = 300* , 400*) .

The symbol * indicates that the signal is in real time (unscaled), whereas the signals without * are in scaled time (compressed by $\sqrt{2}$). The model is treated as full scale in the former case and half scale in the latter case. The acceleration time histories of some of these records and their Fourier spectra are shown in Figs. 4.7-4.10.

4.3.1 Description of Earthquake Inputs

The El Centro 1940 record is a moderately long, extremely irregular motion. The peak acceleration (0.33g) occurred very near the start of the earthquake and other fairly large accelerations occur later in the record after around 12 seconds and 26 seconds. The Taft 1952 record is also moderately long , around 20 seconds, has low peak acceleration and is very characteristic of California earthquakes. The Parkfield 1966 signal comes from a relatively small earthquake. The peak acceleration was above 0.5g but the strong motion lasted only 1.5 seconds. The Pacoima Dam signal differs from the others by having a few high-frequency peak acceleration pulses in the record.

The artificial records used in the tests were the Cal Tech A and Caltrans signals. Cal Tech signal is a long duration record with large displacements and low accelerations but a wide frequency range. Caltrans signal is an accelerogram modified from the El Centro 1940 earthquake signal to be compatible with the Caltrans design spectrum.[37]

4.3.2 Linear Models

First, the linear fractional derivative and linear viscous SDOF models with the parameters determined in Section 4.2.2 are used. The relative displacements of these models can be computed using the numerical L1-algorithm discussed in Chapter 3. (h = 0.05 sec.; N = 40 and 2 for fractional derivative and viscous models, respectively.) The computed responses for both models when subjected to the El Centro earthquake (H=100) are compared with the experimental response in Figs. 4.11 and 4.12. It can be seen that both models can fit the data very well. Nevertheless, the linear FDM gives a better fit than the linear viscous model. The

errors in the maximum positive and maximum negative peaks for the linear FDM are only 0.9% and 0.8% respectively, whereas they are 4.7% and 5.7% for the linear viscous model. For the other five tests, however, both of these linear models do not correlate well with the experimental results. See for example Figs. 4.13 and 4.14 in the case of El Centro earthquake, H=400. This is because the shear displacement of the rubber bearing has exceeded 2 in. and in such cases the nonlinearity, namely the strain-dependency of the shear stiffness of rubber, becomes important. To account for this nonlinear behavior of rubber, it is necessary to develop a nonlinear model and this is discussed in the next section.

4.3.3 Nonlinear Models

It has been found by many researchers that the stiffness of rubber, especially of filled compounds, is strain dependent. Specifically, the shear modulus of rubber is found to often decay exponentially with the strain amplitude. See for examples Ref. 38-40. This is known as the strain effect or amplitude effect of stiffness. In the nonlinear model accounting for such phenomenon, the following empirical stiffness-strain relation is assumed:

$$k = a - b \ln(|\gamma_p|) \tag{4.4}$$

where γ_p is the peak strain, a and b are coefficients to be determined. Note that the stiffness-strain relations found in the literature are usually determined from steady state harmonic tests. In which case the peak strain is simply the magnitude of the harmonic strain. For seismic excitation, there are often many peaks of different magnitudes in the response. It is then not clear how the stiffness of rubber depends on the strain in this transient problem. In search of a simple and yet realistic relation, the following two hypotheses are considered:

(1) γ_p in Eq. (4.4) is the maximum peak strain in the response history.

(2) γ_p is the most recent peak strain.

These two hypotheses are respectively incorporated in the numerical algorithms and tested against the shaking table test results. It is found that the first hypothesis does not lead to good correlation between the experimental and theoretical results, whereas the second

hypothesis does. In both cases, the coefficients are not determined from the harmonic test results. The reason is that the amplification factor is sensitive to slight changes in frequency near resonance where the data points are insufficient for a nonlinear fit and the resolution of frequency is probably not better than 0.02 Hz at these low frequencies. Instead, the coefficients are determined by fitting the overall response time history in two tests (El Centro H=100 and H=400), with ξ and q assumed to be the same as before. The coefficients found in this way are $a = 0.81$ and $b = 0.22$. The nonlinear model with the second hypotheses is found to be in good agreement with the experimental results in general. The comparisons of response time histories for all the eleven runs are presented in Figs. 4.15-4.25. The differences between the experimental and theoretical peak responses range from 0.1% to 15.9% and average about 7.3%. (See Table 2.)

In terms of overall time history of response, this nonlinear model is excellent. In terms of peak response, this model may need improvement, for instance, in the stiffness-strain relation in Eq. (4.4). We should bear in mind that the values of ξ and q were taken to be the same as those found in the harmonic test in order to reduce the number of parameters in the fitting procedure. It is possible that a better fit could have been obtained by adjusting these two parameters, especially in view of the fact that the peak response is sensitive to ξ for low damping. A more rational way (which unfortunately was not done in the experiments) would be to conduct many series of harmonic tests, in each series the relative displacement being controlled at a fixed quantity so as to identify the strain effect independently. It should also be noted that there were inevitably some experimental errors (e.g. measurement and calibration errors), which could also have contributed to the discrepancy between experimental and theoretical results.

CHAPTER 5

DYNAMIC ANALYSIS OF BASE ISOLATED MDOF-STRUCTURE

5.1 Response of 2-DOF System

We first consider a 2 degree-of-freedom (DOF) system, consisting of a single-story shear building mounted on a base deck that is supported by an elastomeric isolation system. The structure is idealized as a SDOF oscillator and the base deck with isolation system as a SDOF fractional oscillator (i.e. q-th derivative model). As shown in Fig. 5.1 , the two degrees of freedom are:

v_0 = displacement of base deck (lumped mass m_0) relative to ground;

v_1 = displacement of structure (lumped mass m_1) relative to base deck.

The equations of motion are

$$m_t \ddot{v}_0(t) + m_1 \ddot{v}_1(t) + c_0 D^q v_0(t) + k_0 v_0(t) = - m_t \ddot{u}_g(t) \tag{5.1}$$

$$m_1 \ddot{v}_0(t) + m_1 \ddot{v}_1(t) + c_1 \dot{v}_1(t) + k_1 v_1(t) = - m_1 \ddot{u}_g(t) \tag{5.2}$$

where

m_t = total mass of base deck and structure (m_0+m_1);

c_0 = damping constant of base isolation system;

k_0 = stiffness constant of base isolation system;

c_1 = damping constant of structure;

k_1 = stiffness constant of structure.

Alternatively ,

$$(D^2 + \bar{c}_0 D^q + \bar{k}_0) v_0 + \gamma_1 D^2 v_1 = - \ddot{u}_g \tag{5.3}$$

$$D^2 v_0 + (D^2 + 2\omega_1 \xi_1 D + \omega_1^2) v_1 = - \ddot{u}_g \tag{5.4}$$

where

$$\bar{k}_0 = k_0/m_t \quad ; \quad \omega_1 = \sqrt{k_1/m_1} \quad ;$$

$$\bar{c}_0 = c_0/m_t \quad ; \quad \xi_1 = c_1/(2m_1\omega_1) \quad ;$$

$$\gamma_1 = m_1/m_t$$

These equations can be solved numerically by employing L1-algorithms for $D^q v_0$ term and central difference scheme for D^2 and D terms.

Numerical Example

As an illustrative example , we consider the following parameters:

$q = 0.13$; $\bar{k}_0 = 10$; $\bar{c}_0 = 3$; $\omega_1 = 2\ Hz$; $\xi_1 = 1\%$; $\gamma_1 = 0.7$.

The excitation is El Centro 1940 earthquake, NS component. The results are plotted in Figs. 5.2 and 5.3 . We can see that the agreement between the L1-solutions and the FFT solutions is very good.

5.2 Response of (N+1)-DOF System

The solution procedure discussed so far can certainly be extended to the analysis of a multi-degree-of-freedom (MDOF) system. However, the solution would be more efficient if we assume that the structure has a proportional damping matrix (e.g. Rayleigh damping matrix).[41] This assumption does not severely affect the accuracy of the solution since the structural damping ratios are small, as compared to the damping in the base isolation system. We can then use mode superposition technique to reduce the number of degrees of freedom as long as the structure is assumed to remain in the linearly elastic range.

Fixed-base Structure

Consider a N-story shear building, having lumped mass m_i , stiffness k_i and damping constant c_i at the i-th floor (Fig. 5.4) . Let us first assume that the structure is fixed-base . Due to an earthquake ground motion, the displacement of i-th floor relative to the ground is v_i and the equations of motion can be written as

$$\mathbf{M}\ddot{\mathbf{v}} + \mathbf{C}\dot{\mathbf{v}} + \mathbf{K}\mathbf{v} = -\mathbf{M}\mathbf{r}\ddot{u}_g \tag{5.5}$$

where $\mathbf{M}$ is the mass matrix, defined as

$$\mathbf{M} = \mathrm{diag}[\, m_1 , m_2 , \cdots , m_N \,] \tag{5.6}$$

C is the damping matrix, defined as

$$\mathbf{C} = \begin{bmatrix} c_1+c_2 & -c_2 & & zeros & \\ -c_2 & c_2+c_3 & -c_3 & & \\ & -c_3 & & & \\ zeros & & & & -c_N \\ & & & -c_N & c_N \end{bmatrix} \tag{5.7}$$

K is the stiffness matrix, defined as

$$\mathbf{K} = \begin{bmatrix} k_1+k_2 & -k_2 & & zeros & \\ -k_2 & k_2+k_3 & -k_3 & & \\ & -k_3 & & & \\ zeros & & & & -k_N \\ & & & -k_N & k_N \end{bmatrix} \tag{5.8}$$

r is the displacement influence vector, defined as

$$\mathbf{r} = [1 \;\; 1 \;\; \cdots \;\; 1]^T \tag{5.9}$$

v is the relative displacement vector, defined as

$$\mathbf{v} = [v_1 \;\; v_2 \;\; \cdots \;\; v_N]^T \tag{5.10}$$

Consider the eigenvalue problem of the undamped system:

$$\mathbf{M}\ddot{\mathbf{v}} + \mathbf{K}\mathbf{v} = \mathbf{0} \tag{5.11}$$

for which the mode shape (eigenvector) is ϕ_i corresponding to the i-th natural frequency ω_i . The mode shapes satisfy the following orthogonality properties:

$$\phi_i^T \mathbf{M} \phi_j = 0 \quad ; \quad \phi_i^T \mathbf{K} \phi_j = 0 \quad \text{for } i \neq j \tag{5.12}$$

By mode superposition method, the displacements can be expressed as

$$\mathbf{v} = \sum_{i=1}^{N} Y_i \phi_i \tag{5.13}$$

where Y_i is the generalized coordinate associated with the i-th vibration mode. As a result of the assumption of proportional damping matrix, Eq. (5.5) reduces to the following uncoupled form:

$$\ddot{Y}_i + 2\xi_i \omega_i \dot{Y}_i + \omega_i^2 Y_i = -L_i \ddot{u}_g \quad \text{for } i = 1,...,N \tag{5.14}$$

where the modal mass, modal frequency, modal damping ratio and modal participation factor are defined respectively as follows:

$$M_i = \phi_i^T \mathbf{M} \phi_i \tag{5.15}$$

$$\omega_i = \left(\frac{\phi_i^T \mathbf{K} \phi_i}{M_i} \right)^{1/2} \tag{5.16}$$

$$\xi_i = \frac{\phi_i^T \mathbf{C} \phi_i}{2 M_i \omega_i} \tag{5.17}$$

$$L_i = \frac{\phi_i^T \mathbf{M} \mathbf{r}}{M_i} \tag{5.18}$$

Base-isolated Structure

The structure is now considered to be supported on a base isolation system. The mathematical model is shown in Fig. 5.5 . The vector $\mathbf{v}$ in this case represents the floor displacements *relative* to the base deck. For this $(N+1)$-DOF system, the equations of motion are

$$m_t \ddot{v}_0 + c_0 D^q v_0 + k_0 v_0 + (\mathbf{r}^T \mathbf{M}) \ddot{\mathbf{v}} = - m_t \ddot{u}_g \tag{5.19}$$

$$\mathbf{M} \mathbf{r} \ddot{v}_0 + \mathbf{M} \ddot{\mathbf{v}} + \mathbf{C} \dot{\mathbf{v}} + \mathbf{K} \mathbf{v} = - \mathbf{M} \mathbf{r} \ddot{u}_g \tag{5.20}$$

where $m_t = \sum_{i=1}^{N} m_i$

If we assume that only the first n modes contribute significantly to the response and higher modes are therefore neglected, the structural response is then approximated by

$$\mathbf{v} = \sum_{i=1}^{n} Y_i \phi_i \tag{5.21}$$

Premultiplying Eqs. (5.19) and (5.20) by ϕ_i^T , and making use of Eqs. (5.21) and (5.15) through (5.18) lead to

$$(D^2 + \bar{c}_0 D^q + \bar{k}_0) v_0 + \sum_{i=1}^{n} \gamma_i D^2 \bar{Y}_i = -\ddot{u}_g \tag{5.22}$$

$$D^2 v_0 + (D^2 + 2\omega_i \xi_i D + \omega_i^2) \bar{Y}_i = -\ddot{u}_g \quad \text{for } i=1,...,n \tag{5.23}$$

where $\gamma_i = L_i^2 M_i / m_t$; $\bar{Y}_i = Y_i / L_i$.

Any nonlinearity of rubber bearings such as the strain effect of shear stiffness can be easily incorporated into Eq. (5.22). These equations are similar to Eqs. (5.3) and (5.4) . Though the equations are still coupled, the computation effort involved in solving for the $n+1$ unknowns is not much increased as compared to the solution of the 2-DOF system discussed earlier. The reason is that, with the assumption of proportional damping matrix for the structure, the numerical scheme at each time step reduces to the following form:

$$\begin{bmatrix} 1 & \boldsymbol{\gamma}^T \\ \mathbf{r} & \mathbf{A} \end{bmatrix} \begin{Bmatrix} v_0 \\ \bar{Y}_1 \\ \bar{Y}_2 \\ \\ \bar{Y}_n \end{Bmatrix} = \begin{Bmatrix} b_0 \\ b_1 \\ b_2 \\ \\ b_n \end{Bmatrix} \tag{5.24}$$

where

$$\boldsymbol{\gamma}^T = [\gamma_1 \ \gamma_2 \ \cdots \ \gamma_n]^T$$
$$\mathbf{A} = \text{diag}[a_1 , a_2 , \cdots , a_n]$$

Since the lower right $n \times n$ submatrix is diagonal, the solution is readily obtained as follows :

$$v_0 = (b_0 - \sum_{i=1}^{n} \frac{b_i \gamma_i}{a_i}) / (1 - \sum_{i=1}^{n} \frac{\gamma_i}{a_i}) \tag{5.25}$$

$$\bar{Y}_i = (b_i - v_0) / a_i \quad \text{for } i = 1,...,n \tag{5.26}$$

CHAPTER 6
CONCLUSIONS

The fractional derivative is a convenient mathematical operator for describing the stress-strain relation of viscoelastic materials. By allowing the order of derivatives in the constitutive relations to be fractional, usually in the range between zero and one, various fractional derivative models can be proposed. Although the fractional derivative is a mathematical representation in time domain, such models have been found by a number of researchers to fit the viscoelastic properties very well in the frequency domain. Its appearance in many fields of physical science suggests that the fractional derivative is not just an abstract or physically meaningless concept; neither is it totally empirical in its application to viscoelastic analysis.

The fractional Kelvin model, in particular, is chosen here in conjunction with a mass term to account for the inertia effect, forming the so called 'fractional oscillator'. The latter is used to model the dynamic behaviors of the rubber bearings used in base isolation systems. This model has the advantages over conventional models that a good fit of material properties, specifically the storage modulus and the loss factor, is obtained by adjusting the additional parameter, which is the order of fractional derivative. In contrast to the use of generalized Kelvin or generalized Maxwell models, the equation of motion remains a second order one.

In this report, a single-degree-of-freedom system is first presented as a simple model for base isolated structures if the structure is approximated as a rigid body supported on base isolation system. For linear systems, the response can be obtained by Laplace or Fourier transformation methods in the same way as in the conventional dynamic analyses with linear viscous or hysteretic damping models. No complication arises due to the use of fractional derivatives since the Laplace and Fourier transforms of fractional derivatives bear the same forms as in the case of derivatives of integral order. Between these two methods, the Fourier approach is preferred for problems with arbitrary excitation because an efficient numerical

algorithm (FFT) is available. Alternatively, one can carry out the step-by-step analysis in the time domain. Shifted linear and quadratic L1-algorithms are developed for the step-by-step integration scheme, which is shown to be consistent and stable under a lenient condition. The number of operations required is found to be comparable to the FFT method. Numerical examples show that the L1-solutions are in good agreement with the Laplace and Fourier solutions. The time domain approach has the advantage that nonlinearity effects can be easily included if necessary.

In the application of fractional derivative model to the shaking table tests of a base-isolated bridge deck which can be very well idealized as a SDOF system, the linear model is first used. To fit the amplification factor curve obtained from the harmonic tests, the linear FDM is found to give a much better fit than the linear viscous or linear hysteretic models. In matching the response time histories during the earthquake simulated tests, however, the linear models are inadequate when the shear strain of rubber is large enough that the strain effect of shear stiffness is important. For this case, a nonlinear FDM is suggested to take into account of the strain effect by assuming an empirical relation between the shear stiffness of rubber bearing and the most recent peak shear strain of rubber. This hypothetical model is found to correlate very well with the results of the shaking table tests in general.

The solution procedures is extended to the dynamic analysis of a multi-degree-of-freedom system, and therefore the effect of higher modes on the response can be studied and included if required. The computation effort can be reduced by making the assumption of a proportional damping matrix for the superstructure.

REFERENCES

1. B. Ross, "A Brief History and Exposition of the Fundamental Theory of Fractional Calculus," in *Lecture Notes in Mathematics*, vol. 457, pp. 1-36, Springer-Verlag, New York, 1975.

2. O. Heaviside, *Electromagnetic Theory*, II, Dover (Reprint), New York, 1950.

3. A. Gemant, "A Method of Analyzing Experimental Results Obtained from Elastoviscous Bodies," *Physics* , vol. 7, pp. 311-317, New York, 1936.

4. A. Gemant, "On Fractional Differentials," *Philosophical Magazine*, vol. 25, pp. 540-549, 1938.

5. K. B. Oldham and J. Spanier, *The Fractional Calculus*, Mathematics and Science and Engineering, 111, Academics Press, New York, 1974.

6. G. W. Scott-Blair and J. E. Caffyn, "An Application of the Theory of Quasi-properties to the Treatment of Anomalous Stress-strain Relations," *Philosophical Magazine*, vol. 40, p. 80, 1949.

7. M. Caputo, "Linear Models of Dissipation whose Q is almost Frequency Independent," *Annali Geofisica*, vol. 19, pp. 383-393, 1966.

8. M. Caputo and F. Minardi, "A New Dissipation Model Based on Memory Mechanism," *Pure & Applied Geophysics*, vol. 91, pp. 134-147, 1971.

9. M. Caputo, "Vibrations of an Infinite Plate with a Frequency Independent Q," *Journal of the Acoustical Society of America*, vol. 60, no. 3, pp. 634-639, Sep. 1976.

10. G. L. Slonimsky, "Laws of Mechanical Relaxation Processes in Polymers," *Journal of Polymer Science : Part C*, no. 16, pp. 1667-1672, 1967.

11. W. Smit and H. de Vries, "Rheological Models containing Fractional Derivatives," *Rheologica Acta*, vol. 9, pp. 525-534, 1970.

12. R. L. Bagley and P. J. Torvik, "Fractional Calculus -- A Different Approach to the Finite Element Analysis of Viscoelastically Damped Structures," *AIAA Journal*, vol. 21, no. 5, pp. 741-748, 1983.

13. R. L. Bagley and P. J. Torvik, "A Generalized Derivative Model for an Elastomer Damper," *Shock and Vibration Bulletin*, vol. 49, part 2, pp. 135-143, Sep. 1979.

14. R. L. Bagley, "Applications of Generalized Derivatives to Viscoelasticity," *Ph.D. Dissertation*, Air Force Institute of Technology, 1979.

15. M. Stiassnie, "On the Application of Fractional Calculus for the Formulation of Viscoelastic Models," *Applied Mathematical Modeling*, vol. 3, no. 4, pp. 300-302, 1979.

16. L. Rogers, "Operators and Fractional Derivatives for Viscoelastic Constitutive Equations," *Journal of Rheology*, vol. 27, no. 4, pp. 351-372, Aug. 1983.

17. R. C. Koeller, "Applications of Fractional Calculus to the Theory of Viscoelasticity," *Journal of Applied Mechanics*, vol. 51, no. 2, pp. 299-307, June 1984.

18. Y. N. Rabotnov, *Elements of Hereditary Solid Mechanics*, Mir Publishers, Moscow, 1980.

19. J. D. Ferry, *Viscoelastic Properties of Polymers*, p. 54, John Wiley & Sons, New York, 1961.

20. P. J. Torvik and R. L. Bagley, "On the Appearance of the Fractional Derivatives in the Behavior of Real Materials," *Journal of Applied Mechanics*, vol. 51, pp. 294-298, June 1984.

21. R. L. Bagley and P. J. Torvik, "A theoretical Basis for the Application of Fractional Calculus," *Journal of Rheology*, vol. 27, no. 3, pp. 201-210, June 1983.

22. B. H. Zimm, "Dynamics of Polymer Molecules in Dilute Solution : Viscoelasticity, Flow Birefringence and Dielectric Loss," *Journal of Chemical Physics*, vol. 24, no. 2, pp. 269-278, 1956.

23. P. B. Lindley, "The Stiffness of Rubber Springs," in *Use of Rubber in Engineering*, ed. by P. W. Allen, P. B. Lindley & A. R. Payne, pp. 1-24, Maclaren & Sons, London, 1967.

24. P. McL. Swift and A. A. Watson, "The Fabrication and Compounding of Rubber," in *Use of Rubber in Engineering*, ed. by P. W. Allen, P. B. Lindley & A. R. Payne, pp. 81-91, Maclaren & Sons, London, 1967.

25. A. R. Payne and J. R. Scott, *Engineering Design with Rubber*, p. 3, Interscience Publishers, New York, 1960.

26. P. B. Lindley, "Design and Use of Natural Rubber Bridge Bearings," *Natural Rubber Technology Bulletin*, Malaysian Rubber Producers' Research Association, 1962.

27. D. J. Derham and R. A. Waller, "Luxury Without Rumble," *The Consulting Engineer*, vol. 39, p. 49, 1975.

28. C. J. Derham and A. P. Plunkett, "Fire Resistance of Steel Laminated Natural Rubber Bearings," *Natural Rubber Technology*, vol. 7, p. 29, 1976.

29. J. M. Kelly, "Aseismic Base Isolation," *The Shock and Vibration Digest*, vol. 14, no. 5, pp. 17-25, May 1982.

30. A. R. Payne, "Dynamic Properties of Rubber," in *Use of Rubber in Engineering*, ed. by P. W. Allen, P. B. Lindley & A. R. Payne, pp. 25-40, Maclaren & Sons, London, 1967.

31. S. H. Crandall, "Dynamic Response of Systems with Structural Damping," in *Air , Space and Instruments , Draper Anniversary Volume*, ed. by H. S. Lees, pp. 183-193, McGraw-Hill, New York, 1963.

32. R. W. Clough and J. Penzien, *Dynamics of Structures*, p. 76, McGraw-Hill, New York, 1982.

33. P. L. Butzer and U. Westphal, "An Access to Fractional Differentiation via Fractional Difference Quotients," in *Lecture Notes in Mathematics*, ed. by A. Dold and B. Eckmann, vol. 457, pp. 116-145, Springer-Verlag, New York, 1975.

34. W. Flügge, *Viscoelasticity,* p. 21, Springer-Verlag, New York, 2 ed., 1975.

35. M. Caputo, "Linear Models of Dissipation whose Q is almost Frequency Independent – II," *Geophysical Journal of the Royal Astronomical Society*, vol. 13, no. 5, pp. 529-539, Nov. 1967.

36. *Malaysian Rubber Producers' Research Association, Engineering Data Sheets, EDS 39,* Tun Abdul Razak Laboratory, Kuala Lumpur, 1979.

37. J. H. Gates, "Factors Considered in the Development of California Design Criteria for Bridges," in *Proceedings of Workshop on Earthquake Resistance of Highway Bridges*, pp. 141-162, Applied Technology Council, ATC-6-1, Palo Alto, California, 1979.

38. S. D. Gehman, "Dynamic Properties of Elastomers," *Rubber Chemistry and Technology*, vol. 30, no. 5, pp. 1202-1250, Dec. 1957.

39. A. R. Payne, "The Dynamic Properties of Carbon Black-Loaded Natural Rubber Vulcanizates," *Rubber Chemistry and Technology*, vol. 36, no. 2, pp. 432-443, 1963.

40. J. E. Cole, "The Effects of Frequency, Amplitude, and Load on the Dynamic Properties of Elastomers," *Shock and Vibration Bulletin*, vol. 49, no. 2, pp. 105-117, Sep. 1979.

41. R. W. Clough and J. Penzien, *Dynamics of Structures,* p. 195, McGraw-Hill, New York, 1982.

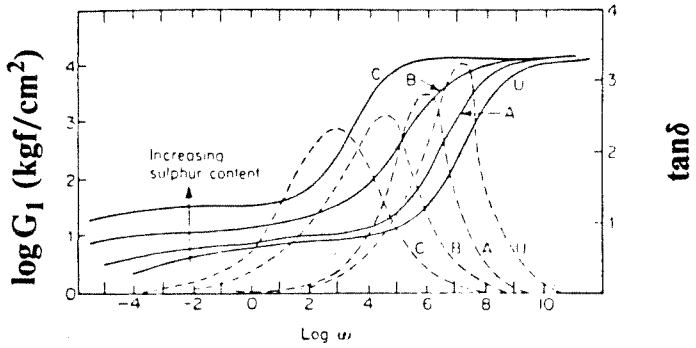

Figure 1.1 Master curves for G_1 (full lines) and $\tan\delta$ (broken lines) for natural rubbers. U: unvulcanized ; A,B,C: 1.5, 3.5, 7.5 pphr sulphur, respectively. Temperature 25° C. (Reference 30)

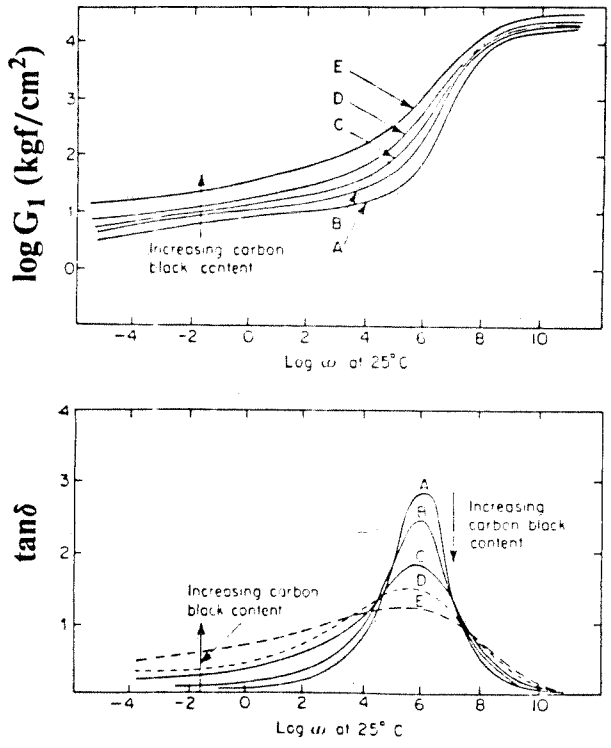

Figure 1.2 Master curves for G_1 (top) and $\tan\delta$ (bottom) for natural rubbers. A: vulcanized with 1.5 pphr sulphur; B-E: 1.5 pphr sulphur + 10,20,30 and 50 pphr HAF black, respectively. 10% shear strain amplitude. Temperature 25° C. (Reference 30)

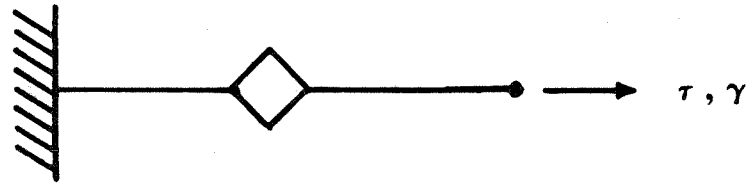

Figure 2.1 Spring-pot element

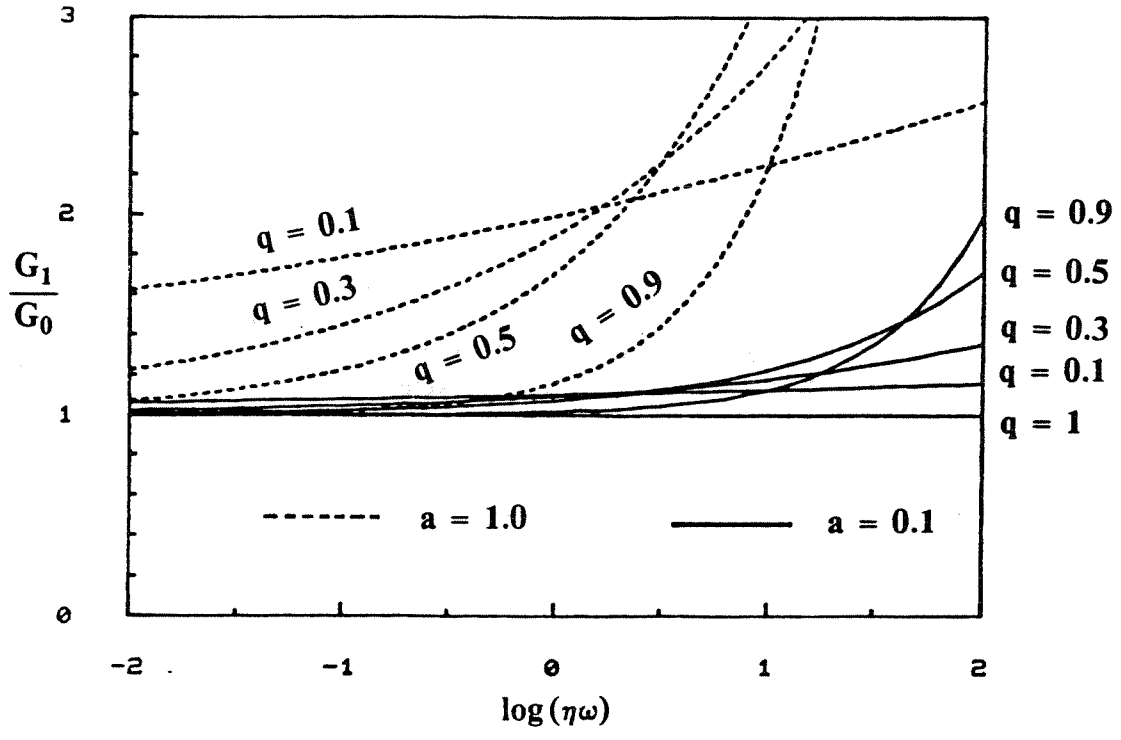

Figure 2.2 Storage modulus curves for FKV model

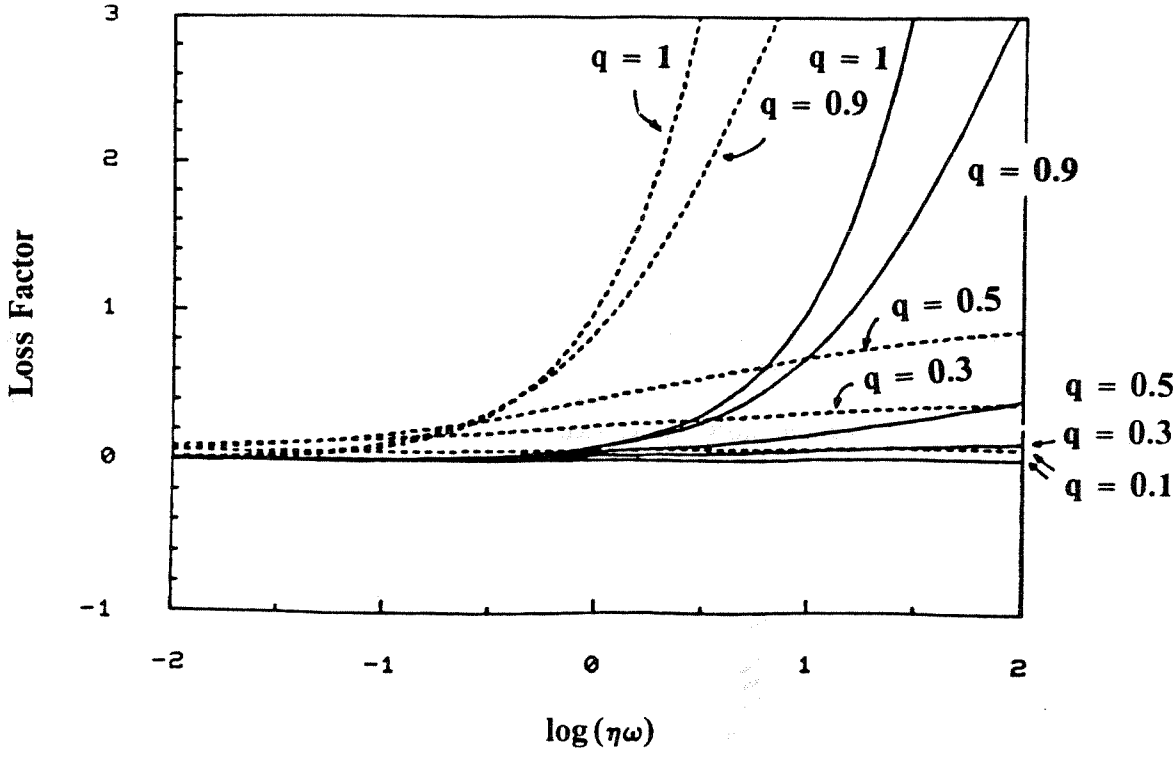

Figure 2.3 Loss factor curves for FKV model

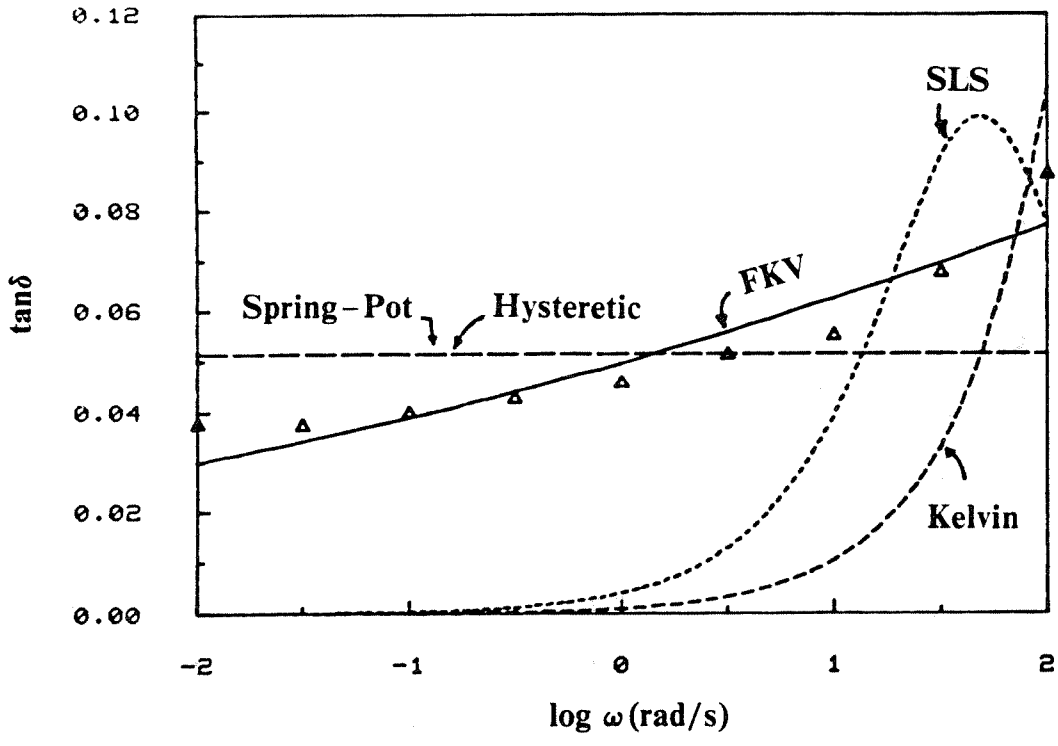

Figure 2.4 Fitting of loss factor curve of lightly vulcanized Hevea rubber by different models.

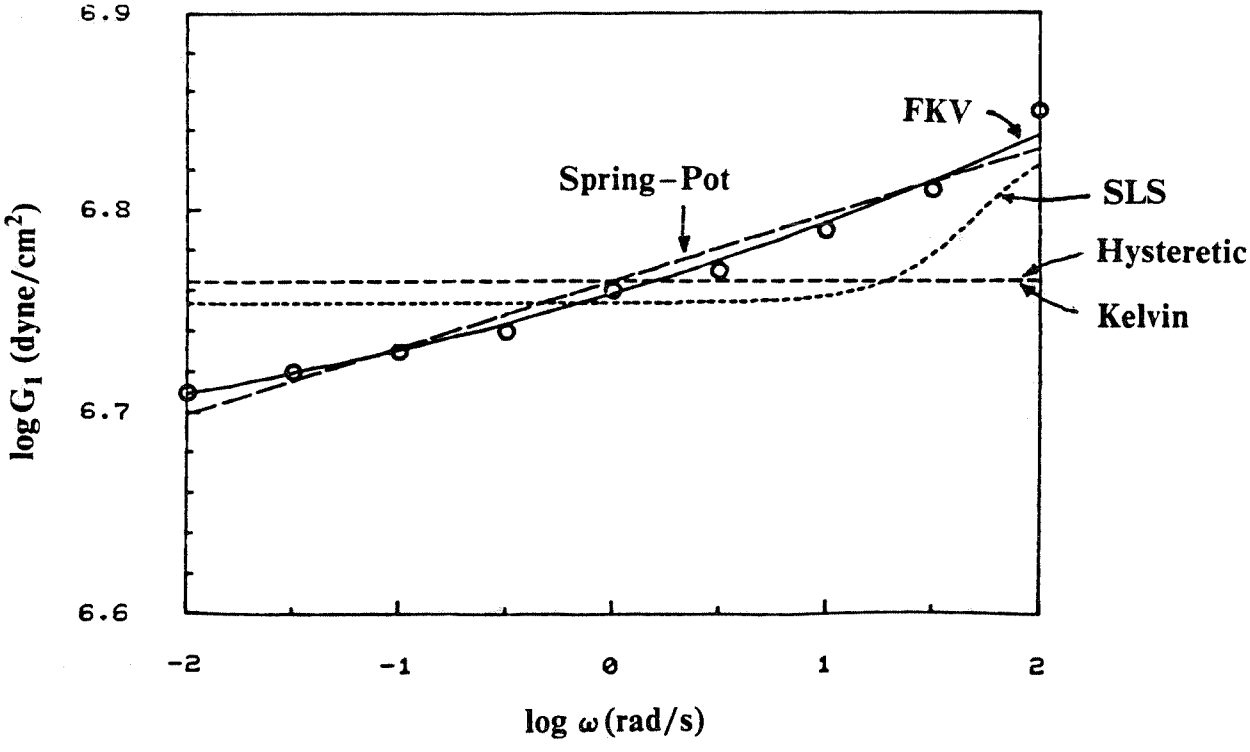

Figure 2.5 Fitting of storage modulus curve of lightly vulcanized Hevea rubber by different models.

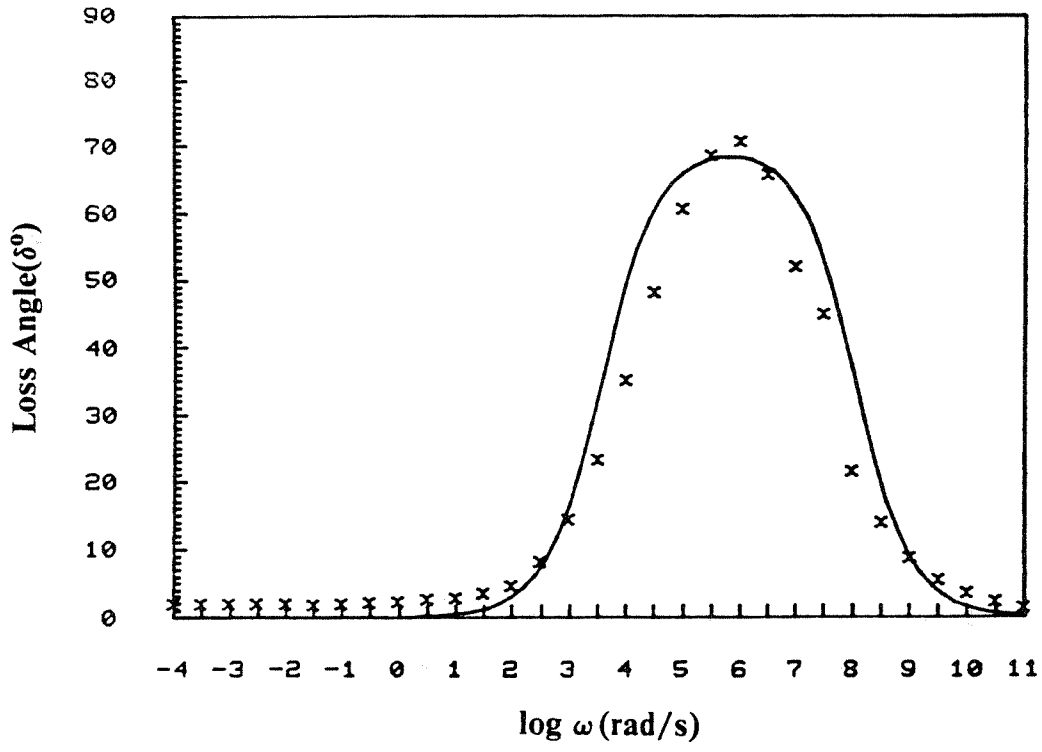

Figure 2.6 Fitting of loss angle curve of Lightly vulcanized Hevea rubber by FSLS model.

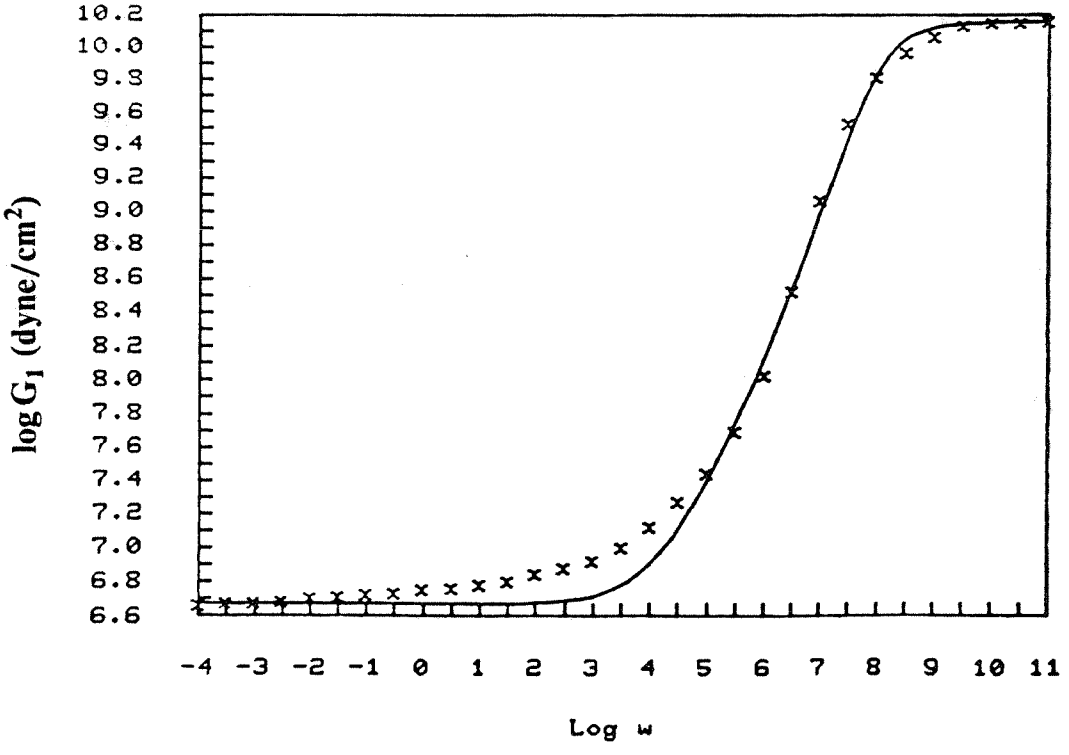

Figure 2.7 Fitting of storage modulus curve of lightly vulcanized Hevea rubber by FSLS model.

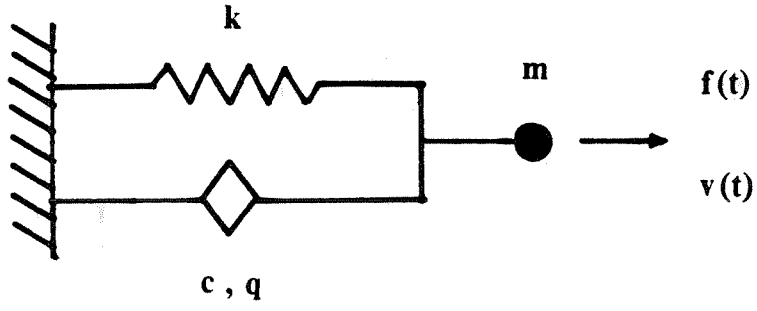

Figure 3.1 SDOF fractional oscillator

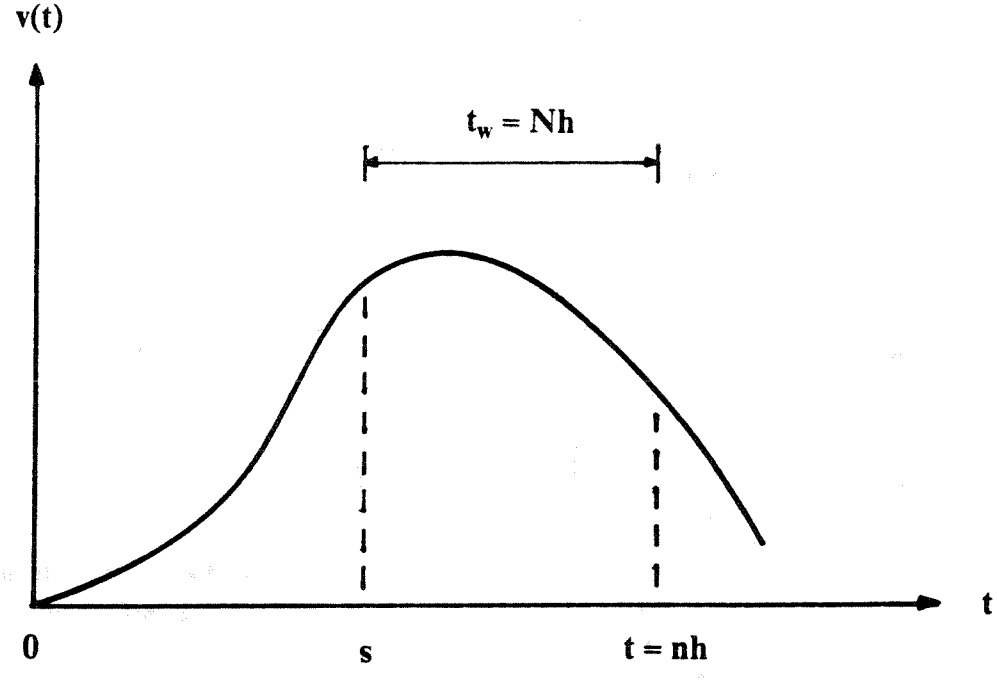

Figure 3.2 Illustration of shifted algorithm

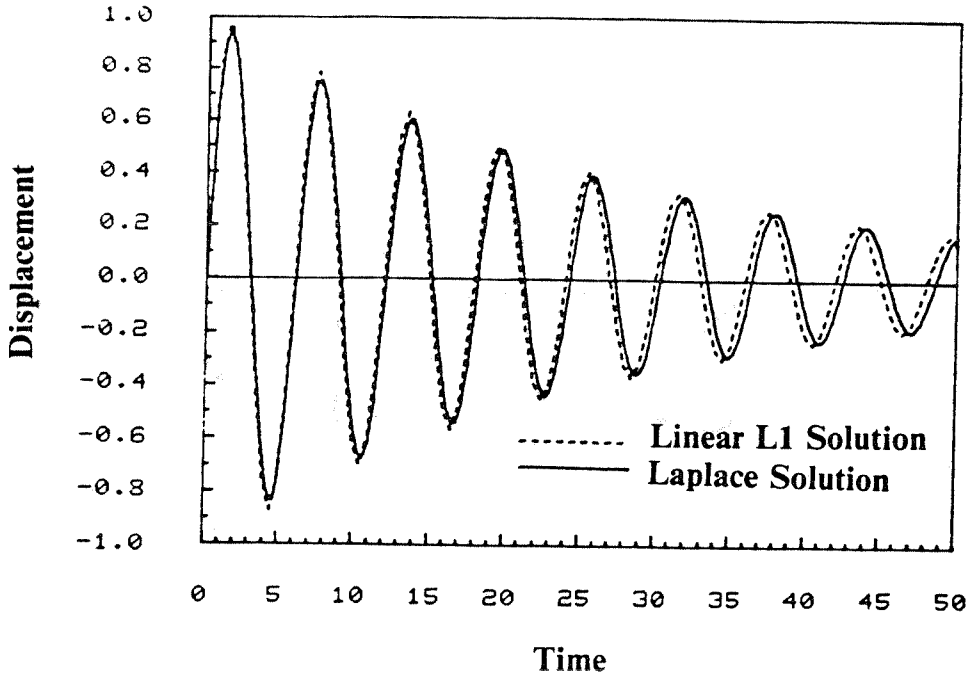

Figure 3.3 Response of SDOF fractional oscillator due to $f(t) = \delta(t)$ ($m = 1$, $k = 1$, $c = 0.1$, $q = 0.5$, $N = 4$, $h = 0.5$)

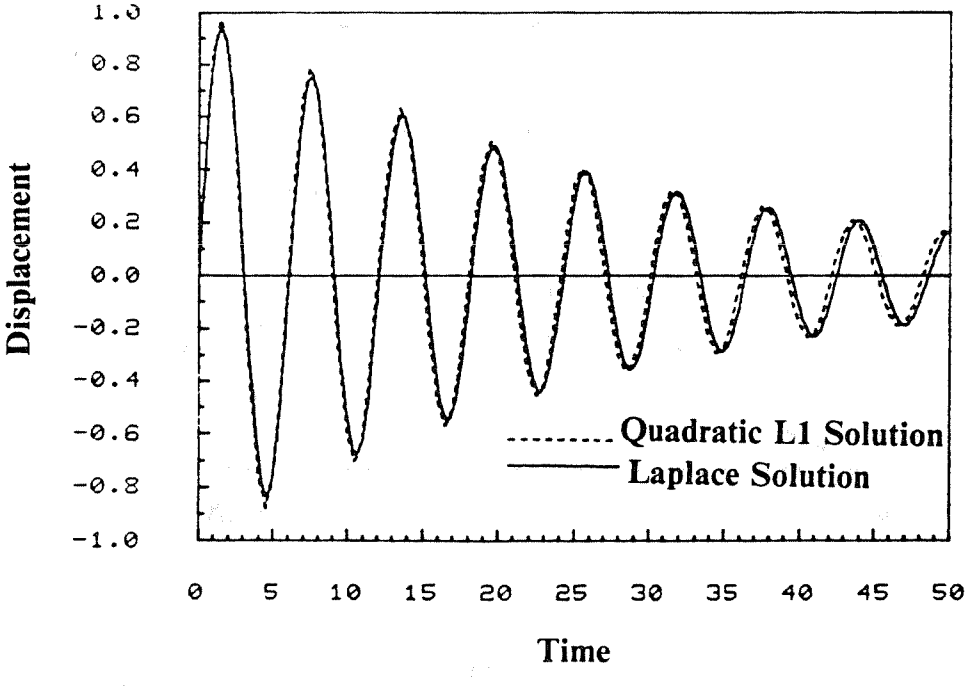

Figure 3.4 Response of SDOF fractional oscillator due to $f(t) = \delta(t)$ ($m = 1$, $k = 1$, $c = 0.1$, $q = 0.5$, $N = 4$, $h = 0.5$)

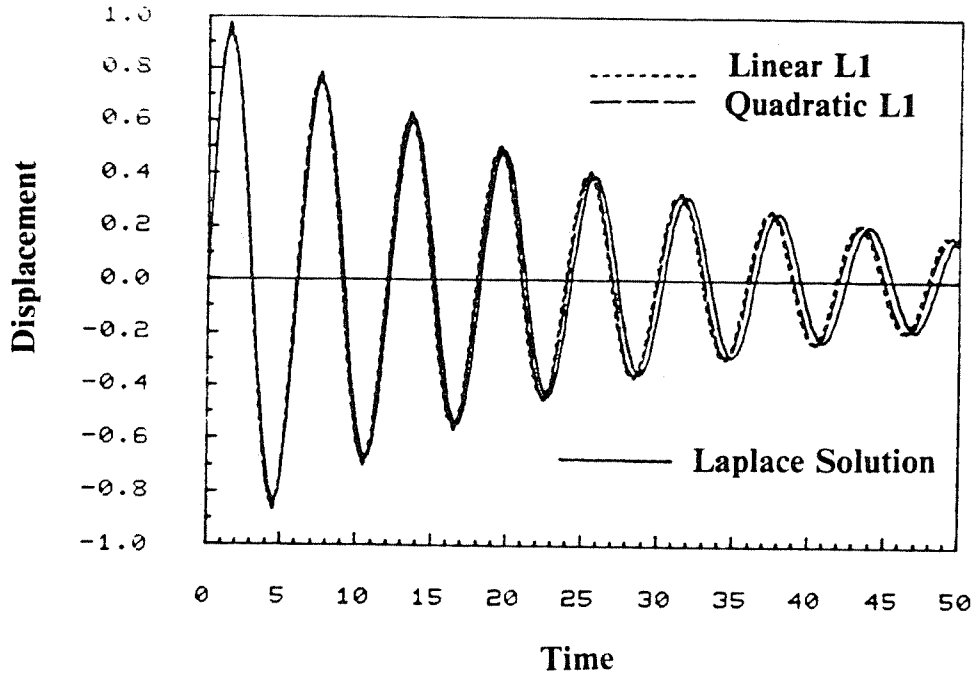

Figure 3.5 Response of SDOF fractional oscillator due to $f(t) = \delta(t)$ ($m = 1$, $k = 1$, $c = 0.1$, $q = 0.5$, $N = 50$, $h = 0.5$)

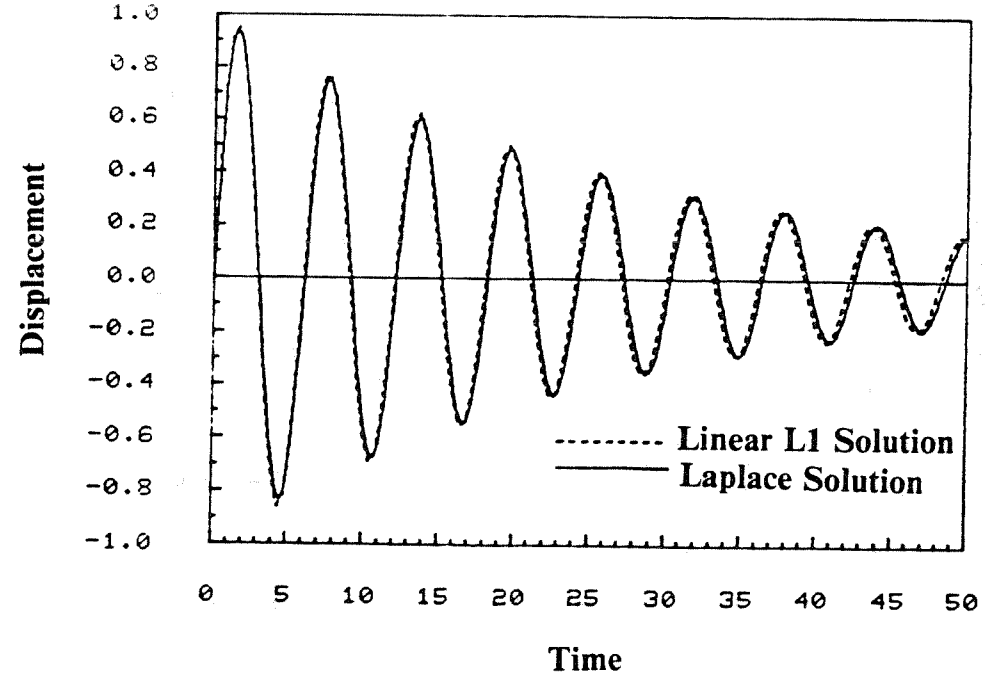

Figure 3.6 Response of SDOF fractional oscillator due to $f(t) = \delta(t)$ ($m = 1$, $k = 1$, $c = 0.1$, $q = 0.5$, $N = 5$, $h = 0.4$)

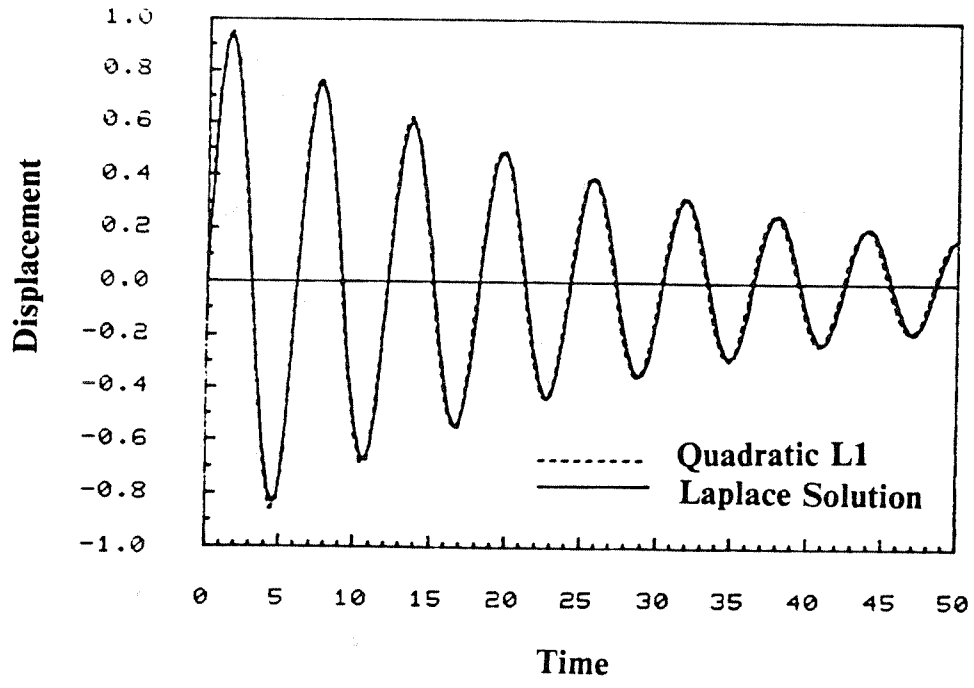

Figure 3.7 Response of SDOF fractional oscillator due to $f(t) = \delta(t)$ ($m = 1$, $k = 1$, $c = 0.1$, $q = 0.5$, $N = 5$, $h = 0.4$)

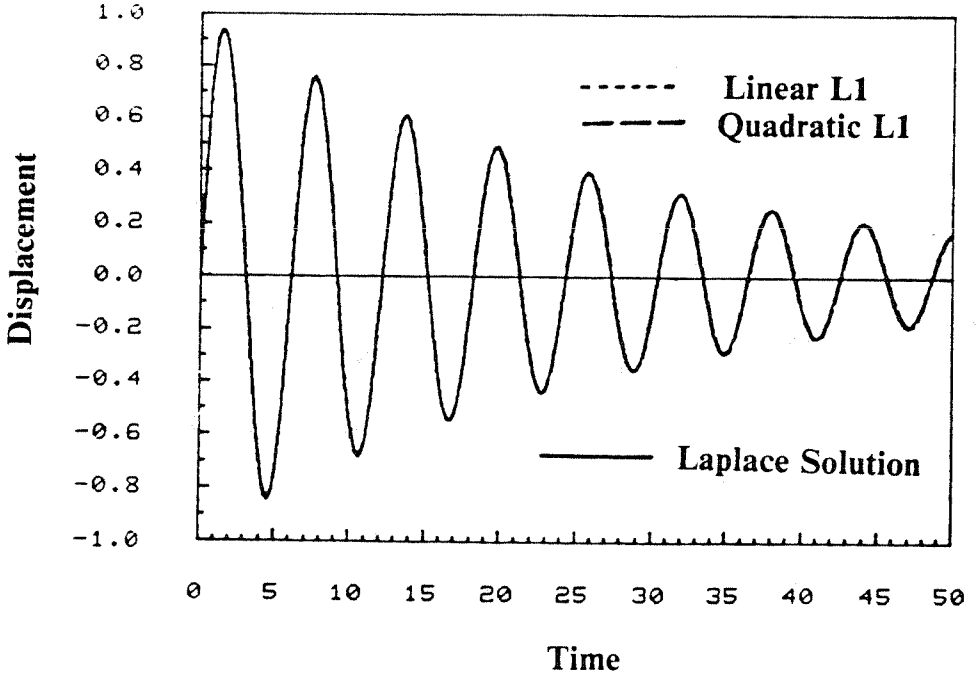

Figure 3.8 Response of SDOF fractional oscillator due to $f(t) = \delta(t)$ ($m = 1$, $k = 1$, $c = 0.1$, $q = 0.5$, $N = 10$, $h = 0.2$)

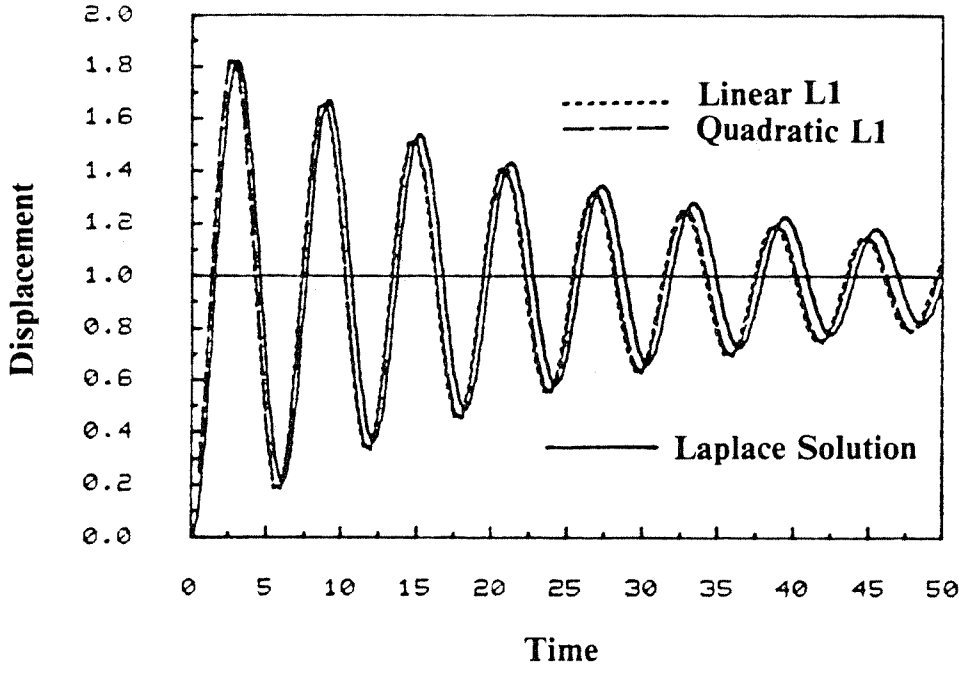

Figure 3.9 Response of SDOF fractional oscillator due to $f(t) = h(t)$ ($m = 1$, $k = 1$, $c = 0.1$, $q = 0.5$, $N = 4$, $h = 0.5$)

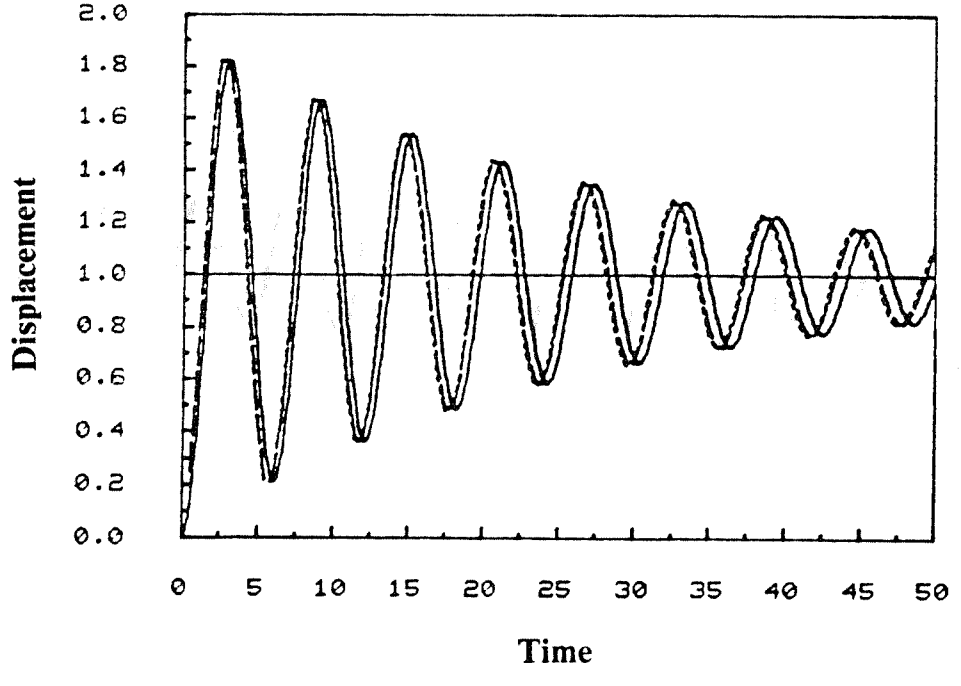

Figure 3.10 Response of SDOF fractional oscillator due to $f(t) = h(t)$ ($m = 1$, $k = 1$, $c = 0.1$, $q = 0.5$, $N = 50$, $h = 0.5$)

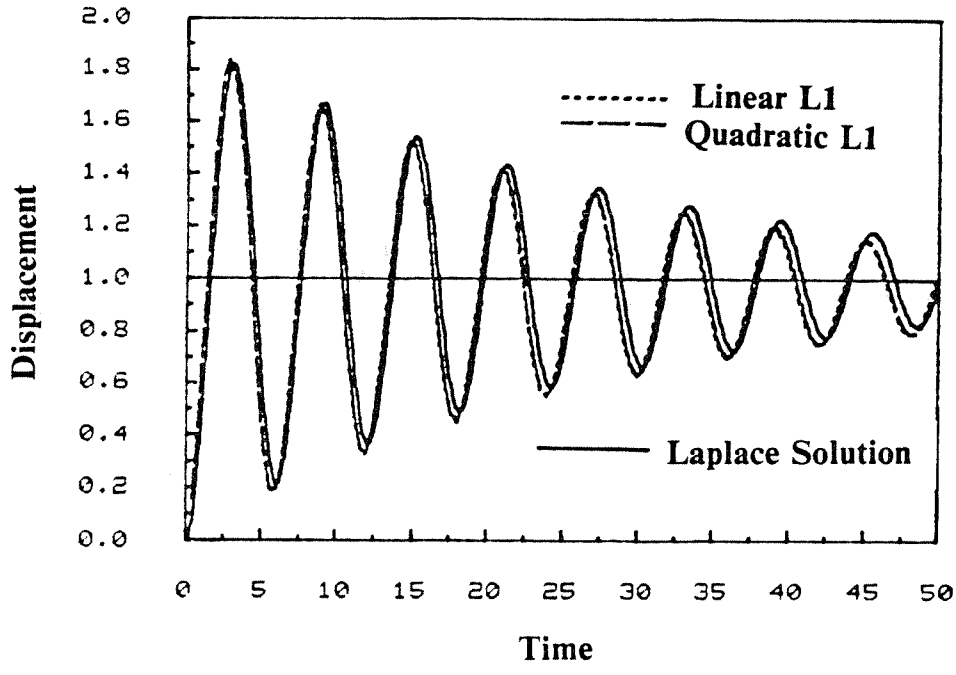

Figure 3.11 Response of SDOF fractional oscillator due to $f(t) = h(t)$ ($m = 1$, $k = 1$, $c = 0.1$, $q = 0.5$, $N = 5$, $h = 0.4$)

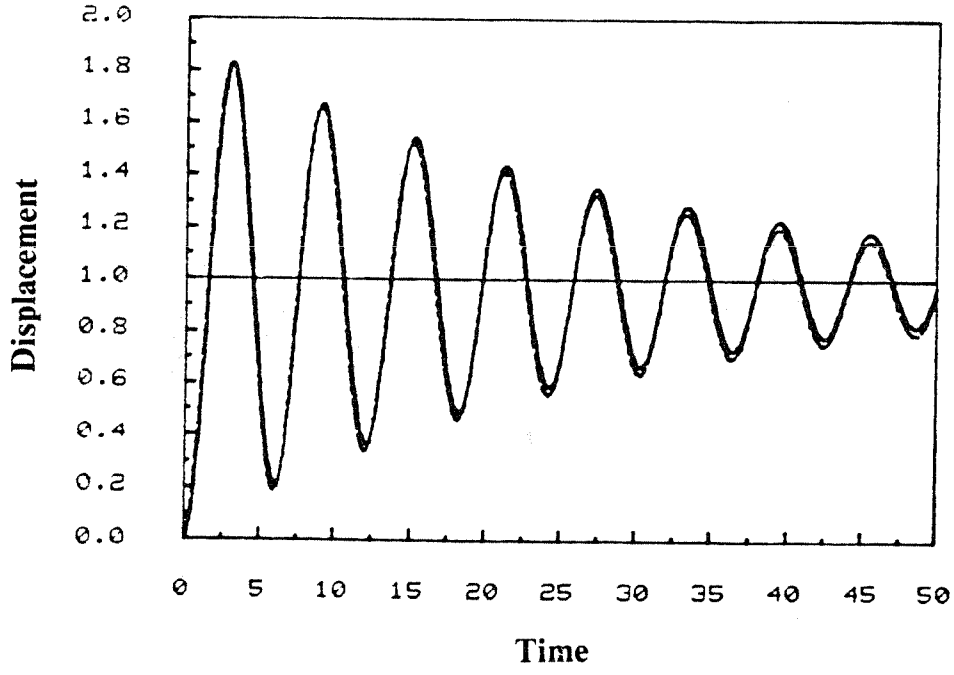

Figure 3.12 Response of SDOF fractional oscillator due to $f(t) = h(t)$ ($m = 1$, $k = 1$, $c = 0.1$, $q = 0.5$, $N = 10$, $h = 0.2$)

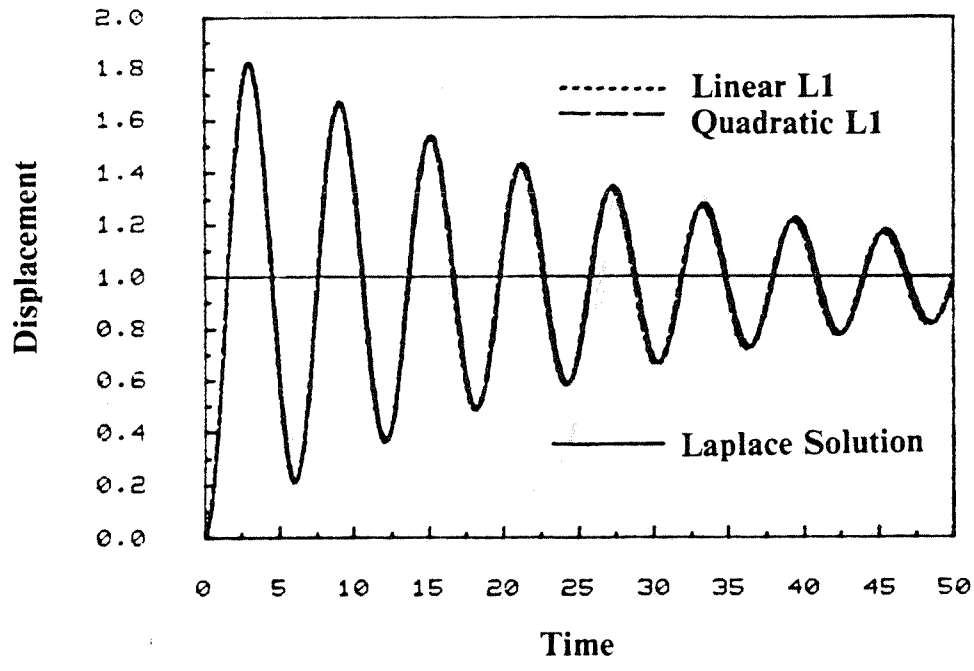

Figure 3.13 Response of SDOF fractional oscillator due to $f(t) = h(t)$
($m = 1$, $k = 1$, $c = 0.1$, $q = 0.5$, $N = 50$, $h = 0.2$)

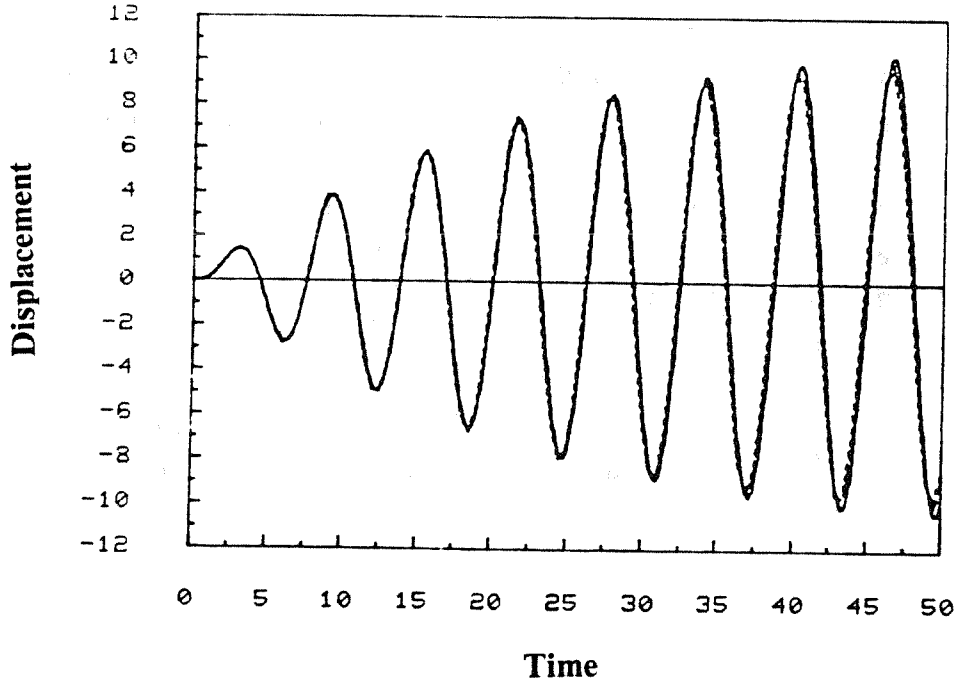

Figure 3.14 Transient Response of SDOF fractional oscillator due to $f(t) = \sin(\bar{\omega}t)$
($m = 1$, $k = 1$, $c = 0.1$, $q = 0.5$, $N = 4$, $h = 0.5$, $\bar{\omega} = 1$)

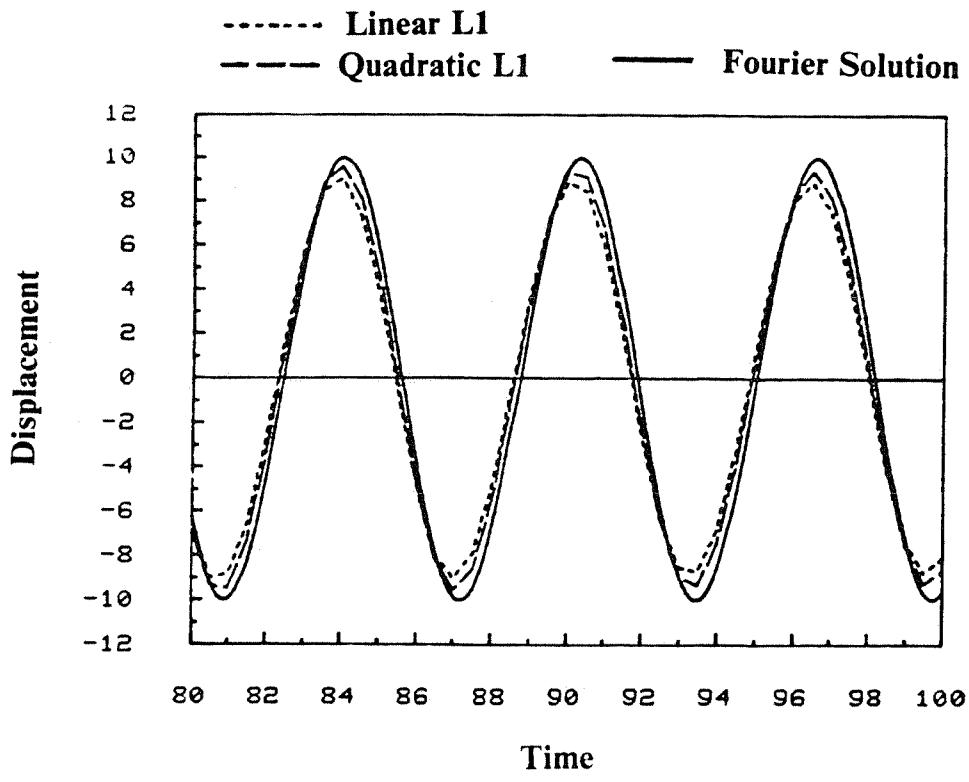

Figure 3.15 Steady-state Response of SDOF fractional oscillator due to $f(t) = \sin(\bar{\omega}t)$
($m = 1$, $k = 1$, $c = 0.1$, $q = 0.5$, $N = 4$, $h = 0.5$, $\bar{\omega} = 1$)

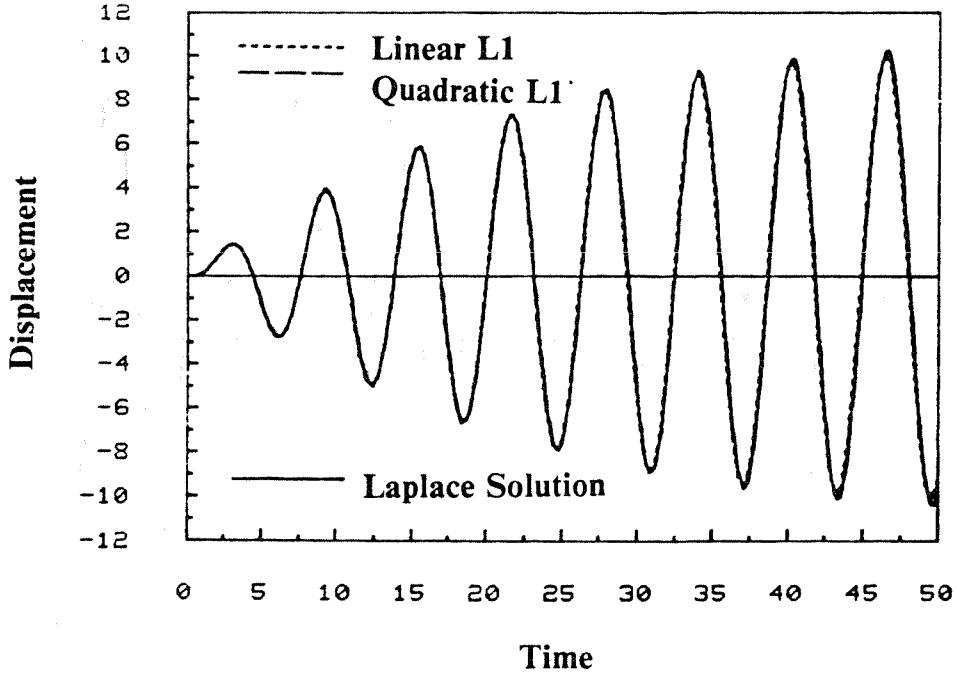

Figure 3.16 Transient Response of SDOF fractional oscillator due to $f(t) = \sin(\bar{\omega}t)$
($m = 1$, $k = 1$, $c = 0.1$, $q = 0.5$, $N = 5$, $h = 0.4$, $\bar{\omega} = 1$)

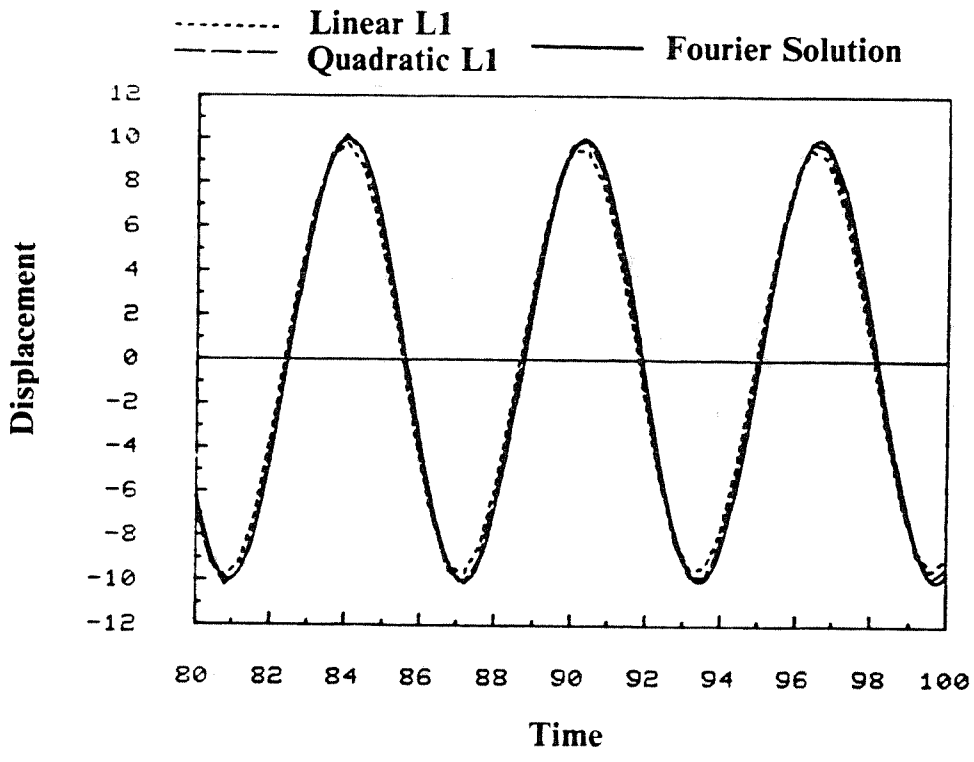

Figure 3.17 Steady-state Response of SDOF fractional oscillator due to $f(t) = \sin(\bar{\omega}t)$
($m = 1$, $k = 1$, $c = 0.1$, $q = 0.5$, $N = 5$, $h = 0.4$, $\bar{\omega} = 1$)

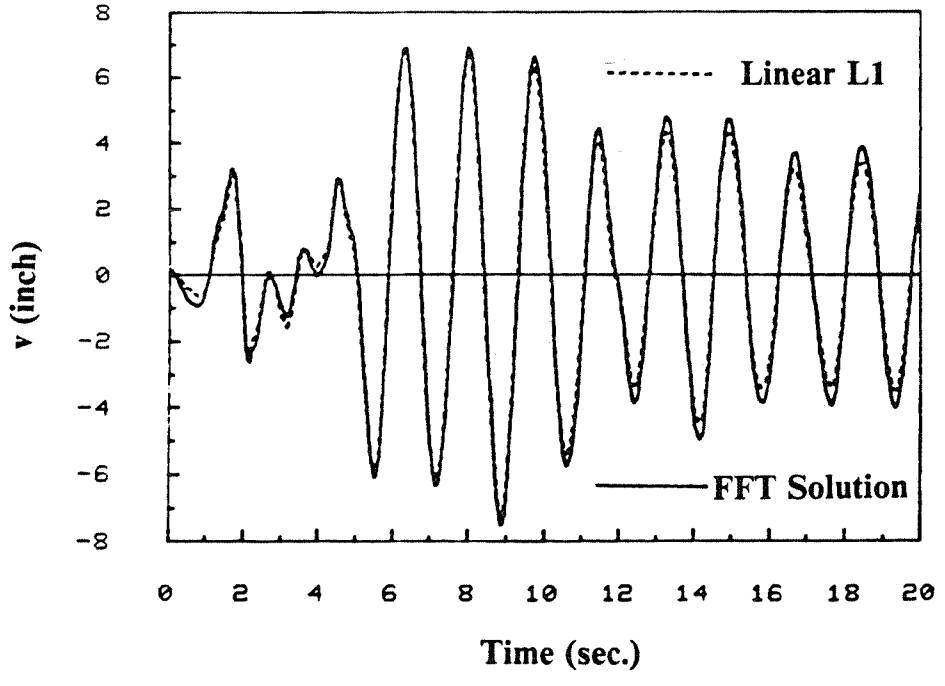

Figure 3.18 Response of SDOF fractional oscillator due to El Centro 1940 earthquake (NS component)
($m = 1$, $k = 10$, $c = 3$, $q = 0.13$, $N=25$, $h = 0.04$)

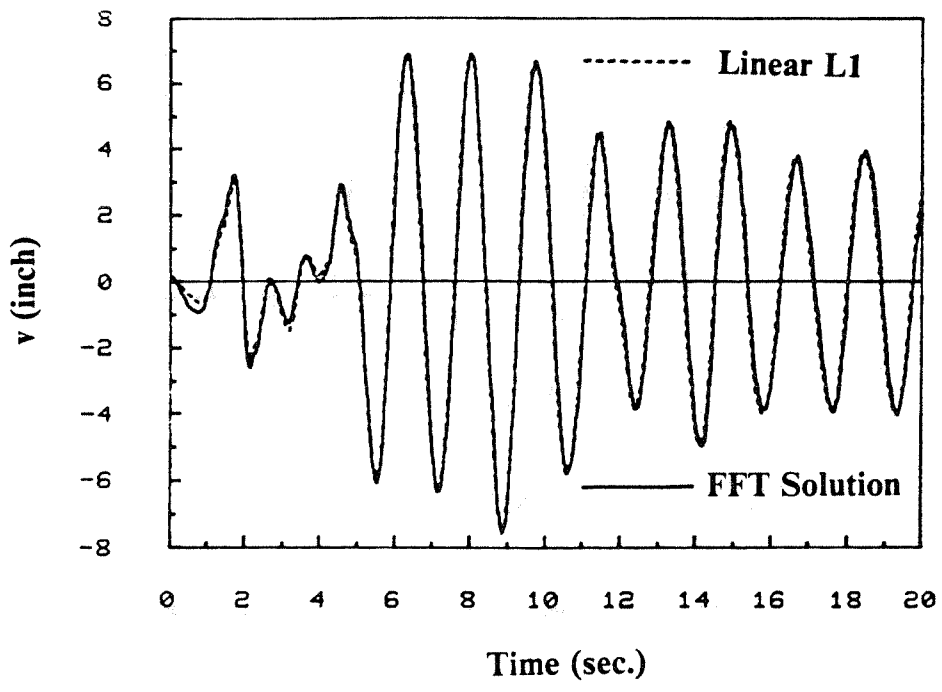

Figure 3.19 Response of SDOF fractional oscillator due to El Centro 1940 earthquake (NS component)

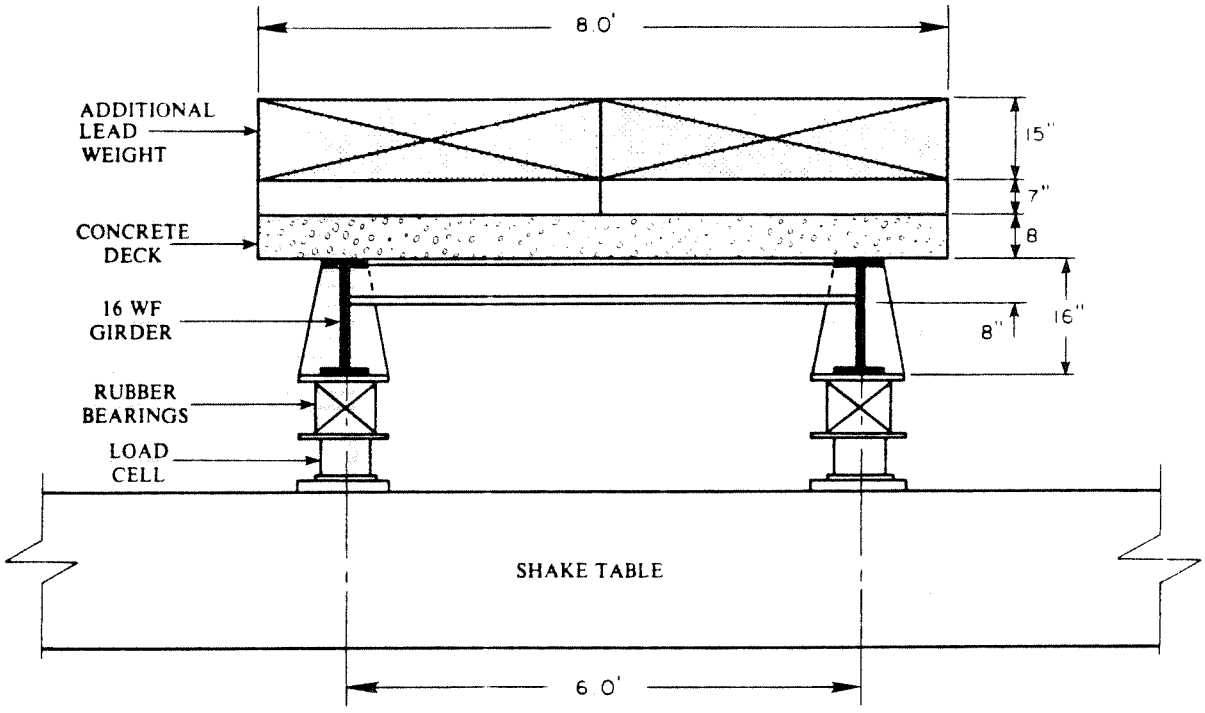

Figure 4.1 Cross-section of base-isolated bridge deck in shaking table tests

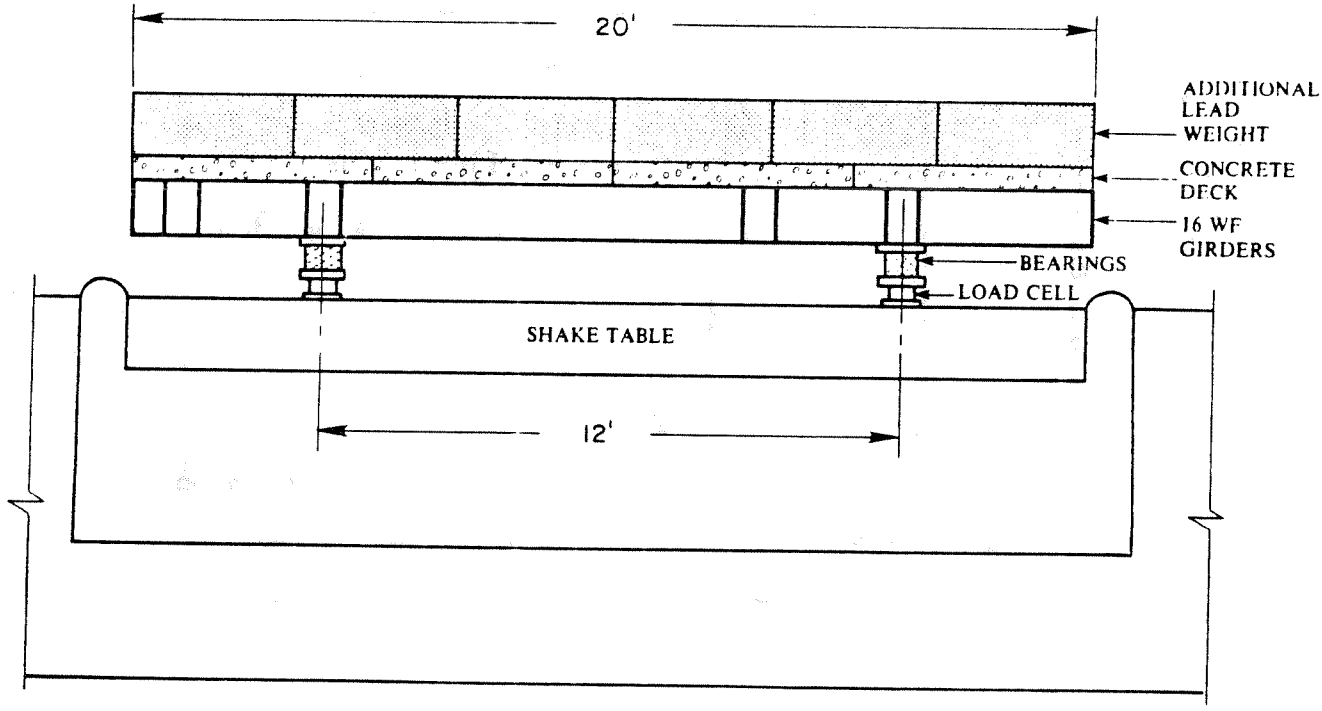

Figure 4.2 Longitudinal elevation of base-isolated bridge deck in shaking table tests

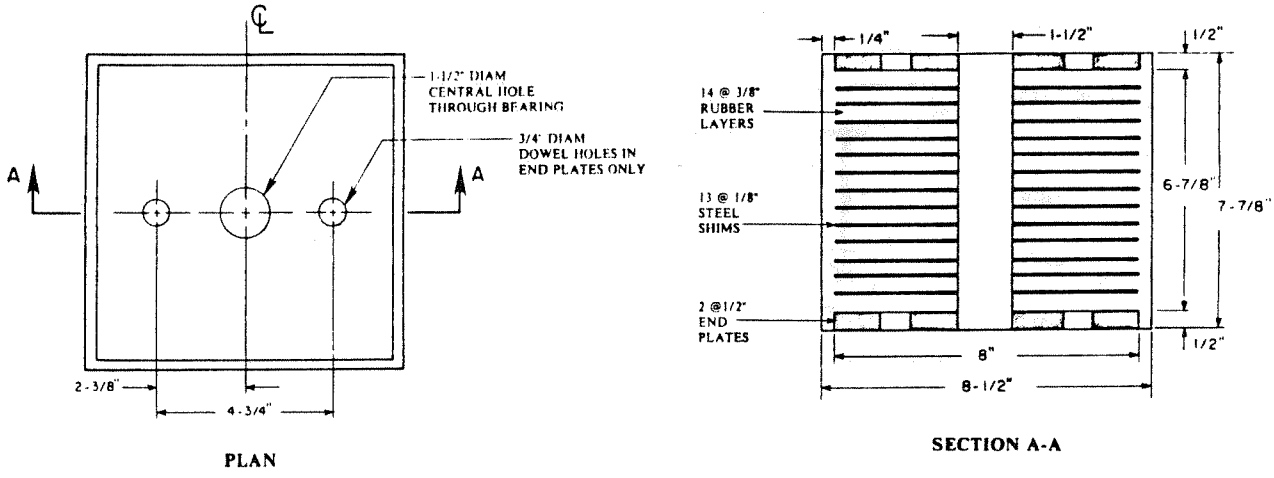

Figure 4.3 Cross-section and plan view of natural rubber isolation bearings

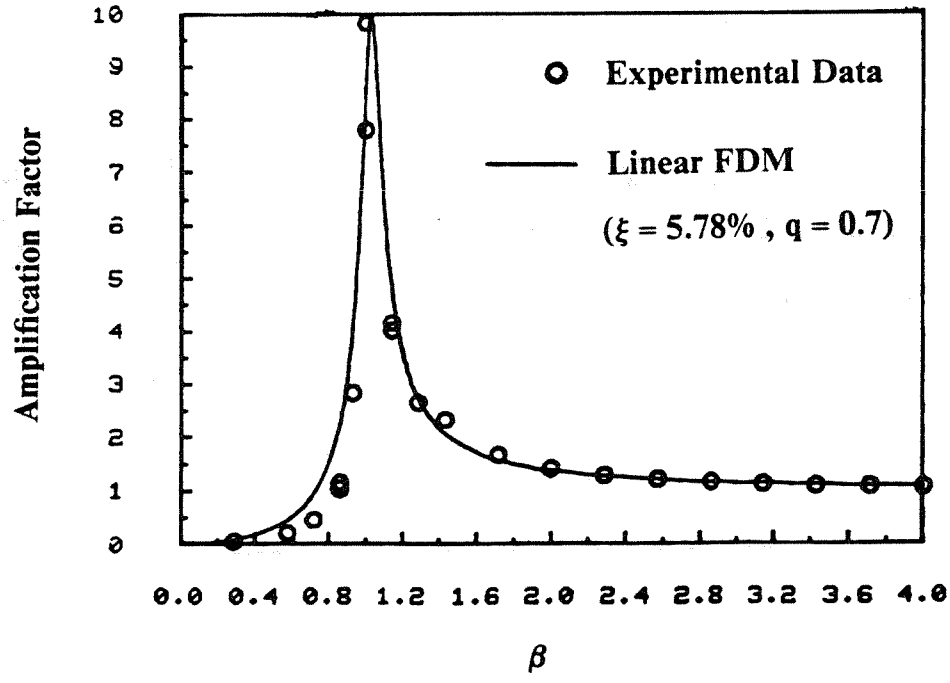

Figure 4.4 Amplification factor obtained in steady-state harmonic tests

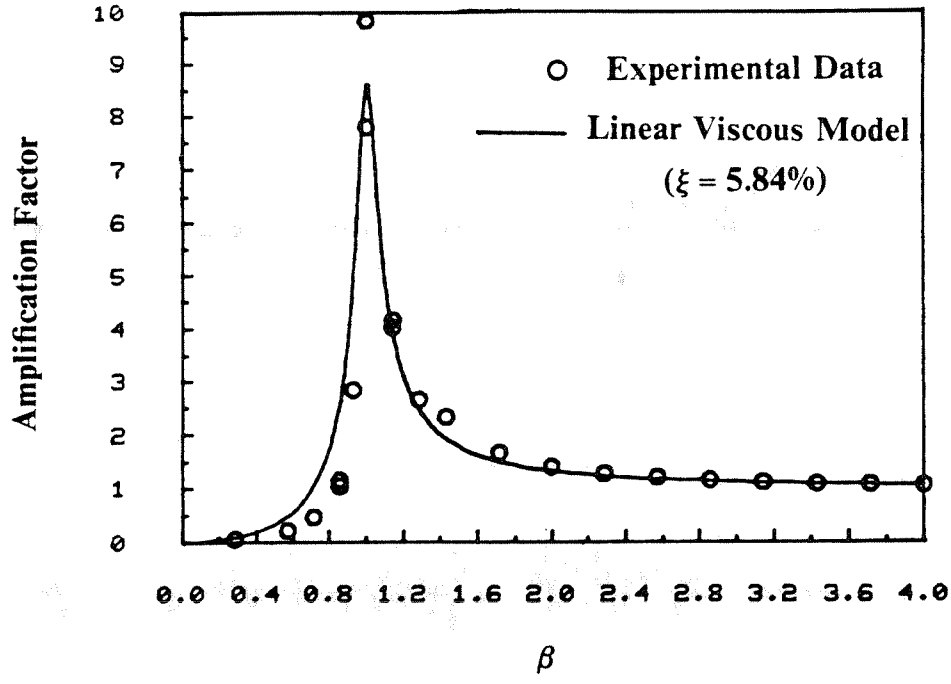

Figure 4.5 Amplification factor obtained in steady-state harmonic tests

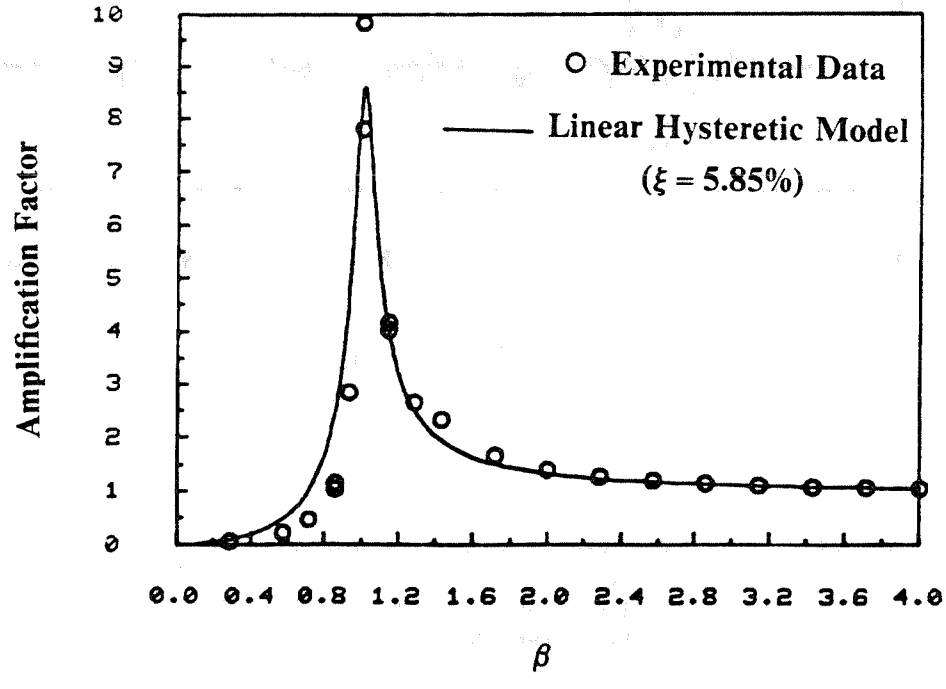

Figure 4.6 Amplification factor obtained in steady-state harmonic tests

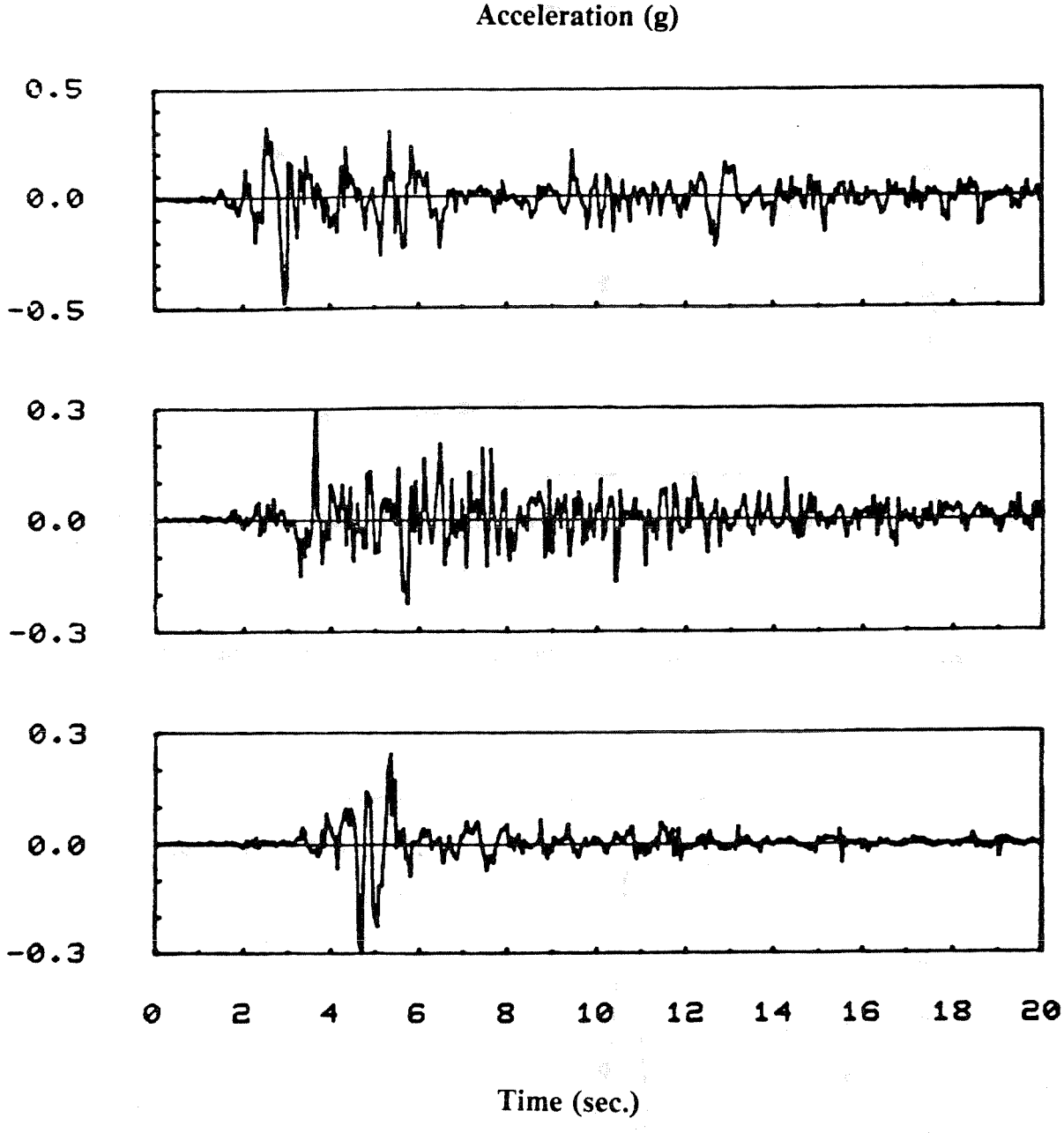

Figure 4.7 Acceleration time histories of input signals :
(a) El Centro 1940 S00E component (H=400) ;
(b) Taft 1952 S69E component (H=750) ;
(c) Parkfield 1966 N65E component (H=750)

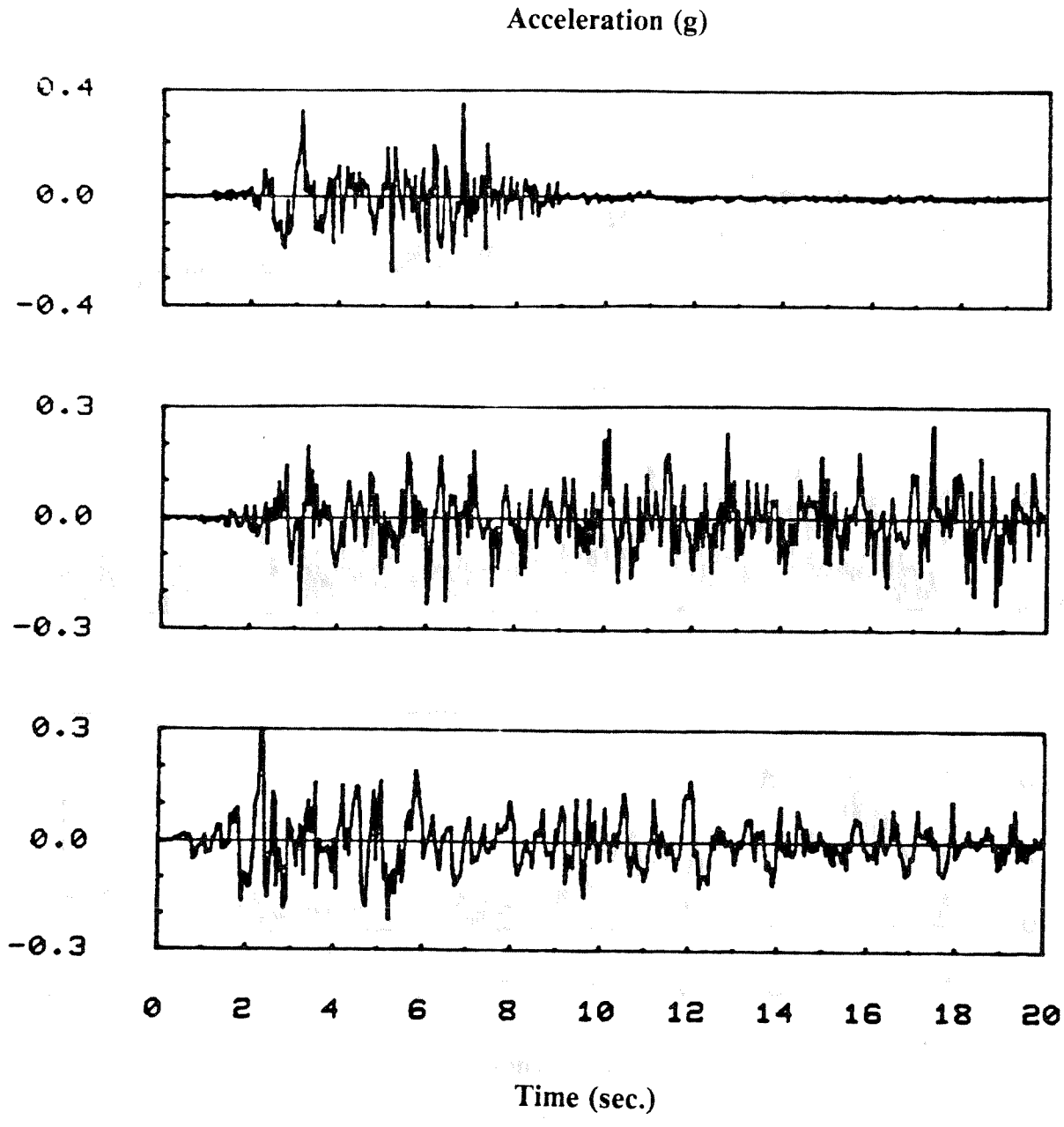

Figure 4.8 Acceleration time histories of input signals :
(a) Pacoima Dam 1971 S14W component (H=750) ;
(b) Cal Tech A artificial record (H=750) ;
(c) Caltrans artificial record (H=400)

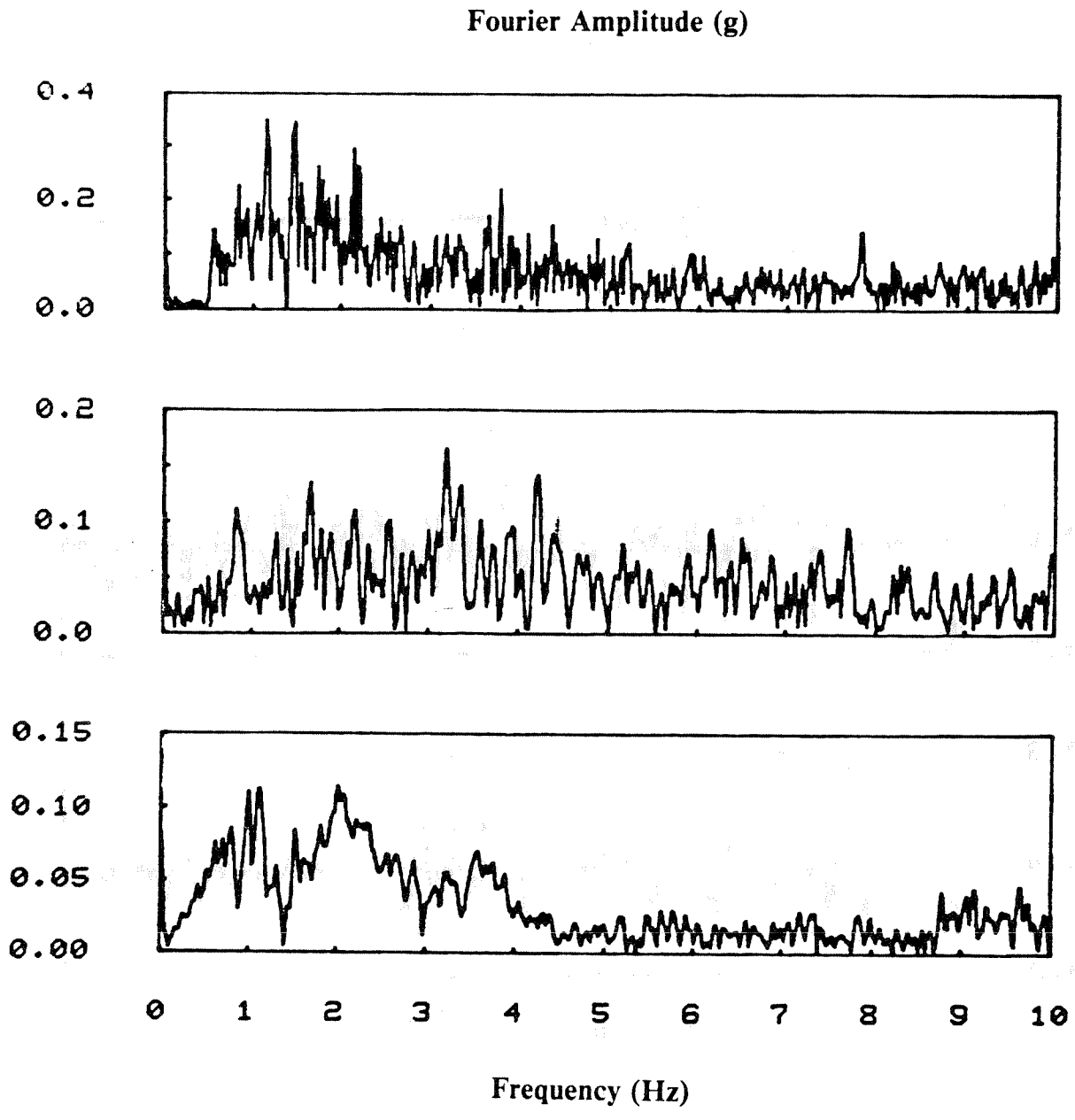

Figure 4.9 Fourier amplitude spectra of input signals :
(a) El Centro 1940 S00E component (H=400) ;
(b) Taft 1952 S69E component (H=750) ;
(c) Parkfield 1966 N65E component (H=750)

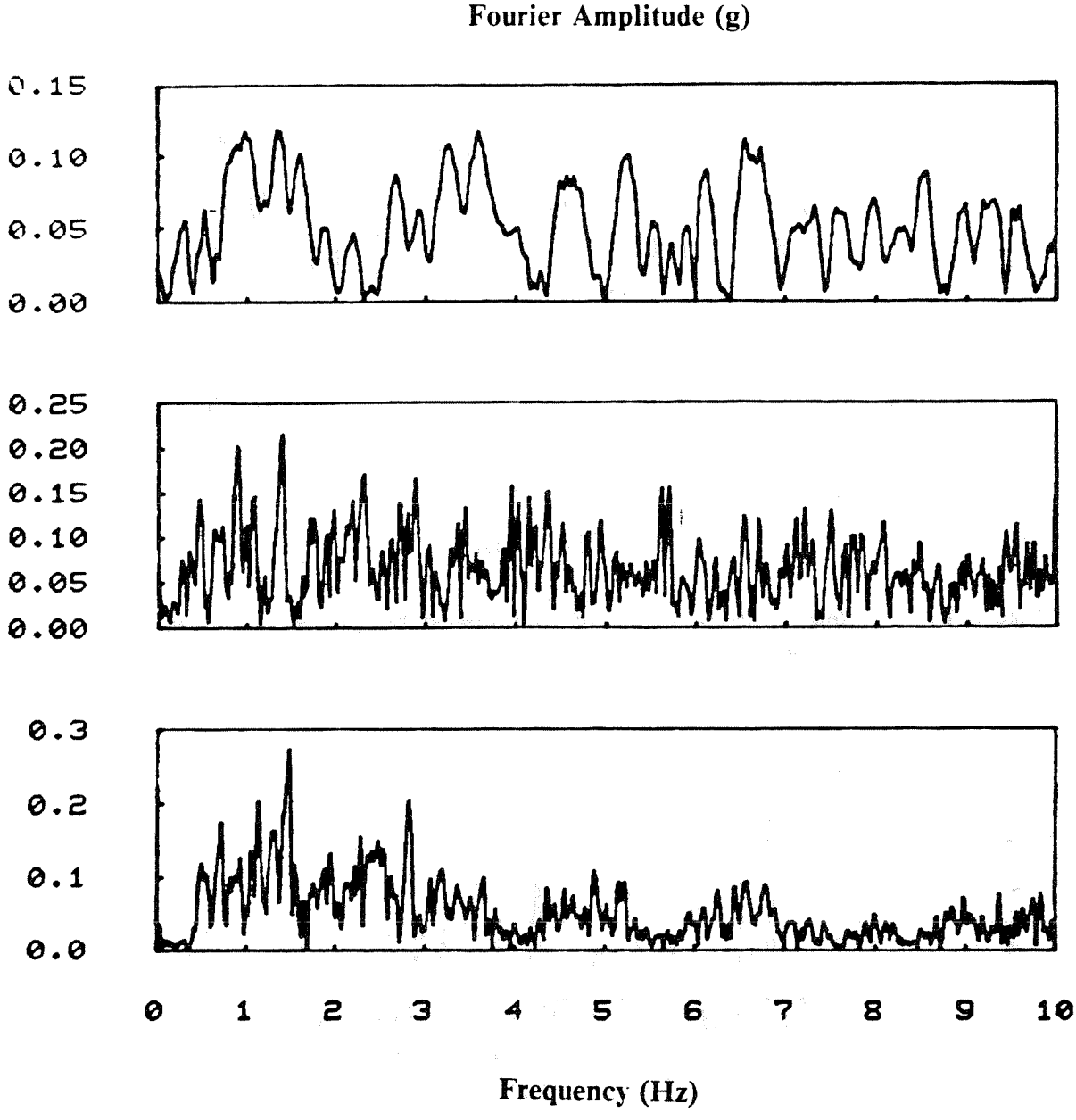

Figure 4.10 Fourier amplitude spectra of input signals :
(a) Pacoima Dam 1971 S14W component (H=750) ;
(b) Cal Tech A artificial record (H=750) ;
(c) Caltrans artificial record (H=400)

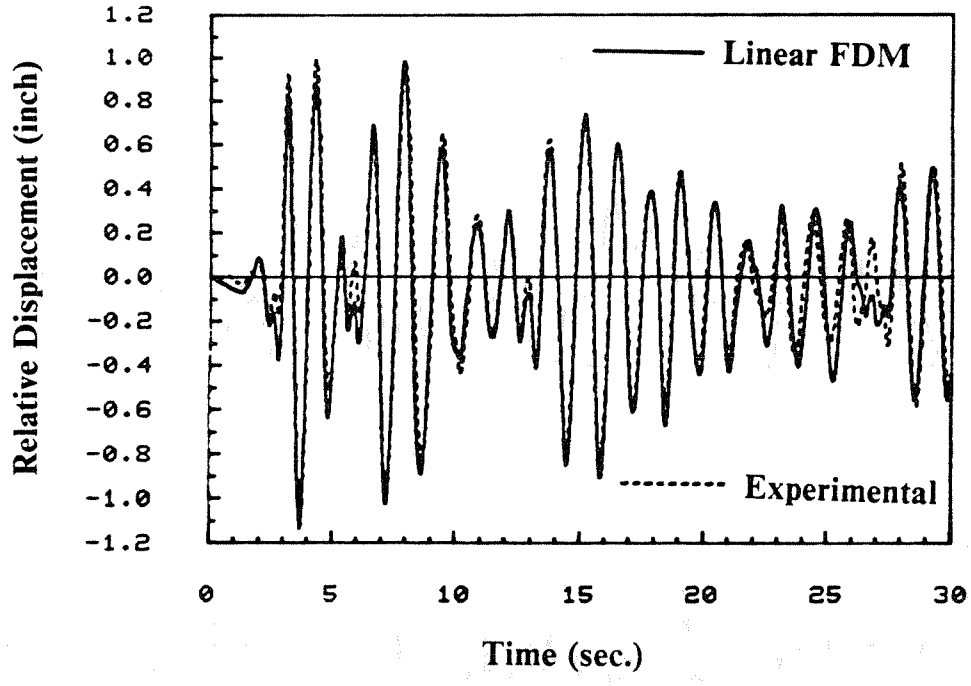

Figure 4.11 Relative displacement of base-isolated bridge deck subjected to El Centro 1940 signal (H=100)

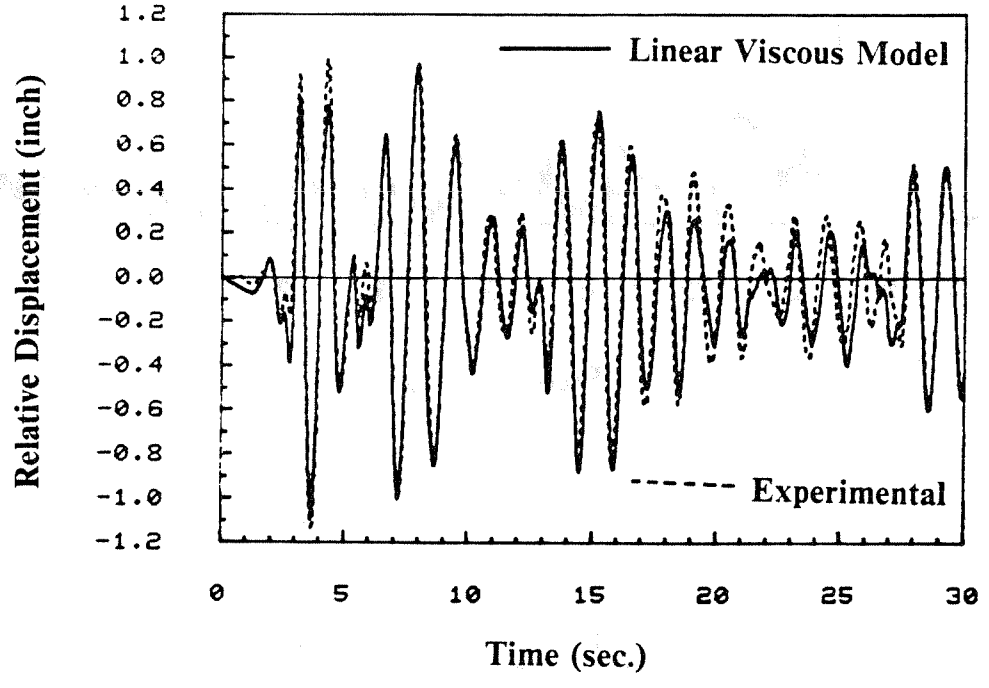

Figure 4.12 Relative displacement of base-isolated bridge deck subjected to El Centro 1940 signal (H=100)

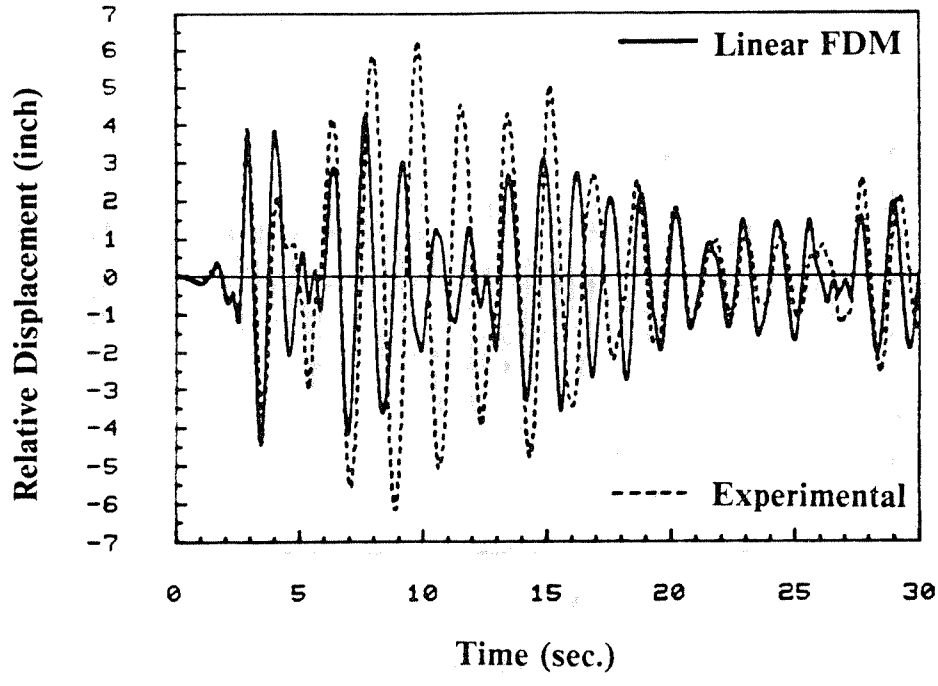

Figure 4.13 Relative displacement of base-isolated bridge deck subjected to El Centro 1940 signal (H=400)

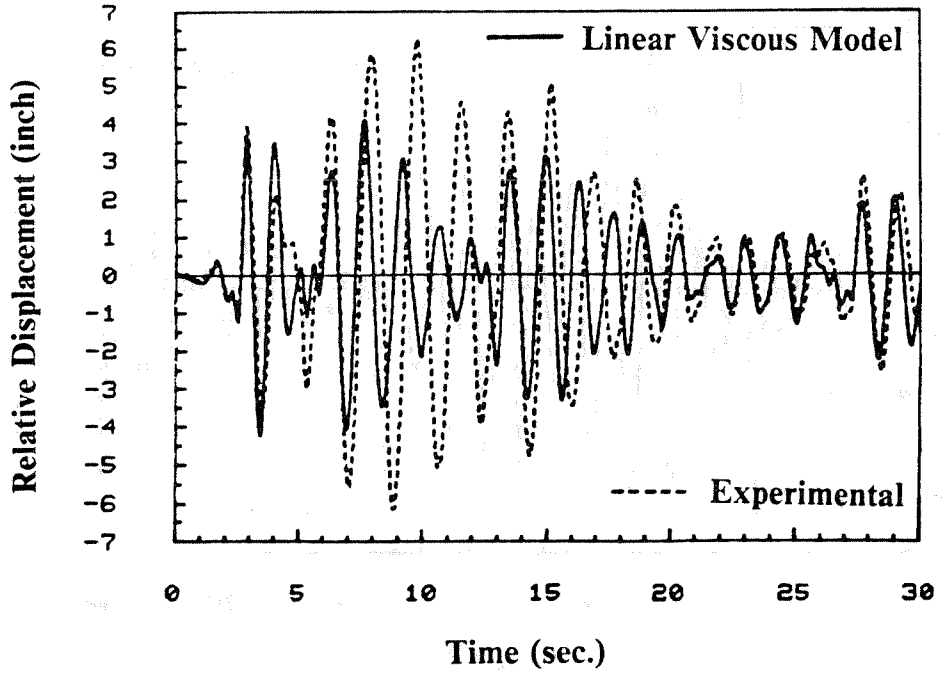

Figure 4.14 Relative displacement of base-isolated bridge deck subjected to El Centro 1940 signal (H=400)

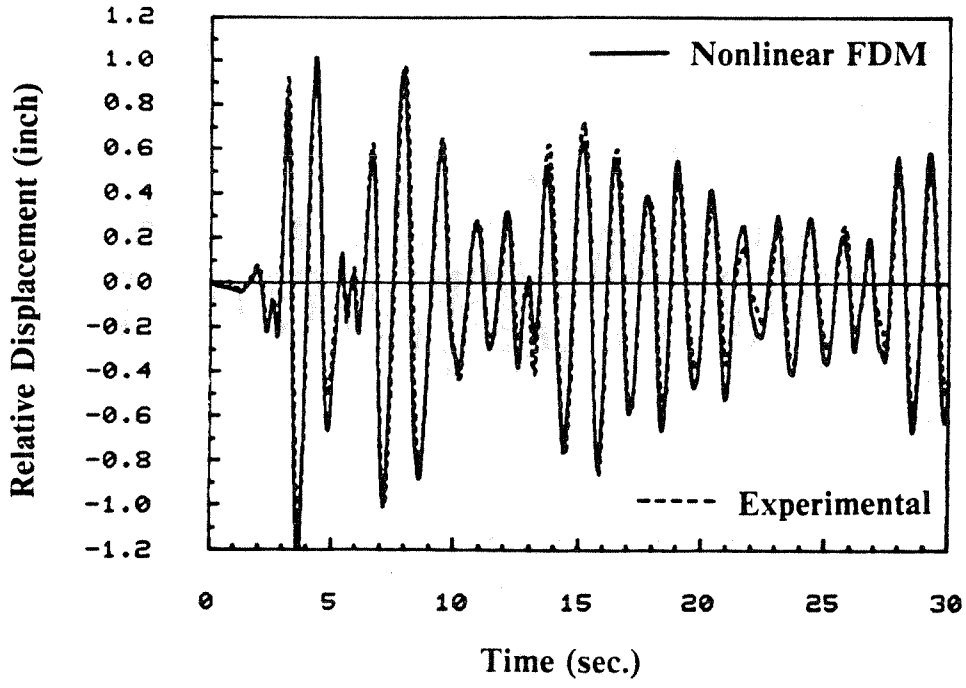

Figure 4.15 Relative displacement of base-isolated bridge deck subjected to El Centro 1940 signal (H=100)

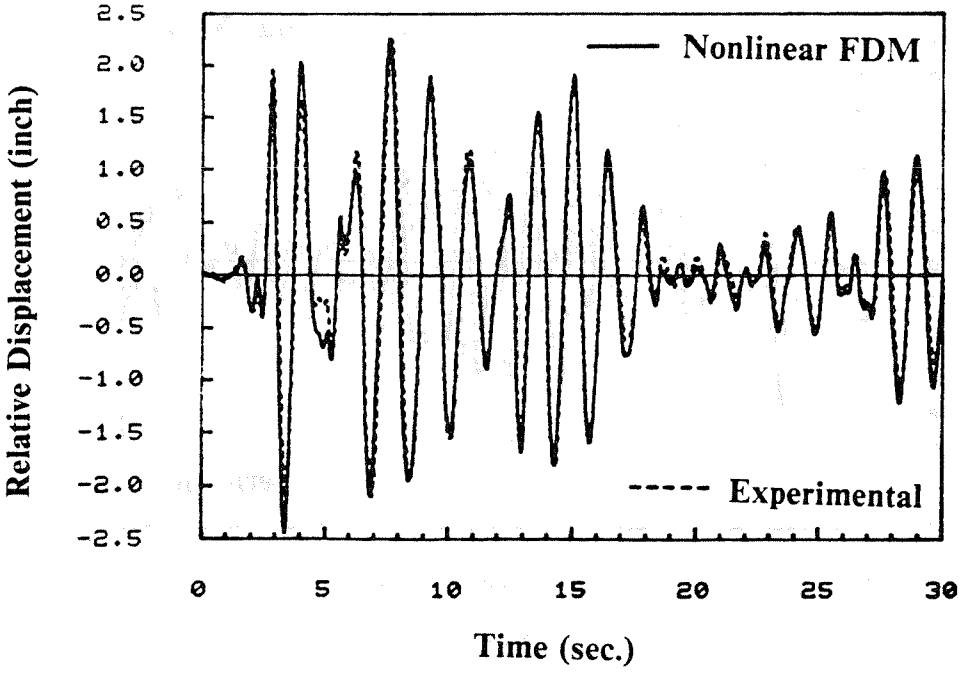

Figure 4.16 Relative displacement of base-isolated bridge deck subjected to El Centro 1940 signal (H=200)

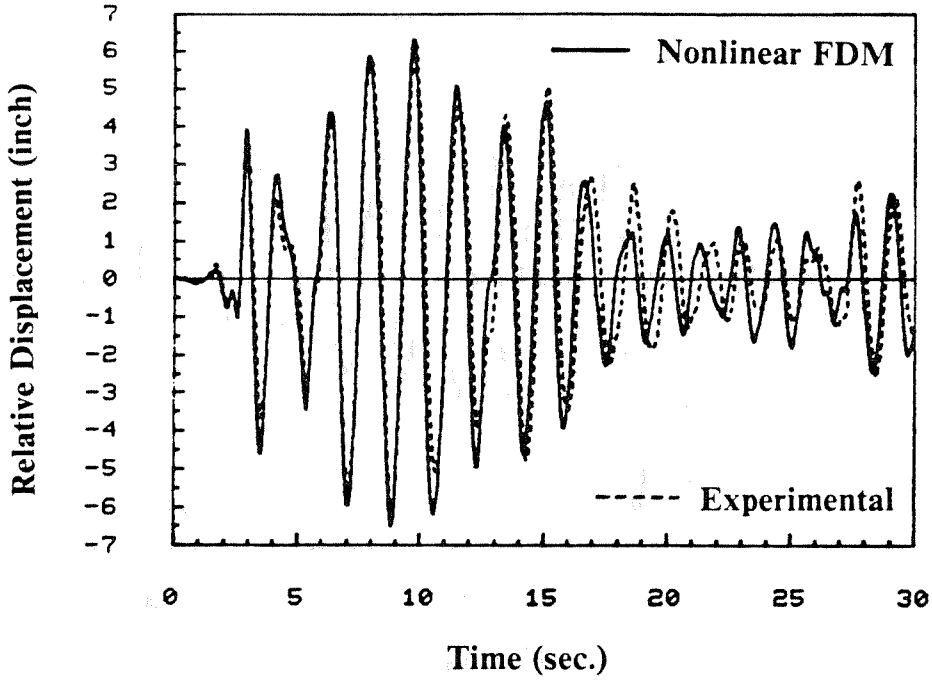

Figure 4.17 Relative displacement of base-isolated bridge deck subjected to El Centro 1940 signal (H=400)

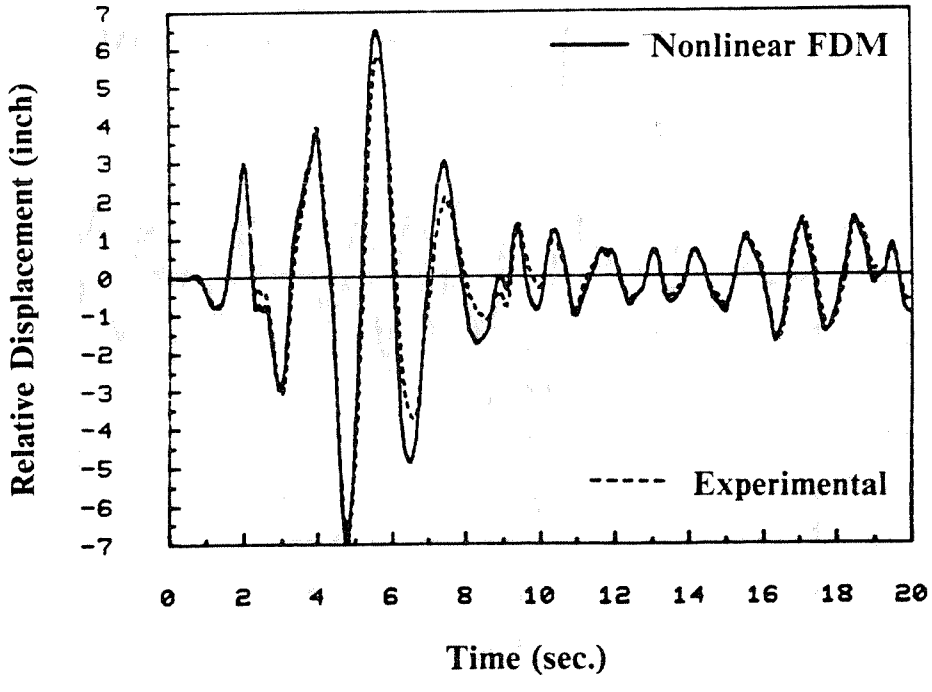

Figure 4.18 Relative displacement of base-isolated bridge deck subjected to El Centro 1940 signal (H=750)

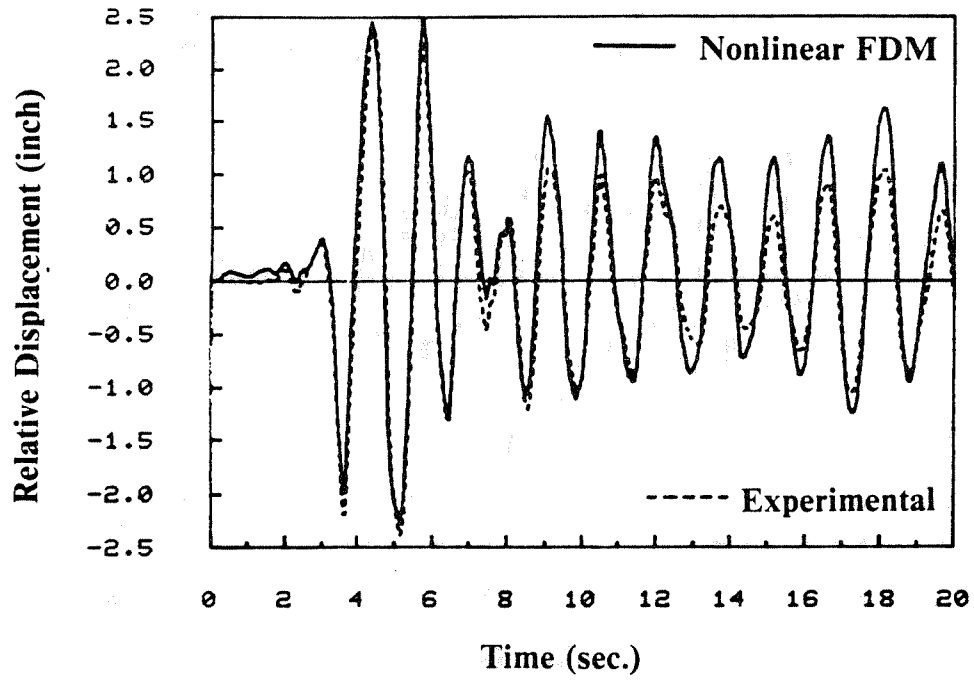

Figure 4.19 Relative displacement of base-isolated bridge deck subjected to Taft 1952 signal (H=750)

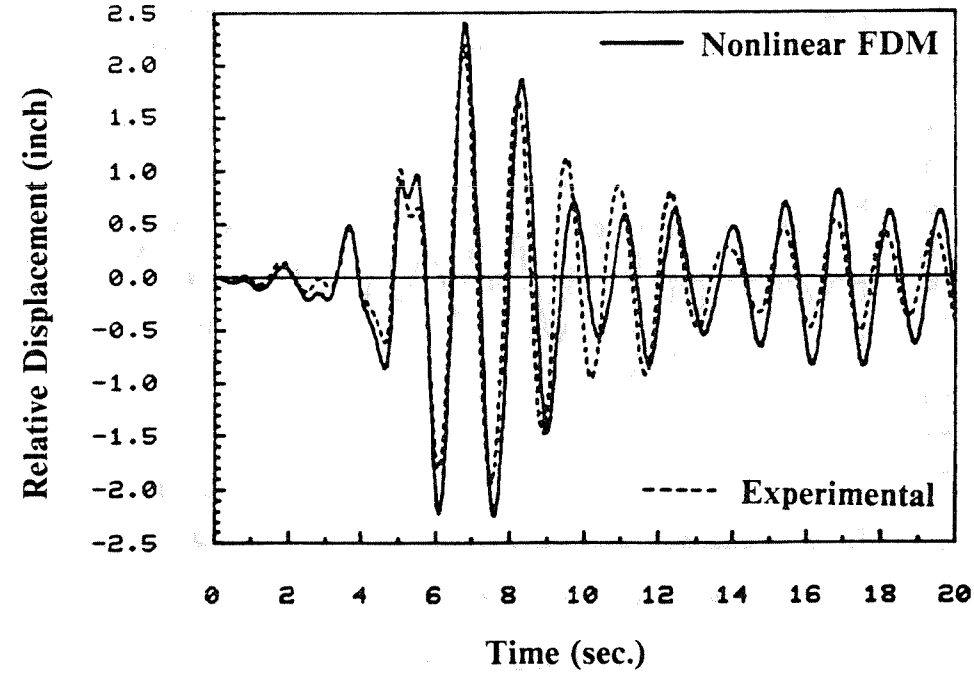

Figure 4.20 Relative displacement of base-isolated bridge deck subjected to Parkfield 1966 signal (H=150)

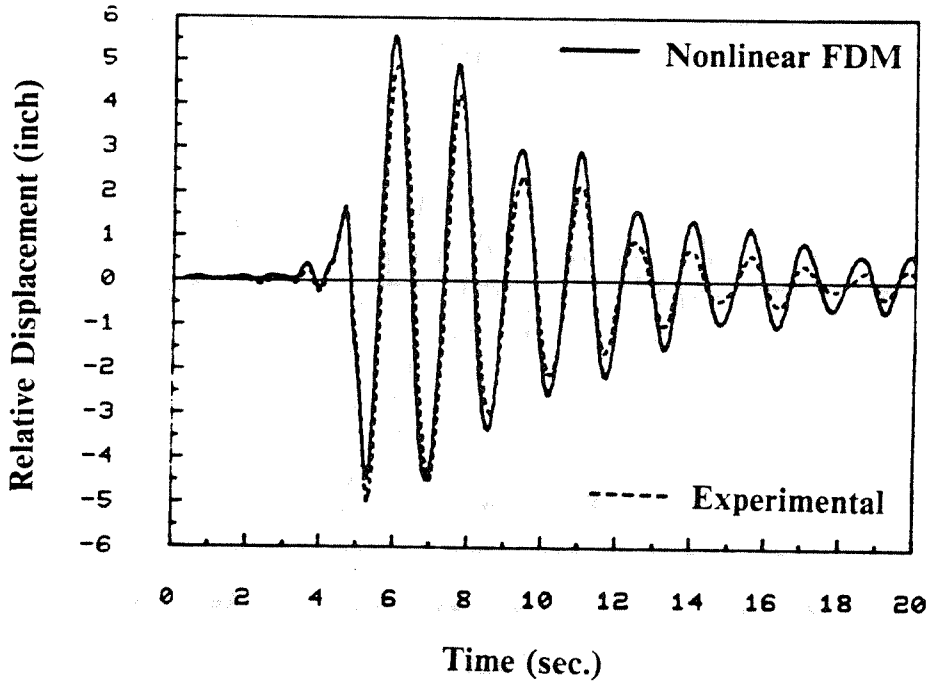

Figure 4.21 Relative displacement of base-isolated bridge deck subjected to Parkfield 1966 signal (H=750)

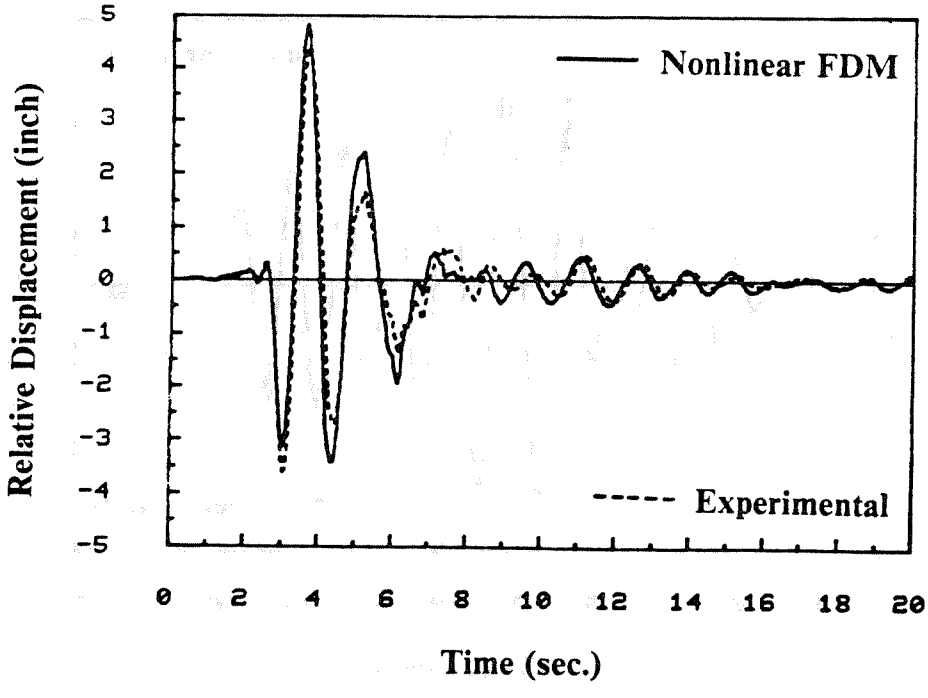

Figure 4.22 Relative displacement of base-isolated bridge deck subjected to Pacoima Dam 1971 signal (H=750)

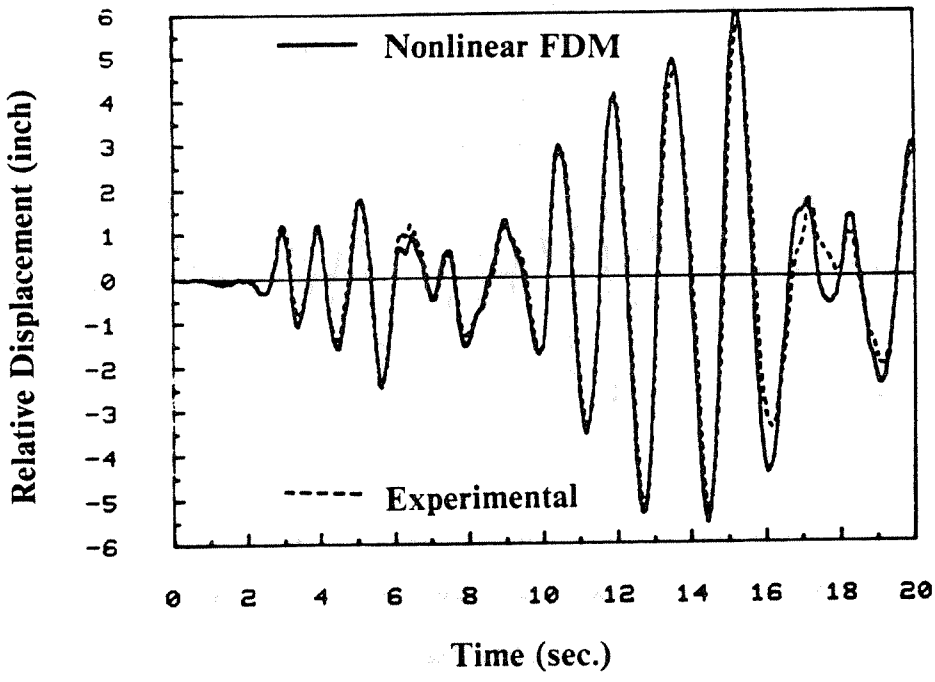

Figure 4.23 Relative displacement of base-isolated bridge deck subjected to Cal Tech A signal (H=750)

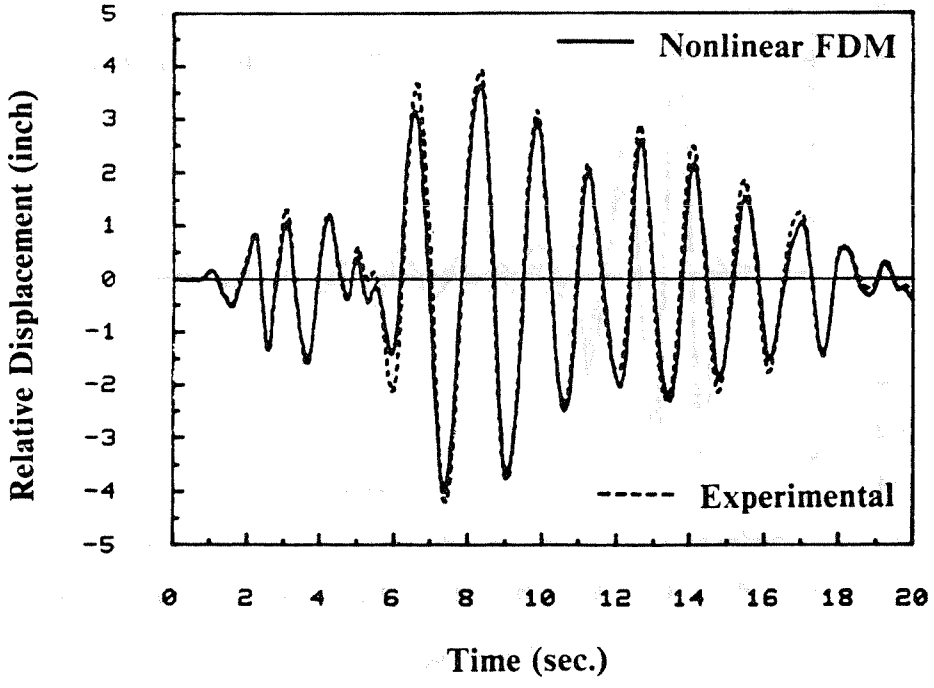

Figure 4.24 Relative displacement of base-isolated bridge deck subjected to Caltrans signal (H=300)

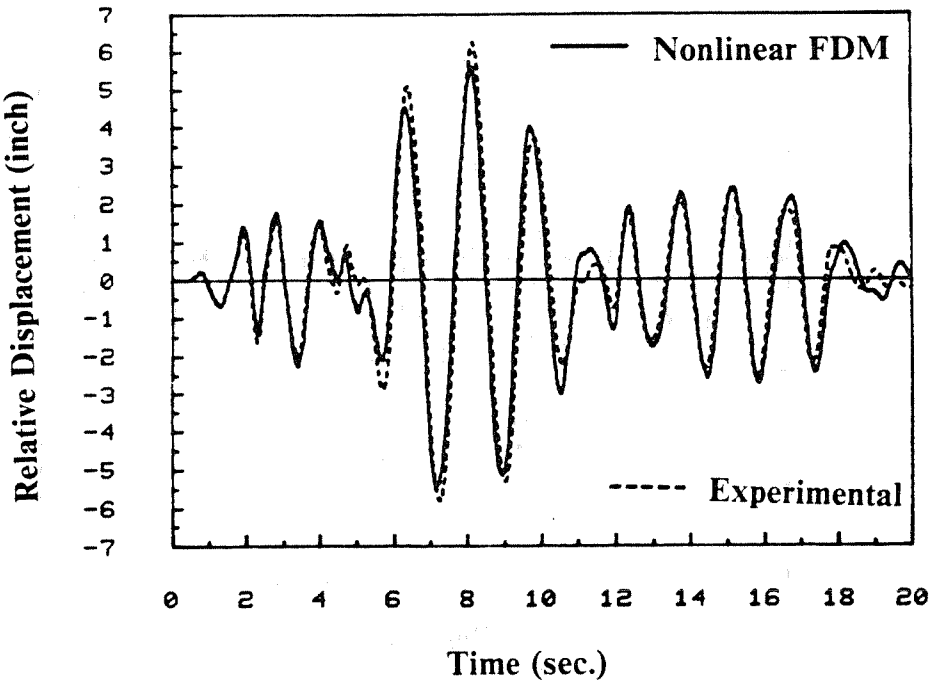

Figure 4.25 Relative displacement of base-isolated bridge deck subjected to Caltrans signal (H=400)

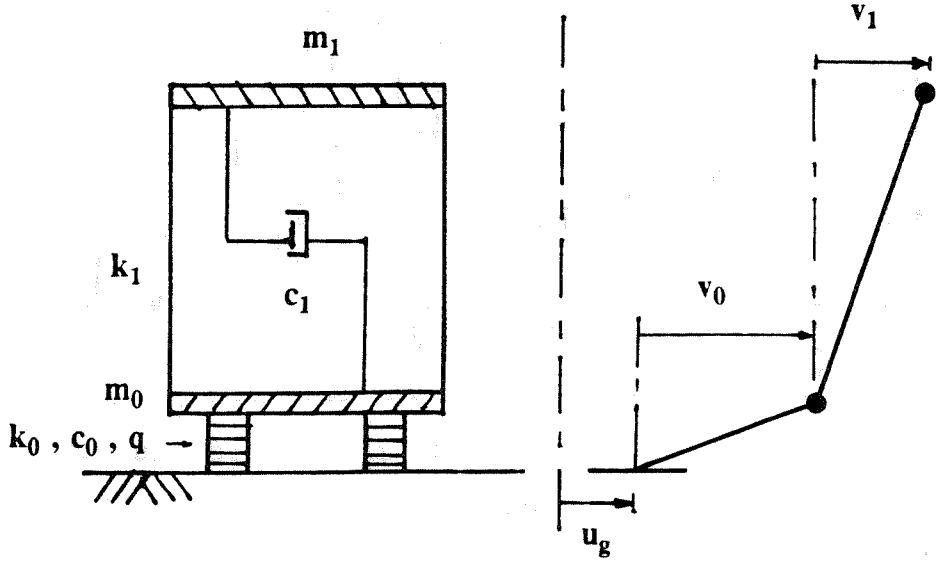

Figure 5.1 Base isolated single-story shear building and the idealized 2-DOF model

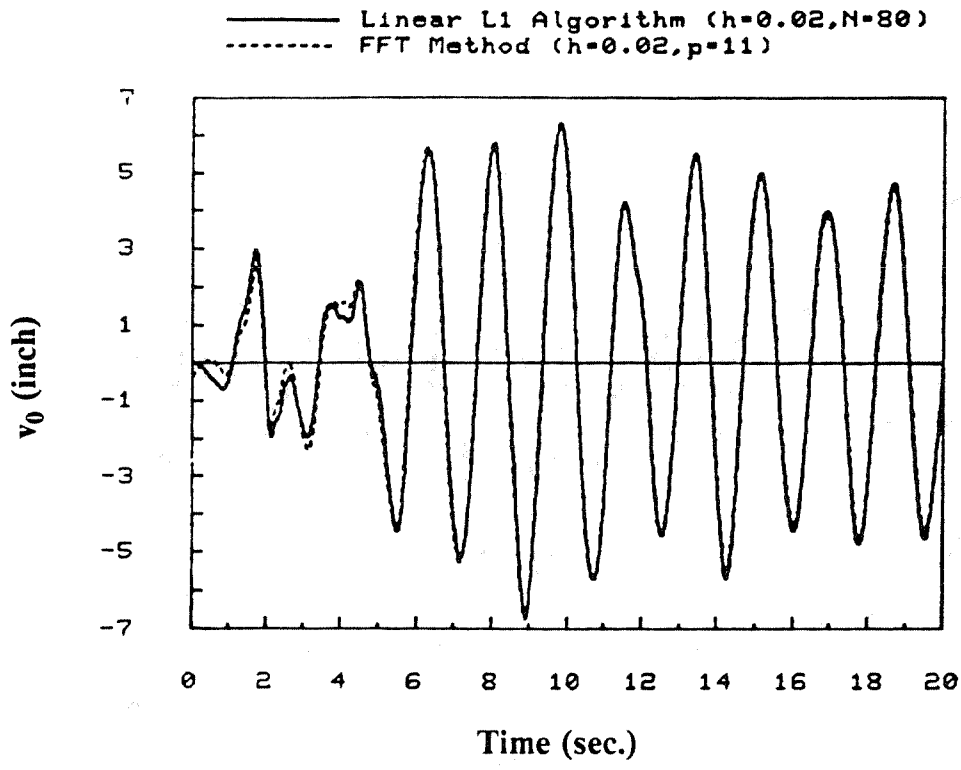

Figure 5.2 Displacement of base deck relative to ground due to El Centro 1940 earthquake (NS)

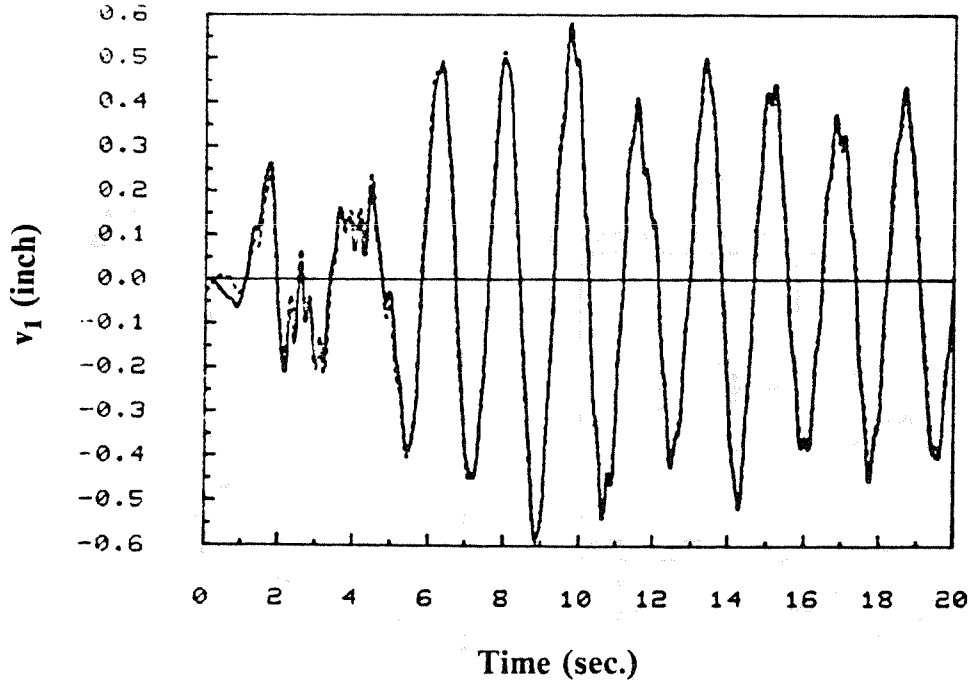

Figure 5.3 Displacement of building relative to base deck due to El Centro 1940 earthquake (NS)

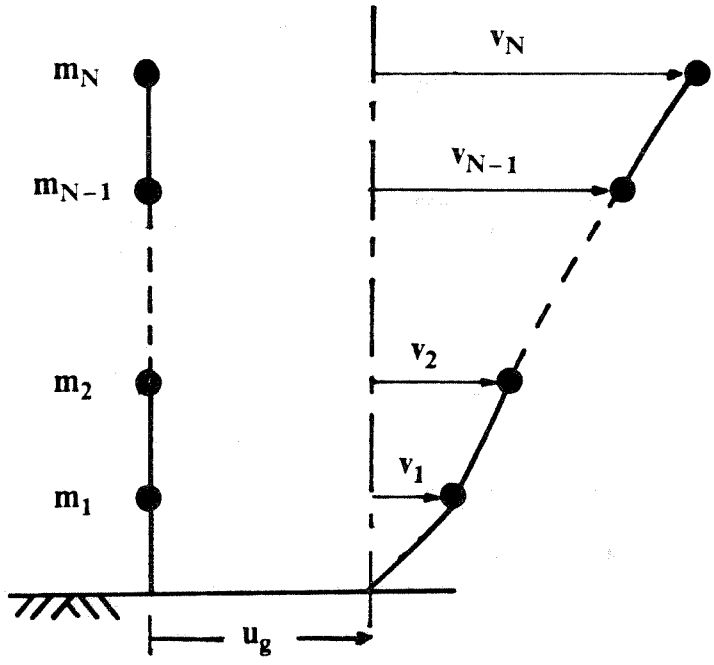

Figure 5.4 Theoretical model of fixed base structure

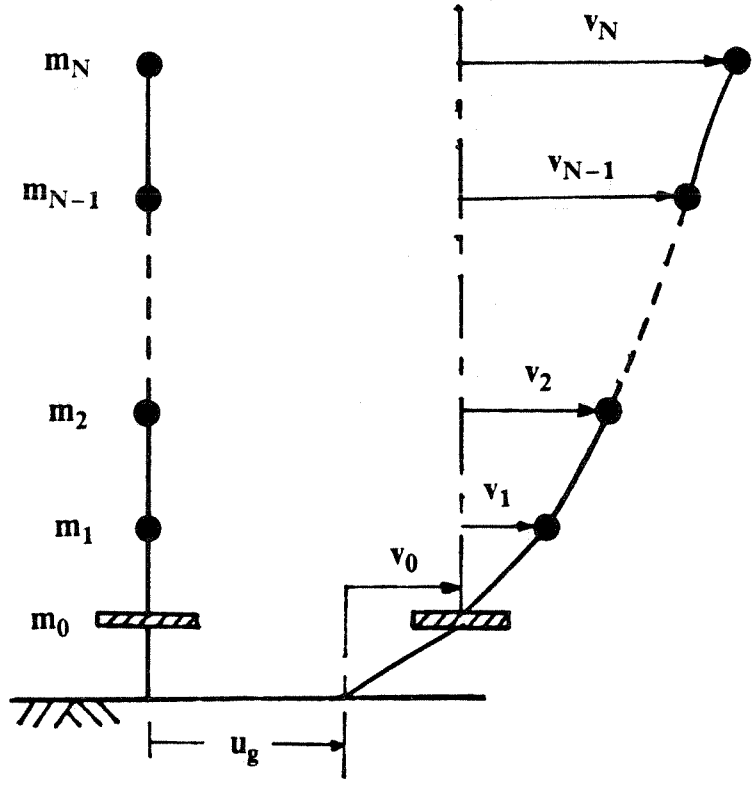

Figure 5.5 Theoretical model of base-isolated structure

TABLE 1

Amplification Factor of Base-Isolated Bridge Deck in Harmonic Tests

Frequency (Hz)	Amplification Factor
0.2	0.07
0.4	0.23
0.5	0.48
0.6	1.06
0.6	1.17
0.65	2.86
0.7	7.81
0.7	9.85
0.8	4.03
0.8	4.17
0.9	2.67
1.0	2.35
1.2	1.68
1.4	1.42
1.6	1.29
1.8	1.22
2.0	1.17
2.2	1.13
2.4	1.10
2.6	1.09
2.8	1.07

TABLE 2

Percentage Differences between

Experimental Response and Nonlinear FDM Response

Simulated Earthquake	H	Max. Positive Peak	Max. Negative Peak
El Centro 1940	100	1.8	10.8
	200	0.1	15.9
	400	0.7	5.8
	750	11.8	0.5
Taft 1952	750	6.0	-5.3
Parkfield 1966	150	10.2	15.2
	750	11.8	-12.6
Pacoima Dam 1971	750	9.6	-4.8
Cal Tech A (Artificial)	750	6.0	4.4
Caltrans (Artificial)	300	-6.4	-4.4
	400	-10.6	-6.6

Note: Negative number means that the predicted response by nonlinear FDM is smaller than the experimental response; conversely for positive number.

APPENDIX A

FOURIER TRANSFORMS OF FRACTIONAL DERIVATIVES

Consider that q is positive and non-integer , and n is the smallest integer larger than q , i.e. $n > q > n-1$. Letting $a = -\infty$ and $\nu = 1+q-n$ in Eq. (2.1a) , we obtain

$$ {}_{-\infty}D_t^q [f(t)] = \frac{1}{\Gamma(1-\nu)} \frac{d^n}{dt^n} [\int_{-\infty}^{t} \frac{f(\tau)}{(t-\tau)^\nu} d\tau] \quad , \tag{A.1} $$

alternatively , in the form of convolution integral :

$$ {}_{-\infty}D_t^q [f(t)] = \frac{d^n}{dt^n} [\int_{-\infty}^{t} f(\tau) g(t-\tau) d\tau] \tag{A.2} $$

where

$$ g(t) = \begin{cases} t^{-\nu}/\Gamma(1-\nu) & t \geq 0 \\ 0 & t < 0 \end{cases} \tag{A.3} $$

Taking the Fourier transforms of Eq. (A.2) gives

$$ F\{ {}_{-\infty}D_t^q [f(t)]\} = (i\omega)^n \, F\{f(t)\} \, F\{g(t)\} \tag{A.4} $$

where

$$ \begin{aligned} F\{g(t)\} &= \int_{-\infty}^{\infty} g(t) exp(-i\omega t) dt \\ &= \frac{1}{\Gamma(1-\nu)} \int_0^{\infty} \frac{exp(-i\omega t)}{t^\nu} dt \\ &= \frac{\omega^{\nu-1}}{\Gamma(1-\nu)} \int_0^{\infty} (\frac{\cos u}{u^\nu} - i \frac{\sin u}{u^\nu}) du \quad ; \quad u = \omega t \end{aligned} $$

Since

$$ \int_0^{\infty} \frac{\cos u}{u^\nu} du = \frac{\pi}{2\Gamma(\nu) cos(\nu\pi/2)} \quad , $$

$$ \int_0^{\infty} \frac{\sin u}{u^\nu} du = \frac{\pi}{2\Gamma(\nu) sin(\nu\pi/2)} \quad , $$

$$ \Gamma(1-\nu)\Gamma(\nu) = \frac{\pi}{\sin(\nu\pi)} \quad , $$

Eq. (A.4) becomes

$$F\{{}_{-\infty}D_t^q[f(t)]\} = (i\omega)^{n-1} F\{f(t)\}\,\omega^{\nu}[\cos(\nu\pi/2) + i\sin(\nu\pi/2)]$$

where

$$\cos(\nu\pi/2) + i\sin(\nu\pi/2) = \exp(i\nu\pi/2) = [exp(i\pi/2)]^{\nu} = i^{\nu} \ ,$$

Therefore ,

$$F\{{}_{-\infty}D_t^q[f(t)]\} = (i\omega)^q F\{f(t)\} \tag{A.5}$$

It should be noted that i^q is multivalued mathematically . Nevertheless , as seen in this derivation , only the principal value is considered , i.e. we would take

$$i^q = \cos(q\pi/2) + i\sin(q\pi/2)$$

If we further assume $f(t) = 0$ for $t < a$, then ${}_{-\infty}D_t^q[f(t)] = {}_aD_t^q[f(t)]$, and hence

$$F\{{}_aD_t^q[f(t)]\} = (i\omega)^q F\{f(t)\} \tag{A.6}$$

APPENDIX B

ERROR BOUND FOR LINEAR L1-ALGORITHM

Consider the subinterval $jh \le \tau \le (j+1)h$ and let $u = \tau - jh$, $l = n-j$ ($t = nh$). By Taylor series expansion, we obtain

$$\dot{v}(t-\tau) = \dot{v}(lh) - u\,\ddot{v}(ph) \quad , \quad l-1 \le p \le l \tag{B.1}$$

In the linear L1-algorithm, $v(t)$ is assumed to be piecewise linear in the subinterval . Thus, $\dot{v}(t-\tau)$ is approximated by $(v_{n-j} - v_{n-j-1})/h$.

Let e_j be the absolute error introduced in the numerical integration of $\int_{jh}^{(j+1)h} \frac{\dot{v}(t-\tau)}{\tau^q}\,d\tau$.

A rather loose bound for e_j can be obtained as follows :

$$\begin{aligned} e_j &\le \int_{jh}^{(j+1)h} \frac{u\ |\ \ddot{v}(ph)\ |}{\tau^q}\,d\tau \\ &\le \max_{jh \le t \le (j+1)h} |\ \ddot{v}\ | \int_{jh}^{(j+1)h} \frac{\tau - jh}{\tau^q}\,d\tau \\ &= \max_{jh \le t \le (j+1)h} |\ \ddot{v}\ |\ h^{2-q} \left\{ \frac{1}{2-q}\left[(j+1)^{2-q} - j^{2-q}\right] - \frac{j}{1-q}\left[(j+1)^{1-q} - j^{1-q}\right] \right\} \\ &\le K\,h^{2-q} \qquad \text{where } K \text{ is some constant.} \end{aligned}$$

The accumulated truncation error at $n-th$ step is thus bounded at most by

$$K\,n\,h^{2-q} = K\,t\,h^{1-q} = O(h^{1-q})$$

APPENDIX C

QUADRATIC L1-ALGORITHM

Let $x_j = jh$, $x = x_N = Nh$, $u = y - x_j$ and $h(u) = f(x-y)$.

$$I_j \equiv \int_{(j-1)h}^{jh} \frac{\frac{d f(x-y)}{dy}}{y^q} dy$$

$$= \int_{-h}^{0} \frac{\frac{dh}{du}}{(u + x_j)^q} dy \tag{C.1}$$

$$h(u) = 1 : \quad I_j = 0 \tag{C.2}$$

$$h(u) = u : \quad I_j = \frac{h^{1-q}}{1-q} [j^{1-q} - (j-1)^{1-q}] \tag{C.3}$$

$$h(u) = u^2 : \quad I_j = 2h^{2-q} \left\{ \frac{1}{2-q} [j^{2-q} - (j-1)^{2-q}] - \frac{j}{1-q} [j^{1-q} - (j-1)^{1-q}] \right\} \tag{C.4}$$

Exact up to polynomials of second order, the integral I_j is evaluated through the following quadrature formula:

$$I_j \approx \frac{1}{h^q} \sum_{i=-1}^{1} A_{j,i} f(x_{j+i}) \tag{C.5}$$

The quadrature weights are $A_{j,1} = b_j + a_j$, $A_{j,-1} = b_j - a_j$, $A_{j,0} = -b_j$ in which

$$a_j = \frac{1}{2} [j^{1-q} - (j-1)^{1-q}]$$

$$b_j = \frac{1}{2-q} [j^{2-q} - (j-1)^{2-q}] - \frac{j}{1-q} [j^{1-q} - (j-1)^{1-q}]$$

The integral in Eq, (3.12) is simply given by

$$I(t = nh) = \sum_{j=1}^{n} I_j$$

$$\approx \frac{1}{h^q} \sum_{j=1}^{n} [A_{j,-1} f(x_{j-1}) + A_{j,0} f(x_j) + A_{j,1} f(x_{j+1})] \tag{C.6}$$

Similar to the procedure in Appendix B, the truncation error can be shown to be at most of order h^{2-q} .

APPENDIX D

LAPLACE SOLUTION OF EQ. (3.3) FOR $q = \frac{1}{2}$

For $q = 1/2$ and $f(t) = \delta(t)$, Eq. (3.3) becomes

$$\bar{v}(s) = \frac{1}{m s^2 + c s^{1/2} + k} \tag{D.1}$$

By partial fraction, Eq. (D.1) can be expressed as

$$\bar{v}(s) = \prod_{i=1}^{4} \frac{1}{\sqrt{s} + a_i} \tag{D.2}$$

where a_i are constants depending on the values of m, c and k. Alternatively,

$$\bar{v}(s) = \sum_{i=1}^{4} \frac{c_i}{\sqrt{s} + a_i} \tag{D.3}$$

where $c_i = \frac{1}{\prod_{j \neq i} (a_j - a_i)}$.

The inverse Laplace transform of $\frac{1}{\sqrt{s} + a}$ is $\frac{1}{\sqrt{\pi t}} - a \exp(a^2 t) \operatorname{erfc}(a\sqrt{t})$ where $erfc$ is the complementary error function defined as

$$\operatorname{erfc}(z) = \frac{2}{\sqrt{\pi}} \int_{z}^{\infty} \exp(-t^2)\, dt \tag{D.4}$$

Thus the inverse Laplace transform of Eq. (D.3) leads to

$$v(t) = \sum_{i=1}^{4} c_i \left[\frac{1}{\sqrt{\pi t}} - a_i \exp(a_i^2 t) \operatorname{erfc}(a_i \sqrt{t}) \right] \tag{D.5}$$

It can be easily shown by comparing the coefficients of Eqs. (D.2) and (D.3) that $\sum_{i=1}^{4} c_i = 0$.

Hence,

$$v(t) = -\sum_{i=1}^{4} a_i c_i \exp(a_i^2 t) \operatorname{erfc}(a_i \sqrt{t}) \tag{D.6}$$

Similarly the analytical solutions for $f(t) = h(t)$ or $\sin \bar{\omega} t$ can be obtained.